Cosmic Strings with Junctions: Dynamics and Cosmological Implications

Alkistis Pourtsidou

The University of
Nottingham

Thesis submitted to the University of Nottingham
for the degree of Doctor of Philosophy, December 2010

Supervisor: Prof. Edmund J. Copeland

Examiners: Dr. Antonio Padilla
Dr. Mairi Sakellariadou

Abstract

Cosmic strings are linear concentrations of energy that may have been formed after cosmological phase transitions in the early universe. Cosmic superstrings are analogous objects arising in string theory, and in particular in models of brane inflation. The latter possess two particular features, which differentiate them from the ordinary cosmic strings: a reduced intercommuting probability, and the ability to form junctions. This thesis is concerned with the dynamics and cosmological implications of cosmic strings and superstrings with junctions.

In Chapter 1, we give a brief introduction to the standard Big Bang model and the inflationary paradigm. We also discuss cosmic string formation after the spontaneous breaking of an Abelian U(1) gauge symmetry in the early Universe. In Chapter 2, we present an overview of cosmic string dynamics using the Nambu-Goto method. We discuss the properties of individual cosmic string segments and loops, as well as network evolution in an expanding Universe. We also introduce cosmic superstrings, and review the Nambu-Goto approach to study the evolution of junctions and the kinematic constraints that govern their formation. We conclude with the study of junctions in an expanding spacetime and present an exact solution for a closed loop of three strings and two junctions in a de Sitter Universe.

In Chapter 3, we compare the two different approaches developed to study the dynamics of strings with junctions. We first extensively study the dynamics and stability of a cosmic string loop with junctions using the modified Nambu-Goto approach. Comparing our results with a field theory model that permits junctions we find very good agreement. The Nambu-Goto method is once again confirmed to be a good approximation for studying cosmic string configurations.

In Chapter 4, we review the observational signatures of cosmic strings. More specifically, we concentrate on their gravitational effects, discussing results and constraints from lensing, gravitational radiation, CMB and pulsar timing. We also present recent results for the case of cosmic (super)-strings with junctions.

Chapter 5 is concerned with the cosmological implications of cosmic superstring networks. We first study the scaling patterns of such networks for different values of the string coupling g_s and different charges (p, q) on the strings. We then focus on their CMB signatures, and derive upper bounds for the fundamental tension μ_F using CMB and pulsar timing constraints. The difference between the scaling behaviour of the networks at high and low values of g_s is imprinted as a movement of the position of the peak in the B-mode spectrum. Together with the constraints on $G\mu_F$ from CMB and pulsar timing, this allows for the exciting possibility to constrain the value of the string coupling g_s using CMB data. We conclude in Chapter 6.

Units and Notation

We employ natural units $\hbar = c = k_B = 1$. Greek indices μ, ν are spacetime indices taking the values $0, 1, 2, 3$ and repeated Greek indices are to be summed over these values. The metric signature is $(+, -, -, -)$. In the following table, we present a summary of the most commonly used symbols in this thesis.

Symbol	Ref.	Definition
a	(1.1)	Scale factor
H	(1.9)	Hubble parameter
μ	Sec. 1.4	Cosmic string tension
σ	Sec. 2.3	Spacelike worldsheet coordinate
L	Sec. 2.3	Length of a cosmic string loop
T	Sec. 2.3	Oscillation period of a cosmic string loop
$\mathcal{P}$	Sec. 2.4	Intercommutation probability
$L(t)$	Sec. 2.4	Correlation length
ξ	Sec. 2.4	The scaling solution $L(t)/t$
ρ	(2.37)	The energy density in the long string network
v	(2.42)	Root mean square velocity of string segments
$\tilde{c}$	(2.46)	Loop formation efficiency
k	(2.48)	Curvature parameter
g_s	(2.58)	String coupling
$s(t)$	(2.60)	The value of σ at a junction
μ_i	(3.6)	The tension of a (p_i, q_i) string in flat spacetime
R	Sec. 3.4	Ratio of tensions $\mu_0/(2\mu_1)$ for the butterfly loop
$\mathcal{R}$	Sec. 3.4	Ratio of tensions $\mu_1/(2\mu_2)$ for the butterfly loop
P	Sec. 4.3	Gravitational radiation power
Γ	(4.14)	Radiative efficiency coefficient
Θ	Sec. 4.4	Fractional temperature fluctuation
$\mathcal{P}_{ij}$	(5.12)	Microphysical intercommuting probability
w	(5.13)	Model-dependent volume parameter
c_i	(5.14)	Self-interaction coefficients
d_{ij}^k	(5.15)	Cross-interaction coefficients
M_i	(5.21)	Power spectrum density

List of Papers

This thesis contains material from the following papers:

1. N. Bevis, E. J. Copeland, P. Y. Martin, G. Niz, A. Pourtsidou, P. M. Saffin and D. A. Steer, "Evolution and stability of cosmic string loops with Y-junctions," Phys. Rev. D **80** (2009) 125030 [arXiv:0904.2127 [hep-th]].

2. A. Pourtsidou, A. Avgoustidis, E. J. Copeland, L. Pogosian and D. A. Steer, "Scaling configurations of cosmic superstring networks and their cosmological implications," [arXiv:1012.5014 [astro-ph.CO]].

3. A. Pourtsidou, A. Avgoustidis, E. J. Copeland, L. Pogosian and D. A. Steer, "Cosmological implications of multi-tension cosmic superstring networks" (*to appear*).

Paper 1 is described in Chapter 3. Papers 2 and 3 are described in Chapter 5.

Acknowledgements

I would first like to thank my supervisor, Ed Copeland, for his guidance and support during my doctoral studies. I am grateful to him for the freedom he gave me to pursue research and explore new ideas, and for encouraging my initiative. I would also like to thank all the members of the Particle Theory group at the University of Nottingham, for creating such a friendly and welcoming atmosphere. I am indebted to Gustavo Niz for his help and mentoring. Thanks to Paul Saffin for many useful discussions and a very fruitful collaboration.

During my PhD, I was also fortunate to work with several people outside Nottingham. I am particularly grateful to Ruth Gregory for her constant support and advice, and for a very enjoyable collaboration. Also, many thanks to Levon Pogosian for his supervision during my visit in Simon Fraser University, and for our countless discussions about politics.

Thanks to: Maria, Lina, Yara, Arianna, Graeme, Mark, Magda, Yiannis, Stelios, Gina, Eleni, Gui, Marina, Asia, Anne, Sam, Lukas, Spyros, Mando, Ruth, Amanda, Toula, Alessandra, Karima, and Fernandito-miau. Your friendship is greatly appreciated, even if I forget to show it sometimes (most of the times).

Last but certainly not least, a million thanks to my family. This thesis is dedicated to my parents, Despina and Tolis, and my little brother, Yiorgos.

Contents

List of Figures

List of Tables

Cosmic Strings with Junctions: Dynamics and Cosmological Implications

Chapter 1

Introduction

1.1 The Standard Cosmological Model

In this chapter, we will introduce the standard cosmological model [1, 2, 3, 4]. We will start with the Friedmann-Lemaître-Robertson-Walker (FLRW) description of our Universe, and then provide a brief overview of its thermal history. The Hot Big Bang model can explain the observed expansion of our Universe, the origin of the Cosmic Microwave Background Radiation, the synthesis of light elements (nucleosynthesis) and the formation of large-scale structure. However, the model requires a set of very peculiar initial conditions. The inflationary paradigm manages to determine these initial conditions, as well as the primordial perturbations that seed the observed structure in the Universe.

As we will see, observations provide very good evidence for our cosmological model until the nucleosynthesis era. Before that, particle physics models predict a series of phase transitions, which are often associated with the production of topologi-

cal defects, and in particular cosmic strings [5, 6]. Cosmic strings are line-like defects which stretch across cosmological sizes and are sufficiently massive to have important gravitational effects. Cosmic superstrings are analogous objects arising in string theory and they have generated a fair amount of interest, since they can provide a link between string theory and cosmology [7, 8, 9, 10].

1.1.1 The FLRW Universe

The *cosmological principle* states that, at any given cosmic time, our Universe looks the same on large scales (> 100 Mpc), independently of the position of the observer or the direction s/he prefers to look in. The spatial isotropy of the Universe on large scales is best indicated by observations of the Cosmic Microwave Background Radiation[1]— it is extremely uniform on large scales, exhibiting only minute fluctuations. We also know that our Universe is expanding, following Hubble's law.

In General Relativity, our spacetime can be written as $\mathbf{R}\times\Sigma$, where $\mathbf{R}$ represents the time whereas Σ is a maximally symmetric three-dimensional space. The line element for an expanding, homogeneous and isotropic Universe can be written as

$$ds^2 = dt^2 - a^2(t)d\ell^2. \tag{1.1}$$

In equation (1.1), t is the cosmic time, dl^2 is the *comoving*[2] three-dimensional line element and $a(t)$ is the scale factor, which describes the scaling of the comoving distances

[1]The Seven-Year Wilkinson Microwave Anisotropy Probe (WMAP) data were released in January 2010, see [11, 12, 13, 14].

[2]In comoving coordinates, the location of a freely moving object (e.g. a galaxy with negligible peculiar velocity) is fixed.

due to the expansion. It will be often useful to define the conformal time τ as

$$d\tau = \frac{dt}{a(t)}, \tag{1.2}$$

and write equation (1.1) as

$$ds^2 = a^2(\tau)\left[d\tau^2 - d\ell^2\right]. \tag{1.3}$$

The metric (1.1) is the Friedmann-Lemaître-Robertson-Walker (FLRW) metric, and in spherical polar coordinates r, θ, ϕ it takes the form [15]

$$ds^2 = dt^2 - a^2(t)\left(\frac{dr^2}{1-kr^2} + r^2 d\theta^2 + r^2 \sin^2\theta d\phi^2\right), \tag{1.4}$$

where k is the constant spatial curvature. It is useful to note that (1.1) is invariant under

$$k \to \frac{k}{|k|}, \tag{1.5}$$

$$r \to \sqrt{|k|}r, \tag{1.6}$$

$$a \to \frac{a}{\sqrt{|k|}}, \tag{1.7}$$

which means that we can consider three cases for the curvature. These are $k = -1, 0$ and 1 for open, flat and closed universes, corresponding to hyperbolic, flat Euclidean and 3-sphere local geometries. There is now strong observational evidence that the geometry of our observable Universe is spatially flat, up to 1% [16]. With $k = 0$, the spatial part of the metric (1.1) is locally Euclidean.

If the comoving distance between two objects is ℓ, their proper ($dt = 0$) radial distance d is

$$d = a(t)\ell. \tag{1.8}$$

Hence the expansion, or recessional, velocity is

$$v = Hd, \tag{1.9}$$

where the rate of expansion $H = \frac{\dot{a}}{a}$ is the Hubble parameter (note that dots denote derivatives with respect to t), which is time dependent[3]. The last equation is Hubble's law: Galaxies far away seem to be receding from us with a velocity proportional to their distance [18]. The Hubble parameter sets the characteristic time and length scale of the observable Universe ($t, d \sim H^{-1}$).

In order to determine the behaviour of the scale factor $a(t)$, we need to solve the Einstein equations in an FLRW background spacetime. They are [15]

$$G_{\mu\nu} \equiv R_{\mu\nu} - \frac{1}{2}Rg_{\mu\nu} = 8\pi G T_{\mu\nu}, \tag{1.10}$$

where $R_{\mu\nu}$ is the Ricci tensor, R the Ricci scalar, $T_{\mu\nu}$ is the energy-momentum tensor and G is Newton's constant. Before we can solve the Einstein equations, we must specify the matter content of the Universe. Following the usual approach, we consider a perfect fluid. The energy-momentum tensor is

$$T^{\mu\nu} = (\rho + p)U^{\mu}U^{\nu} - pg^{\mu\nu}, \tag{1.11}$$

where ρ and p are the energy and pressure densities of the fluid, respectively, and U^{μ} the fluid's four-velocity. Given that the fluid must be at rest in comoving coordinates, we can write

$$U^{\mu} = (1, 0, 0, 0). \tag{1.12}$$

Thus, the form of the energy-momentum tensor compatible with homogeneity and isotropy is

$$T^{\mu}_{\ \nu} = \mathrm{diag}(\rho, -p, -p, -p). \tag{1.13}$$

[3]Today, the Hubble parameter is $H_0 = 74.2 \pm 3.6\,\mathrm{km\,s^{-1}Mpc^{-1}}$ [17].

The energy conservation equation $\nabla_\nu T^{\mu\nu} = 0$ gives the *continuity equation*

$$\dot{\rho} + 3H(\rho + p) = 0. \tag{1.14}$$

Taking the equation of state to be

$$p = w\rho, \tag{1.15}$$

where $w = \text{const}$, we can write equation (1.14) as

$$\frac{\dot{\rho}}{\rho} + 3(1 + w)H = 0. \tag{1.16}$$

Integrating, we find

$$\rho \propto a^{-3(1+w)}. \tag{1.17}$$

We can consider two important cases, namely matter ($w = 0$) and radiation ($w = 1/3$). The case $w = 0$ corresponds to $p = 0$, describing non-relativistic pressureless matter. This is the state of the cold Universe, when atoms are mostly non-interacting. It can also describe collections of stars and galaxies. When the Universe can be well-described by $p = 0$, we say it is *matter-dominated.* On the other hand, when $p = \rho/3$ we are in the *radiation-dominated* era, which describes photons and relativistic particles moving at (almost) luminal speeds. In the matter era, the energy density falls off as

$$\rho_m \propto a^{-3}. \tag{1.18}$$

This can be easily understood as a decrease due to the expansion of the Universe. In radiation, the energy density falls faster,

$$\rho_r \propto a^{-4}, \tag{1.19}$$

due to the additional factor coming from the redshifting of photons. More specifically, the emitted wavelength λ increases as the Universe expands, and its relation with the observed wavelength λ_0 is defined in terms of the redshift z as

$$1 + z = \frac{\lambda_0}{\lambda} = \frac{a_0}{a}. \tag{1.20}$$

Finally, from the Einstein equations (1.10) we find the Friedmann equations

$$\dot{H} + H^2 = \frac{\ddot{a}}{a} = -\frac{4\pi G}{3}(\rho + 3p), \tag{1.21}$$

and

$$H^2 \equiv \left(\frac{\dot{a}}{a}\right)^2 = \frac{8\pi G}{3}\rho - \frac{k}{a^2}. \tag{1.22}$$

From equation (1.21), we see that for an expanding Universe ($\dot{a} > 0$) filled with matter that satisfies the so-called *strong energy condition* $\rho + 3p \geq 0$, we have $\ddot{a} < 0$. Following $a(t)$ backwards in time, we hit a singularity $a = 0$ at $t = 0$.

Now, let us solve equation (1.22) for the explicit dependence of the scale factor on time for both matter and radiation domination for the simplest case of a flat ($k = 0$) Universe. We find

$$a \propto t^{1/2} \tag{1.23}$$

in the case of radiation domination, and

$$a \propto t^{2/3} \tag{1.24}$$

in the case of matter domination. In addition, we find that the energy conservation equation (1.14) can be derived from the Friedmann equations.

We can rewrite (1.22) using the density parameter, defined as

$$\Omega = \frac{8\pi G}{3H^2}\rho = \frac{\rho}{\rho_{crit}}, \tag{1.25}$$

where $\rho_{crit} = 3H^2/8\pi G$ is the so-called *critical* density — substituting $\rho = \rho_{crit}$ in equation (1.22) gives a spatially flat universe. We can therefore write

$$\Omega - 1 = \frac{k}{a^2 H^2}, \tag{1.26}$$

which becomes $\Omega = 1$ for $k = 0$.

The most exciting fact about the evolution of our Universe is the observational evidence that, currently, its expansion is accelerating [19, 20]. This means that $\rho + 3p < 0$ in equation (1.21), so that $\ddot{a}$ is positive. Acceleration can be achieved by adding a cosmological constant term to the Einstein equations. This gives

$$R_{\mu\nu} - \frac{1}{2} R g_{\mu\nu} = 8\pi G T_{\mu\nu} - \Lambda g_{\mu\nu}. \tag{1.27}$$

The cosmological constant represents the vacuum energy, which in turn can be thought of as a fluid with a $w = -1$ equation of state. Thus,

$$p = -\rho, \tag{1.28}$$

and from equation (1.14) the energy density is constant — this means that the cosmological constant term will eventually dominate. Taking $k = 0$, $\rho = \text{const}$ in equation (1.22) and solving for the scale factor a, we find

$$a \propto e^{Ht}. \tag{1.29}$$

The Friedmann equations with a cosmological constant become

$$\frac{\ddot{a}}{a} = -\frac{4\pi G}{3}(\rho + 3p) + \frac{\Lambda}{3}, \tag{1.30}$$

and

$$H^2 \equiv \left(\frac{\dot{a}}{a}\right)^2 = \frac{8\pi G}{3}\rho - \frac{k}{a^2} + \frac{\Lambda}{3}. \tag{1.31}$$

Let us now perform some simple calculations for our flat Universe consisting of different components labelled with the index i, namely radiation, matter and vacuum energy in the form of a cosmological constant (note that the value of the scale factor today is set to unity, $a_0 = 1$). The total energy density of the Universe can be expressed as

$$\rho = \sum_i \rho_i^{(0)} a^{-3(1+w_i)} = \sum_i \rho_i^{(0)} (1+z)^{3(1+w_i)}, \tag{1.32}$$

where from here onwards a superscript or subscript '0' will denote the value of a quantity at the present time. Consequently, the Hubble parameter can be written as

$$H^2 = H_0^2 \sum_i \Omega_i^{(0)} (1+z)^{3(1+w_i)}. \tag{1.33}$$

The age of the Universe is

$$t_0 = \int_0^{t_0} dt = \int_0^{\infty} \frac{dz}{H(1+z)}. \tag{1.34}$$

Today, the radiation term is of course negligible. Combining the above two equations we find

$$t_0 = \int_0^{\infty} \frac{dz}{H_0(1+z)\sqrt{\Omega_m^0 (1+z)^3 + \Omega_\Lambda^{(0)}}}. \tag{1.35}$$

Observations of our Universe find that it is composed of 4% baryonic matter (b), 23% (cold) dark matter (dm) and 73% dark energy [21]. With $\Omega_m^{(0)} = \Omega_b^{(0)} + \Omega_{dm}^{(0)} = 0.27$ and $\Omega_\Lambda^{(0)} = 0.73$ we find $t_0 \simeq 13.5$ Gyr for $H_0 = 74.2$ km s^{-1}Mpc^{-1} [17].

Another important property is the existence of a particle horizon, which determines the size of the observable Universe. More specifically, the particle horizon is defined as the maximum distance a particle could have travelled in the age of the Universe. Photons follow null radial geodesics, so the metric (1.1) gives

$$d_H(t) = a(t) \int_0^t \frac{dt'}{a(t')}. \tag{1.36}$$

For a flat universe, the horizon size is $d_H = 2t$ for radiation and $d_H = 3t$ for matter. Particles separated by a distance $> d_H$ are causally disconnected.

1.1.2 A brief history of the Universe

Following the history of our expanding Universe back in time, we necessarily reach a singularity at $a = 0$ — the Big Bang. There, the energy density approaches infinity and, of course, classical General Relativity breaks down and a quantum theory of gravity is needed. The Hot Big Bang model is the most successful description of our Universe *after* this initial singularity. The associated energy scale, which marks the era of our uncertainty, is known as the *Planck scale*. The corresponding Planck mass is $m_p \simeq 10^{19}$ GeV , the Planck length is $l_p \simeq 10^{-35}$ m , and the Planck time is $t_p \simeq 10^{-43}$ s .

As we saw in the previous subsection, the density of radiation scales as $\rho_r \propto a^{-4}$, faster than the one of non-relativistic matter that scales as $\rho_m \propto a^{-3}$. The present state of the Universe is dominated by a cosmological constant with a significant contribution from matter, while the radiation component is negligible. On the other hand, the very early Universe was radiation dominated. To see when radiation becomes important, we can define the matter/radiation equality time t_{eq} as a time for which

$$\rho_m(t_{eq}) = \rho_r(t_{eq}). \tag{1.37}$$

We then find

$$1 + z_{eq} = \frac{\Omega_m^{(0)}}{\Omega_r^{(0)}} \simeq 3200. \tag{1.38}$$

For $z > z_{eq}$, the Universe is radiation-dominated. We will later show that in the

radiation era we can write

$$\rho_r \propto T^4, \tag{1.39}$$

where T is the temperature. We thus find the important relation

$$T \propto \frac{1}{a}, \tag{1.40}$$

so that, moving back in time, the Universe gets hotter. The energy of particles also increases with increasing temperature. We can therefore deduce that, when the Universe was young, hot and dense, the various particle species were in relativistic motion and were interacting strongly with each other. The basic assumption following this reasoning is that the early universe was in *thermal equilibrium*, and we can use the relativistic perfect gas approximation[4].

The particles in thermal equilibrium are muons, neutrons, protons, electrons, neutrinos and their antiparticles, as well as photons. Fermions (+) are described using Fermi-Dirac distributions, while bosons (−) are described using Bose-Einstein distributions. Let us first define $n_A(P)$ to be the number density of species A in the momentum interval $(P, P + dP)$ and use $c = k_B = \hbar = 1$ units. We then have

$$n_A(P) = \frac{g_A}{2\pi^2} P^2 [e^{E_A(P)/T} \pm 1]^{-1}, \tag{1.41}$$

where $E_A^2 = m_A^2 + P^2$ is the energy of a particle of rest mass m_A and momentum P, while g_A is the number of spin states of the species (e.g., $g_A = 2$ for spin-$\frac{1}{2}$ fermions) and T is the temperature of the distribution. Then, the number density of a particle A can be written as

$$N_A = \frac{g_A}{2\pi^2} \int_0^\infty \frac{P^2 dP}{e^{E_A(P)/T} \pm 1}. \tag{1.42}$$

[4]Considering that the reaction rates change as the number density $n \propto a^{-3}$, while the expansion rate in radiation era scales as a^{-2}, thermal equilibrium should be a very good approximation at early times.

The energy density can be found by multiplying the above integrand by a factor $E_A(P)$. That is

$$\rho_A = \frac{g_A}{2\pi^2}\int_0^\infty \frac{P^2 E_A(P) dP}{e^{E_A(P)/T} \pm 1}. \tag{1.43}$$

For the pressure we have

$$p_A = \frac{g_A}{6\pi^2}\int_0^\infty \frac{P^4 E_A(P)^{-1} dP}{e^{E_A(P)/T} \pm 1}. \tag{1.44}$$

Finally, the entropy density s_A is given by

$$s_A = \frac{p_A + \rho_A}{T}. \tag{1.45}$$

We can immediately see that in the relativistic limit, where $E_A^2 \simeq P^2$, we have $p_A = \rho_A/3$. In the same limit, we find

$$N_A = b_N \left(\frac{g_A \zeta(3)}{\pi^2}\right) T^3 \times \begin{cases} b_N = 1 \text{ for bosons} \\ b_N = 3/4 \text{ for fermions} \end{cases} \tag{1.46}$$

$$\rho_A = b_\rho \left(\frac{g_A \pi^2}{30}\right) T^4 \times \begin{cases} b_\rho = 1 \text{ for bosons} \\ b_\rho = 7/8 \text{ for fermions.} \end{cases} \tag{1.47}$$

Here, $\zeta(3) \simeq 1.202$ is the Riemann zeta function. If $T \gg m$, the masses of the particles can be neglected, so they are essentially behaving like radiation. As we move backwards in time, the temperature is higher by the redshift factor $(1+z)$. This means that for every particle there is a redshift for which $T \sim m$. Before that, the particle behaves like radiation. Hence, we can calculate the total energy density for radiation domination by summing equation (1.47) for ρ over the different relativistic species A. We find

$$\rho_r = \frac{\pi^2}{30} f(T) T^4, \tag{1.48}$$

where we define the effective degrees of freedom $f(T)$ as

$$f(T) = \sum_{bosons} g_A \left(\frac{T_i}{T}\right)^4 + \frac{7}{8} \sum_{fermions} g_A \left(\frac{T_i}{T}\right)^4, \tag{1.49}$$

and $T = (1+z)T_0$ is the temperature of the photons.

For the opposite limit, namely when $m \gg T$, the motion of the particle is non-relativistic. Then, the number density is found to be exponentially suppressed by the Boltzmann factor

$$n_A \propto e^{-m_A/T}, \tag{1.50}$$

as is the energy density, pressure and entropy. Therefore, the dynamics are mainly determined by the particle species that are in relativistic motion. Heavy particles are much fewer in number and their pressure, entropy and energy density are becoming less important with the expansion and cooling of the Universe.

While in thermal equilibrium, we know that the entropy in a comoving volume is conserved. That is

$$\frac{d}{dt}(a^3 s) = 0 \tag{1.51}$$

and, since $s \propto T^3$, we recover equation (1.40) and the radiation era expansion law.

We have seen that the general behaviour of the various particle species depends on the temperature. Of course, massless particles (photons) will always be relativistic. However, the massive particles will be part of the thermal equilibrium as long as their interaction rate Γ is much larger than the rate of expansion H. When this is no longer true, the particles decouple from the thermal bath. At temperatures above $T \simeq 10^{12}\,\mathrm{K} \sim O(100)\,\mathrm{MeV}$ or $t \lesssim 10^{-4}$ sec, photons, muons, electrons, neutrinos (and their antiparticles) are in thermal equilibrium. Soon afterwards, the massive

muons are the first to annihilate. The thermal equilibrium now consists of highly relativistic particles with a temperature $T \propto a^{-1}$. Then, neutrinos begin to decouple. Neutrinos are special, because they are fermions with almost (but not quite) zero mass. Since they are electrically neutral, they interact very weakly, and they decouple from the rest at around 1MeV. At around $t \sim 100$ s and at temperatures of order 0.1 MeV , neutrons and protons are not anymore in thermal equilibrium, so they start producing light nuclei (e.g. deuterium, tritium, helium). This is the *Big Bang Nucleosynthesis* (BBN) era. The observed primordial abundances for the light elements are in remarkable agreement with the theoretical predictions based on the Hot Big Bang model (75% hydrogen, 25% helium and small traces of heavier elements) [22]. At $T \sim$ 1eV, the matter domination era begins (matter-radiation equality). At $t \sim 10^5$ yr, $T \sim 0.1$ eV we have H *recombination* through

$$e + p \rightarrow H + \gamma. \tag{1.52}$$

At redshift $z \simeq 1100$ the mean free path of the photon Γ_γ^{-1} becomes larger than H^{-1}, and photons decouple from matter and propagate freely ("last scattering"). This gas of decoupled photons is the famous Cosmic Microwave Background, a characteristic black-body spectrum of temperature $T = 2.725 \pm 0.001$ K (1σ) [23] which we observe today.

Between the Planck scale and $T \simeq 10^{12}$ K $\sim O(100)$ MeV lies the idea of *Grand Unification*. This idea was inspired by the phenomenal success of the electroweak theory, for which Glashow, Salam and Weinberg were awarded the Nobel Prize in Physics in 1979. This theory unifies two out of the four fundamental forces, the electromagnetic and the weak force, under an $SU(2) \times U(1)$ gauge group. At high energies, above a few hundred GeV, there is an underlying symmetry between the carriers of the two

forces, namely the photon and the W and Z bosons. When the electroweak symmetry becomes spontaneously broken, the W and Z particles acquire masses via the Higgs mechanism, while the photon remains massless. It is then natural to wonder whether the strong force, which is described by the eight-parameter quantum chromodynamics (QCD) SU(3) group, joins the other two at some higher energy scale. In fact, the coupling constants of the three forces, despite their name, depend on the energy, and one finds that they converge to the same value at about 10^{16} GeV. The Standard Model of particle physics combines the electroweak and QCD theories to a single Lagrangian with $SU(3) \times SU(2) \times U(1)$ symmetry. These scenarios gave birth to the so-called Grand Unified Theories (GUTs), which include one or more symmetry-breaking phase transitions from a group G down to the standard model group.

1.2 Topological Defects

Symmetry-breaking phase transitions in the early Universe are often accompanied by the formation of *topological defects* via the Kibble mechanism [24, 25]. Depending on what kind of symmetry is broken, we can have point defects (monopoles), linear defects (cosmic strings), planar defects (domain walls), textures, as well as their combinations (e.g. monopoles connected by strings) [5, 6].

To be more specific, let us consider a phase transition during which an initial symmetry group G is broken down to a subgroup H. The formation or not of topological defects, and their kind, depends on the vacuum manifold $\mathcal{M} = G/H$. As an example, consider the case where the homotopy group $\pi_0(\mathcal{M}) \neq 0$, i.e. $\mathcal{M}$ is not connected. Then, two-dimensional defects will form — domain walls. If $\pi_1(\mathcal{M}) \neq 0$, $\mathcal{M}$ contains

non shrinkable circles and line-like defects, cosmic strings, are formed. Monopoles form when $\pi_2(\mathcal{M}) \neq 0$ and textures when $\pi_3(\mathcal{M}) \neq 0$.

When the broken symmetry is a gauge symmetry, the emerging defects are called *local*, and their energy is strongly confined. *Global* defects are the result of a global symmetry breaking and have long range interactions. Depending on the energy scale of symmetry breaking, local monopoles and domain walls can have disastrous cosmological effects, since they might dominate the energy density of the Universe. Local textures are not cosmologically significant, as they decay quickly with time. Strings, on the other hand, are far more interesting, and they will be studied extensively throughout this thesis. Before starting our discussion of strings, we will talk a bit about inflation, which deals with a few of the problems of standard cosmology, including that of stable catastrophic defects.

1.3 Inflation

The Hot Big Bang model, despite its astonishing successes (e.g. the predictions for the light elements abundances from BBN, the CMB), comes with a few serious shortcomings.

The first is the so-called *flatness problem*. As we already stated, observations tell us that our Universe is spatially flat ($k = 0$), up to 1% [16]. This means that, today, the density parameter Ω is very close to unity. Combining equation (1.26) with the behaviour of the scale factor as a function of time $a \sim t^p$, with $p < 1$, we see that $(aH)^{-2}$ grows with time. Hence, Ω must have been extremely close to one at earlier times, requiring extremely finely tuned initial conditions (for example, $|\Omega - 1| \sim 10^{-16}$

at nucleosynthesis).

In addition, there is the *horizon problem.* The particle horizon at the time of last scattering corresponds to an angular radius of only 1 degree today. However, observations of the Cosmic Microwave Background Radiation show something completely different — the whole sky is smooth, to about ten parts in 10^4. This means that two photons coming from opposite directions on the sky have nearly the same temperature. How can this be explained, if they were not in causal contact at the time of last scattering?

Finally, GUTs predict the formation of massive stable magnetic monopoles. For example, a typical SU(5) GUT monopole has $m \sim 10^{16}$ GeV, hence its energy density scales as $a(t)^{-3}$. On the other hand, the energy density of relativistic fields scales as $a(t)^{-4}$, so monopoles would quickly come to dominate the energy density of the Universe. This is the *monopole problem.*

The inflationary scenario [26, 27, 28, 29, 30] provides a solution to these problems. It is defined as a period of accelerated expansion. That is

$$\ddot{a} > 0. \tag{1.53}$$

From equation (1.21), we see that this means $\rho + 3p < 0$. Also,

$$\frac{d}{dt}(aH)^{-1} < 0. \tag{1.54}$$

The last equation tells us that, during inflation, the comoving Hubble radius decreases with time.

Let us assume an equation of state $p = -\rho$ during inflation, and revisit the flatness

problem. The scale factor evolves as

$$a(t) = e^{Ht}. \tag{1.55}$$

Substituting in equation (1.26), we find $\Omega - 1 \sim e^{-2Ht}$. Thus, any initial curvature will be decreased, and the value $\Omega = 1$ becomes an *attractor*. A similar reasoning solves the horizon problem, since the present observable Universe can originate from a very small causally connected region inside the Hubble radius at the start of inflation, so that photons coming from opposite directions from the sky can actually have the same temperature. The solution of the monopole problem is obvious, as the exponential expansion of space dilutes these defects and they cannot be observed today. Note that, in order for this mechanism to work, the monopoles have to be produced before inflation.

Inflation Dynamics

We saw earlier that, in order to have a period of inflation, we need an equation of state which violates the strong energy condition. To get a system with $p = -\rho$, we introduce scalar fields. Consider a spatially homogeneous scalar field (the so-called *inflaton* field) with potential energy $V(\phi)$. The corresponding Lagrangian is

$$L = \frac{1}{2}(\partial_\mu \phi)(\partial^\mu \phi) - V(\phi). \tag{1.56}$$

The stress-energy tensor is

$$T_{\mu\nu} = (\partial_\mu \phi)(\partial_\nu \phi) - L g_{\mu\nu} \tag{1.57}$$

and, considering an isotropic fluid, we find that the energy density ρ and pressure p are given by

$$\rho = \frac{1}{2}\dot{\phi}^2 + V(\phi) \tag{1.58}$$

$$p = \frac{1}{2}\dot{\phi}^2 - V(\phi). \tag{1.59}$$

From the above equations we can immediately see that, provided $\dot{\phi}^2 \ll V$, we have $p = -\rho$ and the inflaton can successfully drive inflation. Substituting (1.58) and (1.59) into the Friedmann and continuity equations for $k = 0$, we get

$$H^2 = \frac{8\pi G}{3}\left[V(\phi) + \frac{1}{2}\dot{\phi}^2\right], \tag{1.60}$$

$$\ddot{\phi} + 3H\dot{\phi} = -\frac{d}{d\phi}V(\phi) \equiv -V'(\phi). \tag{1.61}$$

Now, in order for inflation to take place, the potential term needs to dominate. This corresponds to a quite flat potential, and using the "slow-roll approximation" we have $\dot{\phi}^2 \ll V$ and $\ddot{\phi} \ll 3H\dot{\phi}$. This gives

$$H^2 \simeq \frac{8\pi G}{3}V(\phi), \tag{1.62}$$

$$3H\dot{\phi} \simeq -V'(\phi). \tag{1.63}$$

The conditions for the slow-roll approximation to hold are that the slow-roll parameters

$$\epsilon \equiv \frac{1}{16\pi G}\left(\frac{V'}{V}\right)^2 \; ; \; \eta \equiv \frac{1}{8\pi G}\frac{V''}{V} \tag{1.64}$$

are very small: $\epsilon, \eta \ll 1$.

Another important quantity is the amount of inflation, defined in terms of the e-foldings number N between some initial time t and the time at the end of inflation t_f.

We define

$$N \equiv \ln \frac{a(t_f)}{a(t)}. \tag{1.65}$$

Inflation ends as the potential steepens with the scalar field oscillating around the minimum. The inflaton's potential energy is transferred to radiation and the Universe is thermalized — this is the *reheating* epoch and it is essential in order to recover the standard Big Bang evolution. The decay of the inflaton field was originally described perturbatively [31], but later a non-perturbative stage, *preheating*, was suggested [32, 33]. A new mechanism that produces cosmic strings after preheating was investigated in [34].

To conclude, we should note that inflation is not only successful in solving the problems of the standard cosmological model, but it also provides an explanation for the origin of the primordial density fluctuations responsible for the observed structure in the Universe and the CMB anisotropy. We will return to this subject in Chapter 4.

1.4 Cosmic Strings

Cosmic strings are linear topological defects that may have been formed as a result of spontaneous symmetry breaking transitions in the early Universe, as originally demonstrated by Kibble [24, 25].

A simple and illustrative model to study the formation of cosmic strings is the Abelian U(1) gauge model. The Lagrangian density is

$$\mathcal{L} = D_\mu \phi (D^\mu \phi)^* - \frac{1}{4} F_{\mu\nu} F^{\mu\nu} - V(\phi), \tag{1.66}$$

where $\phi(x) = \phi_1 + i\phi_2$ is the complex scalar field expressed in terms of two real fields

ϕ_1 and ϕ_2, $D_\mu = \partial_\mu + ieA_\mu$ is the covariant derivative, $F_{\mu\nu} = \partial_\mu A_\nu - \partial_\nu A_\mu$ is the electromagnetic field and the potential $V(\phi)$ can be written as

$$V(\phi) = \frac{1}{4}\lambda(\phi^*\phi - \eta^2)^2 = \frac{1}{4}\lambda(\phi_1^2 + \phi_2^2 - \eta^2)^2;\ \lambda, \eta = \text{const} > 0. \tag{1.67}$$

The Lagrangian has a local U(1) gauge symmetry, i.e. it is invariant under the transformations

$$\phi(x) \to e^{i\alpha(x)}\phi(x) \text{ and } A_\mu(x) \to A_\mu(x) - \frac{1}{e}\partial_\mu\alpha(x). \tag{1.68}$$

As illustrated in Fig. 1.1 (left), the potential (1.67) has a circle of minima $|\phi| = \eta$, while the ground state has a non-zero expectation value

$$\langle 0|\phi|0\rangle = \eta e^{i\alpha}, \tag{1.69}$$

where α is an arbitrary phase angle. This means that the ground state is not invariant under the U(1) phase transformations: The U(1) gauge symmetry is spontaneously broken.

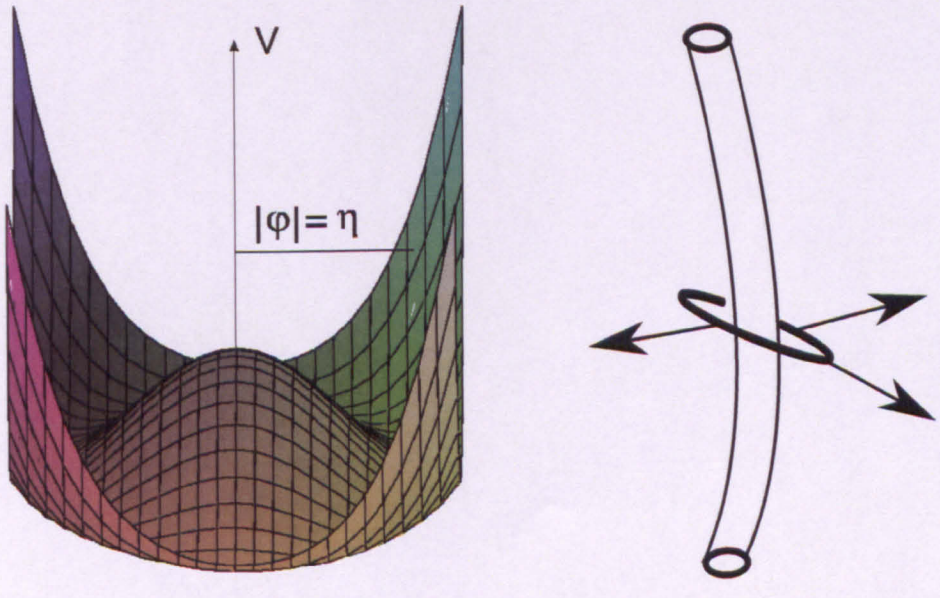

Figure 1.1: *Left:* The potential V has a degenerate ground state where $|\phi| = \eta$, and a central hump. *Right:* A closed loop around a cosmic string — the arrows indicate the different phases α.

However, there exists a ground state where the U(1) symmetry is intact. It is the state where $\langle 0|\phi|0\rangle = 0$, corresponding to the maximum of the potential. This state is unstable. To illustrate this, let us imagine a field at the very early stages of the Universe, where the temperature T is high. There will be large fluctuations in ϕ, so the central hump is unimportant. However, when the Universe cools down the field has to choose a ground state in the valley of minima, as its energy becomes too low to overcome the hump. The symmetry is spontaneously broken and we get two massive particles — the Higgs boson with mass $m_s = \sqrt{\lambda}\eta$ and the gauge (vector) boson with mass $m_v = \sqrt{2}e\eta$.

The choice of vacuum is in principle random, and fields in different patches of the Universe will choose different values of α. Now, imagine a closed loop with α changing from 0 to 2π (Fig. 1.1, right). Then, somewhere in that loop ϕ must rise to the top of the potential lump where it vanishes. As a result, a linear defect will form — a cosmic string. Imagining this process repeating in different regions of the Universe, we can deduce that a random network of cosmic strings will appear.

A string solution to the Abelian-Higgs model was found by Nielsen and Olesen [35]. In cylindrical coordinates ρ, θ, z, and at large distances from the core, the Higgs field has the form

$$\phi \approx \eta e^{in\theta}, \tag{1.70}$$

where n is an integer, the winding number of the string. The gauge field asymptotically becomes

$$A_\mu \approx \frac{1}{ie}\partial_\mu \ln\phi, \tag{1.71}$$

which translates to $A_t = A_\rho = A_z = 0$, $A_\theta = n/e\rho$, as $\rho \to \infty$. Using Stoke's theorem

to integrate around a closed curve enclosing the string, we find a total magnetic flux

$$\Phi_B = \int \mathbf{B} \cdot \mathbf{dS} = \oint \mathbf{A} \cdot \mathbf{dl} = \frac{2\pi n}{e}, \tag{1.72}$$

where $\mathbf{B} = \nabla \times \mathbf{A}$ is the magnetic gauge field. The string carries n quanta of magnetic flux. Note that, far away from the string core, we have $D_\mu \phi \approx 0$ and $F_{\mu\nu} \approx 0$, so the string energy vanishes rapidly away from the core. The radius (width) of the string core is determined by the Compton wavelengths of the Higgs and gauge bosons, $\delta_\phi \propto m_s^{-1}$ and $\delta_v \propto m_v^{-1}$. The total string mass per unit length is

$$\mu \sim \eta^2, \tag{1.73}$$

which gives $\mu \sim 10^{22}$ g cm^{-1} for GUT scale strings.

Note that, in the case where the string's length is much larger than its width, the internal structure of the string is unimportant. The effective energy momentum tensor for a straight string along the z-axis is [36]

$$T^\mu_\nu = \mu\delta(x)\delta(y)\text{diag}(1,0,0,1). \tag{1.74}$$

The string has a large tension equal to the energy density. This implies that curved strings will contract and acquire relativistic velocities.

To conclude, let us return to inflation and the monopole problem. As we already stated, all defects produced before inflation would be diluted to a non-observable level. This means that also cosmic strings will be diluted! Actually, this is not quite true. Early on, it was realised that strings can be formed at the end or near the end of inflation [37, 38, 39]. More recently, it was found that cosmic string formation is generic within supersymmetric grand unified theories (SUSY GUTs) [40, 41]. Another exciting possibility arises in string-theory inspired models of brane inflation. As an example, the popular $D3-\overline{D3}$ inflation model terminates with the collision and annihilation

of a $D3$ and a $\overline{D3}$ brane and the subsequent formation of strings (see, for example, [42, 43, 44, 45, 46]). Another brane inflation model is $D3/D7$, which can end with the formation of semilocal strings (see, for example, [47, 48] and references therein). We will not discuss the details of these models here, as we will refer to them in more detail later in the thesis. The basic idea is that cosmic strings can survive and be observable. The question that immediately arises is how they evolve and what are their cosmological implications. Especially when it comes to cosmic superstrings, one will surely wonder if it is possible to distinguish them from their field-theory analogues, and whether their cosmological consequences can open an observational window to string theory.

Chapter 2

Cosmic String Dynamics

2.1 Introduction

In the previous chapter we described the formation of cosmic strings in the early universe after the spontaneous breaking of a U(1) gauge symmetry. Cosmic strings are linear concentrations of energy which stretch across the universe. They can also form closed loops. Even though they are very thin, they have a huge tension that can trigger observable cosmological effects. In order to quantify these effects, we need to study the dynamics of strings and understand the evolution of a cosmic string network throughout the history of the universe.

In this chapter, we will review some important aspects of cosmic string dynamics (see [5],[6],[49]). We start by deriving the equations of motion for a cosmic string using the Nambu-Goto approach. We solve these equations in Minkowski and FLRW spacetime, and discuss some specific solutions. We then describe the basic features of network evolution, and present the famous 'one-scale model' and its extensions.

We also introduce cosmic superstrings, which are objects analogous to cosmic strings arising in string theory, and in particular in models of brane inflation (see [7, 8, 50]). These objects possess some distinctive features, which can be used in order to distinguish them from the usual, Abelian Higgs cosmic strings. The most striking of these is the ability to form bound states, which results in a configuration with junctions where three strings meet. We present some basic elements of the theory of cosmic strings with junctions, focusing on the Nambu-Goto approach developed by Copeland, Kibble and Steer [51, 52]. We conclude with the study of junctions in an expanding spacetime — an exact solution for a three string loop in a de Sitter universe is derived.

2.2 The Nambu-Goto action

Let us consider a cosmic string moving in a $(3+1)$ dimensional spacetime. When its thickness is much smaller than its radius of curvature, we can effectively treat it as a one-dimensional object. As the string is moving, it spans a two-dimensional surface, the so-called "string worldsheet"

$$x^\mu = x^\mu(\sigma^a),\ a = 0, 1. \tag{2.1}$$

Then, its motion can be described by the Nambu-Goto action, which is proportional to the area swept out by the string. That is [55, 56]

$$S = -\mu \int \sqrt{-\gamma} d^2\sigma, \tag{2.2}$$

where μ is the string's tension, $\gamma_{ab} = g_{\mu\nu}\partial_a x^\mu \partial_b x^\nu$ is the induced metric on the world-sheet with determinant γ, and $g_{\mu\nu}$ is the metric of the background spacetime. The

Nambu-Goto action is invariant under general coordinate transformations, as well as under worldsheet parametrizations $\sigma^a \rightarrow \tilde{\sigma}^a(\sigma^b)$.

Varying equation (2.2) with respect to $x^\mu(\sigma^a)$ we get the equations of motion

$$\nabla^2 x^\mu + \Gamma^\mu_{\nu\rho}\gamma^{ab}\partial_a x^\nu \partial_b x^\rho = 0, \tag{2.3}$$

where

$$\Gamma^\mu_{\nu\rho} = \frac{1}{2}g^{\mu\lambda}(\partial_\rho g_{\lambda\nu} + \partial_\nu g_{\lambda\rho} - \partial_\lambda g_{\nu\rho}) \tag{2.4}$$

is the four-dimensional Christoffel symbol and the covariant Laplacian $\nabla^2 x^\mu$ is given by

$$\nabla^2 x^\mu = \frac{1}{\sqrt{-\gamma}}\partial_a(\sqrt{-\gamma}\gamma^{ab}\partial_b x^\mu). \tag{2.5}$$

Varying the Nambu-Goto action with respect to the background metric $g_{\mu\nu}$, we find that the string energy-momentum tensor $T^{\mu\nu}(x)$ is given by

$$T^{\mu\nu}(x) = \frac{1}{\sqrt{-g}}\mu \int d^2\sigma \sqrt{-\gamma}\gamma^{ab}\partial_a x^\mu \partial_b x^\nu \delta^{(4)}(x^\lambda - x^\lambda(\sigma^a)). \tag{2.6}$$

2.3 String evolution

2.3.1 Minkowski spacetime

In flat (Minkowski) spacetime, the background metric $g_{\mu\nu}$ becomes $g_{\mu\nu} = \eta_{\mu\nu} = \mathrm{diag}(1,-1,-1,-1)$, which gives $\Gamma^\mu_{\nu\rho} = 0$. The string equations of motion (2.3) are then written as

$$\partial_a(\sqrt{-\gamma}\gamma^{ab}\partial_b x^\mu) = 0. \tag{2.7}$$

Since the action (2.2) is worldsheet reparametrization invariant, we can choose a gauge. A very useful choice is to fix $\gamma_{01} = 0$ and $\gamma_{00} + \gamma_{11} = 0$. This gives

$$\dot{x}^\mu x'_\mu = 0;\ \dot{x}^\mu \dot{x}_\mu + x'^\mu x'_\mu = 0, \tag{2.8}$$

where dots and primes denote derivatives with respect to σ^0 and σ^1, respectively. This is called the conformal gauge.

Using the conformal gauge, the equation of motion (2.7) becomes

$$\ddot{x}^\mu - x''^\mu = 0, \tag{2.9}$$

which is the well known wave equation. Furthermore, we can use the remaining gauge freedom to set the timelike worldsheet coordinate σ^0 equal to the Minkowksi time t. Thus, we have

$$t = x^0 = \sigma^0. \tag{2.10}$$

Then, we can immediately write the corresponding equations for the string's trajectory using the three-vector $\mathbf{x}(\sigma, t)$, where $\sigma = \sigma^1$ is the spacelike worldsheet coordinate. Equations (2.8) can be written as

$$\dot{\mathbf{x}} \cdot \mathbf{x}' = 0, \tag{2.11}$$

$$\dot{\mathbf{x}}^2 + \mathbf{x}'^2 = 1, \tag{2.12}$$

$$\ddot{\mathbf{x}} - \mathbf{x}'' = 0. \tag{2.13}$$

The first equation tells us that the velocity of the string is perpendicular to its tangent - that is, $\dot{\mathbf{x}}$ is the physical velocity. In our chosen gauge, the string energy-momentum tensor can be written as

$$T^{\mu\nu}(\mathbf{x}, t) = \mu \int d\sigma (\dot{x}^\mu \dot{x}^\nu - x'^\mu x'^\nu) \delta^{(3)}(\mathbf{x} - \mathbf{x}(\sigma, t)). \tag{2.14}$$

Using this expression and equation (2.12), we find

$$E = \int T_0^0 d^3x = \mu \int d\sigma, \tag{2.15}$$

so that the spacelike coordinate σ is proportional to the energy of the string.

The wave equation (2.13) has an elegant solution in terms of right and left movers. That is

$$\mathbf{x}(\sigma, t) = \frac{1}{2}[\mathbf{a}(\sigma + t) + \mathbf{b}(\sigma - t)]. \tag{2.16}$$

The right and left movers satisfy the constraints

$$\mathbf{a}'^2 = \mathbf{b}'^2 = 1, \tag{2.17}$$

with $\mathbf{b}' = \mathbf{x}' - \dot{\mathbf{x}}$ and $\mathbf{a}' = \mathbf{x}' + \dot{\mathbf{x}}$ (note that, when applied to $\mathbf{b}(\sigma - t)$ and $\mathbf{a}(\sigma + t)$, primes denote derivatives with respect to $(\sigma - t)$ and $(\sigma + t)$, respectively). These functions live on a sphere with unit radius, known as the Kibble-Turok sphere [57]. It is important to note that, although the right and left movers have to obey the above constraints, they are otherwise arbitrary shaped waves which travel along the string with the velocity of light.

Let us now consider what happens when the string forms a closed loop. If the loop has length L (with $0 \leq \sigma < L$), the requirement of spatial periodicity gives

$$\mathbf{x}(\sigma, t) = \mathbf{x}(\sigma + L, t). \tag{2.18}$$

In the centre-of-mass frame the right and left movers are also spatially periodic, that is

$$\mathbf{a}(\sigma, t) = \mathbf{a}(\sigma + L, t); \ \mathbf{b}(\sigma, t) = \mathbf{b}(\sigma + L, t).$$

As for the time periodicity, it is clear that the loop has to be periodic in time with the same period L. In fact, the actual period is $T = L/2$ [57], as we can easily check that

$$\mathbf{x}(\sigma + L/2, t + L/2) = \mathbf{x}(\sigma + L, t). \tag{2.19}$$

This equation tells us that the two halves of the loop are interchanged every $T = L/2$.

The properties of the closed loop solutions give rise to a set of very special points on the string. In particular, there are points on the string that can reach the velocity of light for an instant during the loop's motion [58]. As we mentioned before, the functions $\mathbf{a}'$ and $\mathbf{b}'$ live on the surface of the unit sphere. Considering a closed loop in its center-of-mass frame, we have

$$\int_0^L \mathbf{x}' d\sigma = \int_0^L (\mathbf{a}' + \mathbf{b}') d\sigma = 0; \quad \int_0^L \dot{\mathbf{x}} d\sigma = \int_0^L (\mathbf{a}' - \mathbf{b}') d\sigma = 0.$$

Thus

$$\int_0^L \mathbf{b}' d\sigma = -\int_0^L \mathbf{a}' d\sigma = 0, \tag{2.20}$$

which means that the functions $\mathbf{b}'$ and $-\mathbf{a}'$ trace closed curves on the unit sphere centered on the origin, as σ runs from 0 to L. Therefore, they cannot lie only in one hemisphere of the unit sphere, hence they will generally intersect. In that case, we will have $\mathbf{b}' = -\mathbf{a}'$[1] and the tangent vector $\mathbf{x}'$ vanishes. The loop's velocity squared is

$$\dot{\mathbf{x}}^2(\sigma, t) = \frac{1}{4}[\mathbf{a}'(\sigma + t) - \mathbf{b}'(\sigma - t)]^2, \tag{2.21}$$

which gives $\dot{\mathbf{x}}^2 = 1$. These points are called *cusps*.

There can be also sharp corners on the loop, where the functions $\mathbf{a}'$ and $\mathbf{b}'$ are discontinuous [59]. These points are called *kinks*, and they appear after every string intercommutation. They then travel along the string and away from each other at luminal speed. This leads to the build-up of additional small-scale structure ('wiggliness') on the strings. We will return to the rôle of small-scale structure in Sec. 2.4.

[1] Note that this condition is only a matter of convention — if we define $\mathbf{b} = \mathbf{b}(t-\sigma)$ and $\mathbf{a} = \mathbf{a}(t+\sigma)$, the same discussion holds for $\mathbf{b}' = \mathbf{a}'$.

Another property of loops in Minkowski spacetime is that their mean square velocity is [5]

$$\langle v^2 \rangle = \int_0^T \frac{dt}{T} \int_0^L \frac{d\sigma}{L} \dot{\mathbf{x}}^2 = \frac{1}{2}. \tag{2.22}$$

2.3.2 Loop solutions

We will now present a few representative exact solutions for closed loops in Minkowski spacetime. We will start with a description of the main features of the circular loop, which will be useful in Chapter 3. Then, we will briefly discuss some well-known families of loop solutions.

The simplest loop solution is the initially static planar circular loop. Letting $L = 2\pi$, we can write

$$\mathbf{x} = \cos t(\cos \sigma, \sin \sigma, 0). \tag{2.23}$$

In Fig. 2.1 we illustrate the evolution of the circular loop. As we can see, the loop collapses to a point at $t = \pi/2$ and then re-expands[2]. We can easily check that, at the collapse time $t = \pi/2$, the whole loop takes the form of a *cusp*.

In 1982 Kibble and Turok [57], motivated by the possibility that cosmic strings are responsible for the density perturbations needed for galaxy formation showed that any initially static loop of string collapses after half a period of oscillation. However, they discovered that if one perturbs slightly the collapsing solutions, one can get a class of non-intersecting loops, which can have sufficiently long lifetimes. Letting $L = 2\pi$ (and $u = \sigma + t, v = \sigma - t$), the Kibble-Turok family of loop solutions can be written

[2]This picture is not quite realistic. As Hawking showed [60], a circular loop will eventually form a black hole after radiating away at most 29% of its energy.

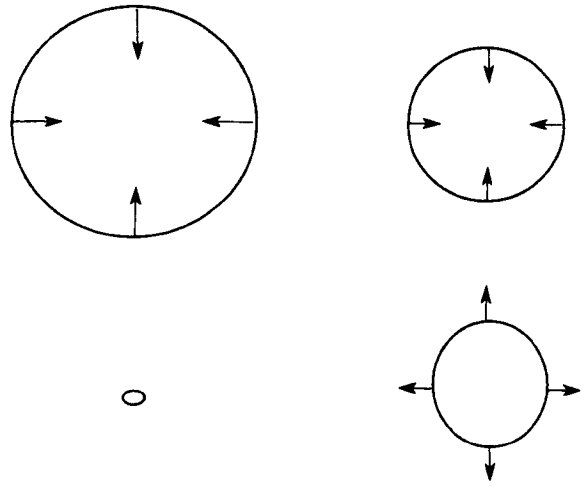

Figure 2.1: The evolution of the initially static circular loop. It collapses to a point at $t = \pi/2$, and then starts re-expanding. The arrows show the direction of the velocity.

as

$$\mathbf{x}(\sigma,t) = \frac{1}{2}\mathbf{e}_1[(1-\alpha)\sin v + \frac{1}{3}\alpha\sin 3v + \sin u] \tag{2.24}$$
$$-\frac{1}{2}\mathbf{e}_2[(1-\alpha)\cos v + \frac{1}{3}\alpha\cos 3v + \cos u]$$
$$-\mathbf{e}_3[\alpha(1-\alpha)]^{1/2}\cos v.$$

They found that these strings do not intersect themselves for $0 < \alpha < 1$, i.e. there is no trivial solution of the equation $\mathbf{x}(\sigma,t) = \mathbf{x}(\sigma',t)$ for this parameter range.

In 1985, Burden [61] extended the previous work of Kibble and Turok and presented a broad class of loop solutions. Using our previous conventions, they can be written as

$$\mathbf{x}(\sigma,t) = \frac{1}{2}[M^{-1}\cos(Mv)\hat{\mathbf{e}}_3 + M^{-1}\sin(Mv)\hat{\mathbf{e}}_1 \tag{2.25}$$
$$+N^{-1}\cos(Nu)\hat{\mathbf{e}}_3 + N^{-1}\sin(Nu)$$
$$(\cos\psi\hat{\mathbf{e}}_1 + \sin\psi\hat{\mathbf{e}}_2)],$$

with M and N relatively prime. If either $M = 1$, $N \neq 1$ (or *vice versa*), the loop does not self-intersect.

As we already stated, a generic feature of *smooth* loops is the presence of cusps [58]. Garfinkle and Vachaspati [59] constructed a class of cuspless kinked loops by

connecting straight segments to form a rectangle. Of course, kinks are formed naturally when loops self-intersect. In addition, kinks can prevent the formation of cusps, as they correspond to discontinuities on the Kibble-Turok sphere. Cusps and kinks are very important for the gravitational radiation signature of cosmic (super)strings. Unfortunately, important questions such as how many cusps are found per oscillation and what is the percentage of non-self-intersecting loops in a network are still unanswered. In Chapter 4, we will present calculations of radiated power from closed loops. We will also discuss gravitational wave bursts from cusps and kinks in a cosmic string network.

2.3.3 FLRW spacetime

After studying the string's equation of motion in flat spacetime, we will now briefly discuss what happens when we consider a background similar to the one of the observable universe [5]. In an FLRW spacetime, the line element can be written as

$$ds^2 = a(\tau)^2(d\tau^2 - d\mathbf{x}^2), \tag{2.26}$$

where $d\mathbf{x}^2$ is the line element on a flat 3D space, $a(\tau)$ is the scale factor, and the conformal time τ is related to the physical time t via $dt = ad\tau$. For fixing the gauge, we can again identify $\sigma^0 = \tau$ but we can only keep the transverse gauge condition $\dot{\mathbf{x}} \cdot \mathbf{x}' = 0$. The string equations of motion are [62]

$$\ddot{\mathbf{x}} + 2H(1 - \dot{\mathbf{x}}^2)\dot{\mathbf{x}} = \frac{1}{\epsilon}\left(\frac{\mathbf{x}'}{\epsilon}\right)', \ \dot{\epsilon} + 2H\epsilon\dot{\mathbf{x}}^2 = 0 \tag{2.27}$$

where $H = \dot{a}/a$, $\epsilon^2 = \mathbf{x}'^2/(1 - \dot{\mathbf{x}}^2)$, while dots and primes denote derivatives with respect to τ and σ, respectively. As we can see, the expansion of the universe has a

damping (friction) effect on the string's motion. After a little algebra, we calculate the energy of the string as

$$E = \mu a(\tau) \int \epsilon d\sigma. \tag{2.28}$$

Note that ϵ is equal to unity for a Minkowski spacetime.

The trivial solution of equation (2.27) is a straight static string

$$\mathbf{x}(\sigma) = \mathbf{A}\sigma; \ \mathbf{A} = \text{const.}, \tag{2.29}$$

which just gets stretched by the expansion. Considering *perturbations* on a straight static string [63]

$$\mathbf{x}(\sigma) = \mathbf{c}\sigma + \delta\mathbf{x}(\tau, \sigma), \tag{2.30}$$

and taking $a(\tau) = \tau^{\alpha}$, the linearised (in $\delta\mathbf{x}$) equations of motion (2.27) give

$$\delta\ddot{\mathbf{x}} + \frac{2\alpha}{\tau}\delta\dot{\mathbf{x}} - \delta\mathbf{x}'' = 0, \tag{2.31}$$

$$\mathbf{c} \cdot \delta\dot{\mathbf{x}} = 0. \tag{2.32}$$

The solution of (2.31) is a superposition of waves with mode frequency k. That is

$$\delta\mathbf{x}(\tau, \sigma) = \mathbf{A}\tau^{-\nu} J_{\nu}(k\tau) e^{ik\sigma}, \tag{2.33}$$

where J_{ν} is the Bessel function of the first kind, $\mathbf{A} \cdot \mathbf{c} = 0$ and $\nu = \alpha - 1/2$.

Since we are working with comoving coordinates, the physical wavelength of the perturbations is

$$\lambda = a(\tau)\frac{2\pi}{k}. \tag{2.34}$$

Therefore, the quantity $k\tau \sim t/\lambda$ represents the ratio of the horizon size to the wavelength (size) of the mode.

We can now investigate the two extreme cases. When $k\tau \ll 1$, i.e. when the wavelength of the mode is much larger than the horizon size, we find that

$$\delta\mathbf{x} \approx \mathbf{A}\left(\frac{k}{2}\right)^{\nu} \frac{e^{ik\sigma}}{\Gamma(\nu+1)}, \tag{2.35}$$

which tells us that the comoving amplitude is constant in time. This means that both the physical wavelength and the amplitude of the perturbations are proportional to the scale factor. The string is conformally stretched, while its shape remains the same. When $k\tau \gg 1$, i.e. when the mode is well inside the horizon, we find

$$\delta\mathbf{x} \approx \mathbf{A}\tau^{-\alpha}\sqrt{\frac{2}{\pi k}}\cos(k\tau - \alpha\pi/2)e^{ik\sigma}. \tag{2.36}$$

This means that, while the wavelength grows with the scale factor, the physical amplitude $a(\tau)\delta\mathbf{x}$ stays constant. The mode straightens.

The aforementioned results can in fact be applied to the case of strongly curved strings [63, 64] hence they are important for the treatment of loops. When a loop is outside the horizon, it is conformally stretched. While it enters the horizon, its radius progressively decreases and its shape is smoothed out. Finally, when the loop becomes much smaller than the horizon, the effects of expansion become insignificant and it starts oscillating freely — effectively, small loops in the universe behave as they would in flat spacetime.

2.4 Network evolution

As we stated in Chapter 1, strings are formed after a symmetry breaking phase transition in the early universe. Simulations have shown that the formed string network consists of a random (Brownian) tangle of infinite straight strings and closed loops

[65, 66, 67]. In this section, we will discuss the basic properties of the evolution of a cosmic string network (see [5],[6]).

Immediately after the network is formed, the string's evolution is determined primarily by damping effects due to the high radiation backreaction density. However, strings will eventually begin to oscillate freely. We then have to take into account two competing effects. The expansion of the universe, which stretches the strings, and the energy loss through string interactions and self-intersections.

In order to understand the effect of string interactions, we need field theory simulations. That is because the Nambu-Goto approach is only accurate as long as the strings under consideration do not intersect with themselves or with each other. When two Abelian-Higgs cosmic string segments meet, there are two possible outcomes: the strings just pass through one another, or they *intercommute* (exchange partners and reconnect). Abelian-Higgs simulations have shown that strings prefer intercommuting (Fig. 2.2), with a probability $\mathcal{P}$ almost equal to unity [68, 69]. An exception seems to be possible when the relative velocity of the strings approaches the speed of light [70].

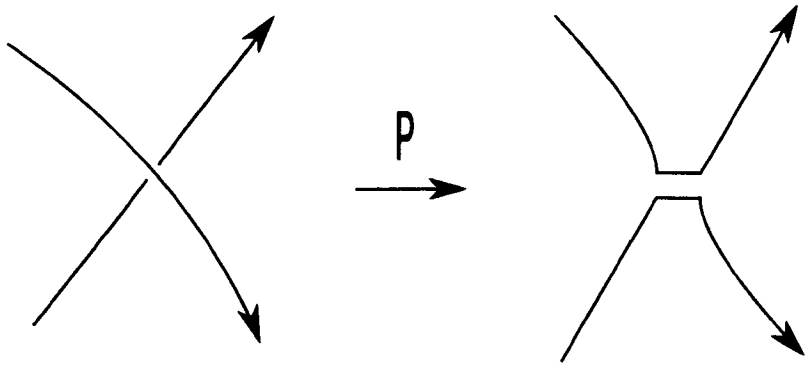

Figure 2.2: String Reconnection.

If long strings are meeting at two points, or if they self-intersect, they can form closed loops (Fig. 2.3). These loops will eventually radiate their energy, hence they are

an important energy loss mechanism for the network.

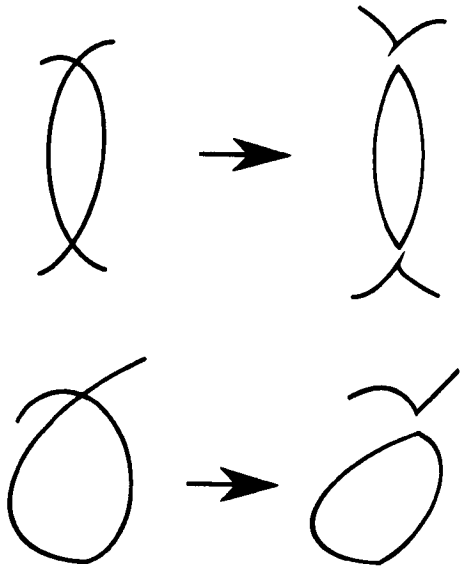

Figure 2.3: Loop formation mechanisms: *Upper*: Two strings meet at two points *Lower*: Self-intersection.

The so-called 'one-scale model' assumes that the string network can be characterised by a single length scale, namely the correlation length L defined by

$$\rho = \frac{\mu}{L^2}\,, \tag{2.37}$$

where ρ is the energy density in the long string network and μ is the string tension. In other words, we expect (on average) one string segment with length L in any volume L^3.

In principle, there are at least two different fundamental length scales in the network — the typical "smoothness" length L of long strings, and the average distance between strings $\bar{L}$. The one-scale model takes the two lengths to be equal (L=$\bar{L}$), an approximation which appears to be reasonably well satisfied [71] for a network of NG strings of tension μ with intercommutation probability $\mathcal{P} = 1$.

The energy loss rate can be approximated by [72]

$$\dot{\rho} \approx -2\frac{\dot{a}}{a}\rho - \frac{\rho}{L}, \tag{2.38}$$

where $\cdot = d/dt$ and $a(t)$ is the scale factor. The first term accounts for the expansion of the universe, and the second for string interactions with associated loop-formation. The network evolves towards a scaling regime, in which L is constant relative to the horizon $d_H \sim t$ [72]. Indeed, setting $L(t) = \xi(t)t$, it follows from equation (2.38) that

$$\frac{\dot{\xi}}{\xi} = \frac{1}{2t}\left(2(\beta - 1) + \frac{1}{\xi}\right), \tag{2.39}$$

where $a(t) \sim t^{\beta}$ ($\beta = 1/2$ in a radiation era, $\beta = 2/3$ in a matter era). The attractor scaling solution of equation (2.39) is

$$\xi = [2(1 - \beta)]^{-1}. \tag{2.40}$$

This scaling solution is independent of the initial conditions — if the initial network is very dense, there will be sufficient intercommuting producing loops which will radiate their energy away. On the other hand, if the initial density is small, intercommuting will be rare. Both of the initial states will eventually reach the scaling regime. Numerical simulations have confirmed the scaling behaviour of cosmic string networks (for example, see [73], [74] and [75]).

As an aside, it is worth noting that, if the energy loss due to loop formation was absent, the strings would soon dominate the energy density of the universe. Assuming Hubble expansion only, we have

$$\rho_{str} \propto a(t)^{-2}, \tag{2.41}$$

while $\rho_{mat} \propto a(t)^{-3}$ and $\rho_{rad} \propto a(t)^{-4}$.

Early numerical simulations also revealed the presence of small scale structure on long strings [75, 76], and more complicated analytic modelling was performed in order to incorporate its possible influence on the network's dynamics. Austin, Copeland

and Kibble developed a 'three-scale' model, keeping L and $\bar{L}$ separate and including an additional length scale ζ to account for the structure in the smallest scales [71]. Allen and Caldwell [77], as well as Austin [78], developed "kink-counting" models to describe small-scale structure.

In the following, we will concentrate on the "Velocity-dependent One-Scale" (VOS) model, developed by Martins and Shellard [79, 80]. VOS calculates the macroscopic quantitative properties of a string network, it is simpler than the other analytic models and has been successfully tested against both field theory and Nambu-Goto numerical simulations [81]. It introduces a dynamical velocity component v to the equations, describing the root mean square (rms) velocity of string segments

$$v^2 = \frac{\int \dot{\mathbf{x}}^2 \epsilon d\sigma}{\int \epsilon d\sigma}. \tag{2.42}$$

Let us start by the equation

$$E(\tau) = a(\tau)\mu \int \epsilon d\sigma. \tag{2.43}$$

Differentiating with respect to conformal time and using $\dot{\epsilon} = -2\frac{\dot{a}}{a}\dot{\mathbf{x}}^2\epsilon$ we find

$$\dot{E} = \frac{\dot{a}}{a}(1 - 2v^2)E. \tag{2.44}$$

Consequently, for the energy density $\rho \propto E/a^3$ we have

$$\frac{\dot{\rho}}{\rho} = -2\frac{\dot{a}}{a}(1 + v^2). \tag{2.45}$$

To this, we add a phenomenological term which describes loop production:

$$\frac{\dot{\rho}}{\rho} = -2\frac{\dot{a}}{a}(1 + v^2) - \tilde{c}\frac{v\rho}{L}. \tag{2.46}$$

Here, $\tilde{c}$ represents the efficiency of loop formation. The equation for the velocity is found to be

$$\dot{v} = (1 - v^2)\left(\frac{k}{L} - 2\frac{\dot{a}}{a}v\right), \tag{2.47}$$

where k is the curvature parameter which indirectly encodes information about the small-scale structure on strings. It can be expressed as a function of the velocity [80]

$$k = \frac{2\sqrt{2}}{\pi}\left(\frac{1-8v^6}{1+8v^6}\right), \tag{2.48}$$

and it incorporates the Virial condition $v^2 \leq \frac{1}{2}$, observed in simulations.

Following the same procedure as before, one now finds a scaling solution with

$$\xi^2 = \frac{k(k+\tilde{c})}{4\beta(1-\beta)}, \tag{2.49}$$

$$v^2 = \frac{k(1-\beta)}{\beta(k+\tilde{c})}. \tag{2.50}$$

Of particular note is that the velocity also enters a scaling regime (2.50) in which it stays constant in time. This solution depends on cosmology (through the expansion exponent β) and on the loop formation efficiency, $\tilde{c}$, which, by comparison with numerical simulations, is of order unity [79].

Before ending our discussion we should note that, even though pioneering analytical and numerical modelling of cosmic string networks has been performed, there still exist some unresolved issues. We stated earlier that the production and decay of closed loops is an important energy loss mechanism for the network. The basic question is what is the typical size ℓ of these loops and what is the precise rôle of small scale structure (for a very recent study on loop distribution combining analytical and numerical methods, see [82]).

When a loop is formed after an intercommutation of two strings or after a string self-intersection, it oscillates with period $\ell/2$ while losing its energy through gravitational radiation. The loop's lifetime is estimated as [83]

$$t_\ell \approx \frac{\ell}{\Gamma G\mu} \approx 10^4 \ell \tag{2.51}$$

for GUT strings (the parameter $\Gamma \sim 60$). This lifetime is quite large, and sufficiently big loops (i.e. loops with a size ℓ close to the characteristic length L of the network, which scale in the same way as the long strings) can meet another segment of string and reconnect to the long-string network. However, simulations in flat and FLRW background spacetimes [74, 75, 76, 84] showed that the loops were in fact much smaller than the horizon. Recent simulations showed [85, 86, 87] that many of these small loops are produced only in a transient regime and they are not expected to be present at the later stages of the network's evolution. In addition, the simulations of [86] find a sub-population of loops which exhibit scaling in radiation and matter (also see [88, 89]). Recent analytical studies support that both small and large loops (with $\ell/t \sim 0.1$) will appear [90, 91, 92].

The typical size and distribution of loops in a cosmic string network is a subject still under debate, mainly because of numerical issues due to the length and time scales involved. Another issue is whether the most important energy loss mechanism of a network is gravitational radiation. A different suggestion, based on Abelian Higgs simulations, is that the string network loses energy because of *particle emission* [84, 93, 94].

An important property of long strings is the small-scale structure, which is responsible for the production of tiny loops. Long strings are smooth on the horizon scale, but on much smaller scale there is a significant sub-structure, with wiggles and kinks. Kinks are a result of string intersections, and they straighten slowly due to the expansion of the universe [75]. The study of small-scale structure, or 'wiggliness', is difficult numerically, due to the smallness of the scales in question. Gravitational radiation from opposite travelling waves was believed to be responsible for damping the

wiggles, but it is now proven to be suppressed [95].

2.5 Cosmic Superstrings

In 1985, Witten [96] was the first to consider the tantalising possibility that fundamental (F) strings produced in the early universe could progressively stretch to cosmic size. Unfortunately, this possibility was quickly ruled out, at least in the context of perturbative string theory. The fundamental strings are expected to have a huge tension, $G\mu \geq 10^{-3}$, close to the Planck scale. Thus, they would produce big fluctuations in the cosmic microwave background, incompatible with measurements demanding $G\mu \leq 10^{-5}$. Moreover, such high tension strings cannot be produced after inflation, as their tension exceeds the upper bound on the energy scale of the inflationary vacuum. On the other hand, if they are produced before inflation, they will be inevitably diluted, together with the other kinds of topological defects which could have disastrous effects for the universe (monopoles and domain walls). Finally, some instabilities were identified [96], which suggested that, even if these strings were successfully produced in the early universe, they would be unable to survive until today.

Some years later, the ideas of braneworlds, extra dimensions and warped spacetime [97, 98, 99, 100] gave a different twist to the story, describing our Universe as a D3-brane embedded in a higher dimensional space, the *bulk*. Only gravity can propagate in the bulk, while the standard model particles are confined to live on the brane. In 10D superstring theory models, Dp-branes of various dimensionality can exist. These branes interact, unwind and evaporate, leading to a system of D3-branes, one of which can play the rôle of our universe [101].

According to the braneworld scenario, the extra dimensions can be warped. This can provide a solution to the cosmic superstring tension problem, in the same way that it was employed to deal with the hierarchy problem. When we allow for spacetime to be warped, we can write the line element as [7, 99]

$$ds^2 = A(\hat{y})(dt^2 - d\mathbf{x}^2) - d\hat{y}^2, \tag{2.52}$$

where $\hat{y}$ denotes the extra dimensions. If this is the case in 10D superstring theory models (with 6 warped extra dimensions), then the fundamental string tension μ_f could in fact be close to the Planck scale, giving a much smaller *effective* tension μ on the brane. If the strings are localized at $\hat{y} = \hat{y}_s$, we will have

$$\mu = A(\hat{y}_s)\mu_f, \tag{2.53}$$

which can be much smaller than μ_f if $A(\hat{y}_s) \ll 1$.

The aforementioned approach provides a neat way around the tension problem. But what about inflation? Surely, these strings must be produced after inflation, otherwise they will be diluted. It turns out that the braneworld scenario can also provide a way to realise inflation in string theory, together with the production of cosmic strings. In models of the so-called *brane inflation* [42, 43, 44, 102, 103], a brane-antibrane pair slowly move towards each other, collide and finally annihilate. Each brane carries a U(1) gauge symmetry. During annihilation, tachyon rolling leads to spontaneous symmetry breaking, and two kinds of strings are produced via the Kibble mechanism: F-strings and D-strings [45, 46, 102, 104, 105, 106]. F-strings are quantum mechanical objects, while D-strings are very similar to the usual cosmic strings. Note that the catastrophic topological defects, i.e. domain walls and monopole-like defects, are not being produced.

To summarise, there are three necessary conditions for the existence of cosmic superstrings [107]:

- The strings must be produced after inflation.
- They must be stable on cosmological scales.
- They must be observable, but not already excluded.

These conditions are satisfied in the context of brane inflation. Another *desirable* condition is that cosmic superstrings should be distinguishable from 'usual' (solitonic) cosmic strings.

Having established that cosmic superstrings can be produced and be stable at cosmological scales, we will now turn to the equally important issue of *distinguishability*. Can we differentiate a cosmic superstring network from a solitonic one? The answer is yes, because cosmic superstrings carry two unique characteristics: a reduced intercommuting probability [105], and the formation of junctions [108].

We have already mentioned that for usual Abelian cosmic strings, the intercommuting probability is essentially one. This is an extremely important feature, giving rise to the scaling solution being a strong attractor - otherwise, the strings would soon dominate the universe.

For cosmic superstrings, the situation is very different (see [8, 9, 107] and references therein). First of all, these strings travel in the extra dimensions, and they can easily miss each other. Secondly, even when they eventually meet, they do not necessarily intercommute, because of charge conservation. To be more specific, let us denote as (p, q) a string carrying p quanta of F charge and q quanta of D charge. In general, a

(p, q) and a (p', q') string can form a $(p + p', q + q')$ or a $(p - p', q - q')$ string. Their crossing results in a configuration of two trilinear vertices (junctions) connected by the segment of the produced string. For example, consider an F-string (1,0) meeting a D-string (0,1). They cannot simply intercommute, but they can form a bound state, an FD-string (1,1) (see Fig. 2.4).

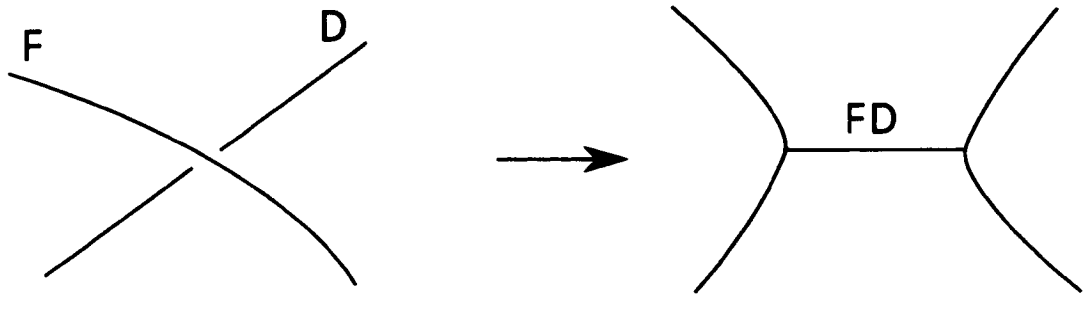

Figure 2.4: An F string interacts with a D string, forming an FD string.

The (p, q) bound states were originally found using the $SL(2, \mathbb{Z})$ duality of the IIB superstring theory in ten dimensions [109]. One starts from the general ten-dimensional supergravity action

$$S_0 = \frac{1}{2\kappa^2} \int d^{10}x\sqrt{-g} \times \left(R - \frac{1}{2}(\partial\phi)^2 - \frac{1}{12}e^{-\phi}H^2 \right), \tag{2.54}$$

where H is a three-form field strength ($H = dB$), and ϕ is the dilaton. The type IIB theory has two three-form field strengths $H^{(i)} = dB^{(i)}, i = 1, 2$. $H^{(1)}$ belongs to the NS-NS (Neveu-Schwarz-Neveu-Schwarz) sector. $H^{(2)}$ belongs to the R-R (Ramond-Ramond) sector. We also have two scalar fields, the dilaton ϕ in the NS-NS sector, and the field χ which belongs to the R-R sector, combined into a complex field

$$\lambda = \chi + ie^{-\phi}. \tag{2.55}$$

Setting the five-form field strength equal to zero (as the corresponding charges are carried by a self-dual three-brane, whereas we are interested on charges carried by

strings) the covariant action for this system can be written as

$$S_0 = \frac{1}{2\kappa^2}\int d^{10}x\sqrt{-g}\left(R + \frac{1}{4}\mathrm{tr}(\partial\mathcal{M}\partial\mathcal{M}^{-1}) - \frac{1}{12}H^T\mathcal{M}H\right), \tag{2.56}$$

where $H^{(1)}$, $H^{(2)}$ are combined into a vector $H = dB$ and the matrix M is given by

$$\mathcal{M} = e^{\phi}\begin{pmatrix} |\lambda|^2 & \chi \\ \chi & 1 \end{pmatrix}. \tag{2.57}$$

The symmetry of this system, studied in [109], suggests that the solutions should carry both $H^{(1)}$ and $H^{(2)}$ electric charge. The F- and D-string can be mapped to each other via S-duality. Measured in units of Q, where Q is the $B_{\mu\nu}$ electric charge carried by the string, we can consider solutions carrying charges $(q_1, q_2) = (p, q)$, where p and q are relatively prime integers. These solutions are now interpreted as bound states of p $F1$-branes and q $D1$-branes [110], and their tension in flat ten-dimensional type-IIB theory is

$$\mu_{(p,q)} = \frac{\mu_F}{g_s}\sqrt{g_s^2(p-\chi q)^2 + q^2}, \tag{2.58}$$

where $g_s = e^{\phi}$ is the string coupling. Note that $(p, q) = (1, 0)$ corresponds to the fundamental F-string, while $(p, q) = (0, 1)$ corresponds to the D-string. The interaction forming an FD bound state is mediated by the RR scalar χ, and the merging occurs with the F string passing its flux to the D string.

Cosmic strings also arise in Grand Unified Theories (GUTs). In a recent publication [41], the authors investigated cosmic string formation in supersymmetric GUTs, and examined all possible spontaneous symmetry breaking schemes from the GUT scale down to the standard model gauge group. Their conclusion is that all phenomenologically consistent theories predict cosmic string formation at the end of the inflationary period.

The aforementioned features provide the fascinating possibility of distinguishing cosmic superstrings, thus opening a window to string theory through cosmology. An important question is immediately raised: Since the intercommuting probability of cosmic superstrings is lower than unity, how will their network behave? Will it scale? Network evolution and cosmological implications of cosmic superstring networks will be the main subject later in this thesis. Before that, we need to introduce the theory of cosmic strings with junctions and study their dynamics and stability.

2.6 Cosmic Strings with Junctions

2.6.1 Introduction

As already stated, cosmic superstrings can bind together, forming an entangled three string configuration. The first study of the dynamics of three-string junctions in a local cosmic string network was performed by Copeland, Kibble and Steer (hereafter CKS) in [51, 52], using an approach which had been previously adopted for representing baryons as pieces of open string connected at a common point [53, 54]. Assuming that the strings have no long-range interactions, the Nambu-Goto approximation can be used.

In this section, we will review the CKS approach for the study of three semi-infinite strings meeting at a junction. We will start by constructing the Nambu-Goto action for a three string vertex, and then analyse the equations of motion and present a simple exact solution [51].

The basic result of the CKS analysis is that the formation of junctions after the col-

lision of two cosmic superstrings is governed by kinematic constraints, which depend on the tensions and the collision angle. This will have important consequences for the evolution of a cosmic superstring network.

2.6.2 Equations of motion

Following the standard approach, we use the conformal gauge, which imposes the constraints

$$\dot{\mathbf{x}} \cdot \mathbf{x}' = 0, \qquad \dot{\mathbf{x}}^2 + \mathbf{x}'^2 = 1, \tag{2.59}$$

where $\dot{\mathbf{x}} = \partial_t \mathbf{x}$ and $\mathbf{x}' = \partial_\sigma \mathbf{x}$.

We consider a junction of three strings of tensions μ_j, $(j = 1, 2, 3)$, and coordinates $\mathbf{x}_j(\sigma, t)$ (Fig. 2.5). The convention for σ is that it increases towards the junction for all three strings. The action for this system is the sum of the Nambu-Goto actions for each

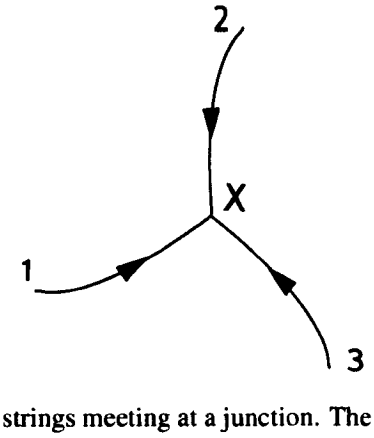

Figure 2.5: Three semi-infinite strings meeting at a junction. The arrows show the chosen convention for the direction of increasing σ_i.

string, together with extra terms to assure that the strings meet at the junction. These

can be written as constraints using Lagrange multipliers. That is [51]

$$S = -\sum_j \mu_j \int dt \int d\sigma\, \Theta(s_j(t)-\sigma)\sqrt{\mathbf{x}_j'^2(1-\dot{\mathbf{x}}_j^2)} + \sum_j \int dt\, \mathbf{f}_j(t)\cdot[\mathbf{x}_j(s_j(t),t)-\mathbf{X}(t)], \tag{2.60}$$

where $\mathbf{X}$ is the position of the vertex, $\mathbf{f}_j$ are the Lagrange multipliers, and the $s_j(t)$ are the values of the spatial world sheet coordinates at the vertex.

Varying the action with respect to $\mathbf{x}_j$ and using the gauge conditions (2.59) we get the usual equation of motion

$$\ddot{\mathbf{x}}_j - \mathbf{x}_j'' = \mathbf{0}, \tag{2.61}$$

with solution

$$\mathbf{x}_j(\sigma,t) = \frac{1}{2}[\mathbf{a}_j(\sigma+t)+\mathbf{b}_j(\sigma-t)], \tag{2.62}$$

while the gauge conditions impose

$$\mathbf{a}_j'^2 = \mathbf{b}_j'^2 = 1. \tag{2.63}$$

We also get (from the terms proportional to $\delta(s_j(t)-\sigma)$)

$$\mu_j(\mathbf{x}_j' + \dot{s}_j\dot{\mathbf{x}}_j) = \mathbf{f}_j, \tag{2.64}$$

where the functions are evaluated at the vertex $(s_j(t),t)$. Varying with respect to the Lagrange multipliers we get the boundary conditions

$$\mathbf{x}_j(s_j(t),t) = \mathbf{X}(t), \tag{2.65}$$

and varying with respect to $\mathbf{X}$ we find

$$\sum_j \mathbf{f}_j = \mathbf{0}. \tag{2.66}$$

We can now write (2.65) as

$$\mathbf{a}_j(s_j + t) + \mathbf{b}_j(s_j - t) = 2\mathbf{X}(t), \tag{2.67}$$

and then use (2.64) and (2.66) to get

$$\sum_j \mu_j[(1 + \dot{s}_j)\mathbf{a}'_j + (1 - \dot{s}_j)\mathbf{b}'_j] = \mathbf{0}. \tag{2.68}$$

Now, let us consider a junction for which the incoming waves are the $\mathbf{b}'_j(s_j - t)$'s, which are determined using the initial conditions. We then calculate the outgoing waves $\mathbf{a}'_j(s_j + t)$ as follows. We begin by differentiating (2.67) with respect to t:

$$(1 + \dot{s}_j)\mathbf{a}'_j - (1 - \dot{s}_j)\mathbf{b}'_j = 2\dot{\mathbf{X}}. \tag{2.69}$$

Substituting for the unknown waves $\mathbf{a}'_j$ into equation (2.68), we find

$$\sum_j \mu_j(1 - \dot{s}_j)\mathbf{b}'_j = -(\mu_1 + \mu_2 + \mu_3)\dot{\mathbf{X}}. \tag{2.70}$$

Eliminating $\dot{\mathbf{X}}$ from the above pair of equations we get an expression for each (unknown) $\mathbf{a}'_j$ as a function of the (known) $\mathbf{b}'_j$'s. However, we still have to calculate the evolution of the junction in σ-space, namely $\dot{s}_j$. Using the gauge conditions $\mathbf{a}'^2_j = 1$, we get a differential equation for $\dot{s}_j$ as a function of the string tensions and the scalar products

$$c_{ij} = \mathbf{b}'_i(s_i - t) \cdot \mathbf{b}'_j(s_j - t) = c_{ji}. \tag{2.71}$$

For example, the corresponding equation for $\dot{s}_1$ is

$$\frac{\mu_1(1 - \dot{s}_1)}{\mu_1 + \mu_2 + \mu_3} = \frac{M_1(1 - c_{23})}{M_1(1 - c_{23}) + M_2(1 - c_{31}) + M_3(1 - c_{12})} \tag{2.72}$$

where $M_1 = \mu_1^2 - (\mu_2 - \mu_3)^2$, with similar definitions for M_2 and M_3. The equations for $\dot{s}_2$ and $\dot{s}_3$ can be obtained by cyclic permutations of equation (2.72).

Given that $|\dot{s}_j| \leq 1$ and $|c_{ij}| \leq 1$, it follows that all $M_j \geq 0$. This means that our configuration must satisfy the triangle inequalities: no string tension can exceed the sum of the other two for the configuration to be stable.

Another important result is the relation

$$\mu_1 \dot{s}_1 + \mu_2 \dot{s}_2 + \mu_3 \dot{s}_3 = 0, \tag{2.73}$$

which expresses energy conservation. This can be obtained by summing equations (2.72), although a more elegant way of deriving the same equation will be presented in Chapter 3.

As we can see, equations (2.72) are differential equations for s_j. This means that, in general, numerical methods will be required to solve for the evolution of a string configuration with junctions. Once the values of $s_j(t)$ are known, we can use equations (2.69) and (2.70) to find the values of $\mathbf{a}'_j(s_j + t)$, and then integrate to obtain $\mathbf{a}_j$. It is important to note that this can be done as long as the incoming waves $\mathbf{b}'_j$ are determined by the initial conditions. The effects of other junctions will eventually start affecting the incoming waves, which will be then determined by the dynamics of these junctions (see Chapter 3 for a complete treatment).

There exists an exceptionally simple analytic solution [51] describing three semi-circular arcs symmetrically arranged around a common diameter (see Fig. 2.6). With $\mu_1 = \mu_2 = \mu_3$, it can be written as

$$\begin{aligned}
\mathbf{x}_1(t,\sigma) &= \cos t(\cos\sigma, 0, \sin\sigma) \\
\mathbf{x}_2(t,\sigma) &= \cos t(-\frac{1}{2}\cos\sigma, \frac{\sqrt{3}}{2}\cos\sigma, \sin\sigma) \\
\mathbf{x}_3(t,\sigma) &= \cos t(-\frac{1}{2}\cos\sigma, -\frac{\sqrt{3}}{2}\cos\sigma, \sin\sigma)
\end{aligned}$$

with $|\sigma| \leq \pi/2$ and $\dot{s}_j = 0$, so that $s_j = \frac{\pi}{2}$ for all t. It is obvious that it is a gen-

eralisation of the well-known collapsing circular loop solution. The loops keep their semicircular shape and collapse to a point at $t = \frac{\pi}{2}$.

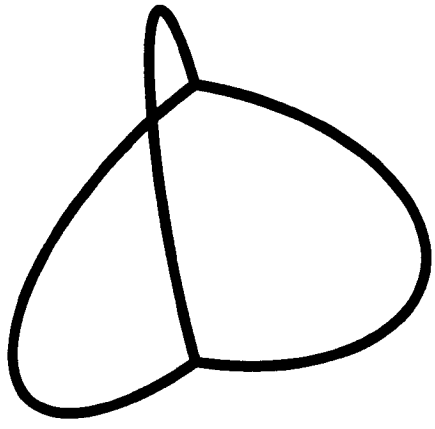

Figure 2.6: Three semicircular arcs symmetrically arranged around a common diameter - initial configuration.

2.7 Collisions of strings with Y junctions

In this section, we will present the CKS approach for studying the problem of the collision of two strings which become linked by a third one.

Let us first consider two straight strings with equal tensions $\mu_1 = \mu_2$, which move towards each other along the z-axis and collide at $t = 0$ [51]. For $t < 0$, we can write

$$\mathbf{x}_{1,2}(\sigma, t) = (-\gamma^{-1}\sigma\cos\alpha, \mp\gamma^{-1}\sigma\sin\alpha, \pm vt). \tag{2.74}$$

where v is the string velocity and $\gamma^{-1} = \sqrt{1-v^2}$. This gives

$$\begin{aligned} \mathbf{a}'_{1,2} &= (-\gamma^{-1}\cos\alpha, \mp\gamma^{-1}\sin\alpha, \pm v), \\ \mathbf{b}'_{1,2} &= (-\gamma^{-1}\cos\alpha, \mp\gamma^{-1}\sin\alpha, \mp v). \end{aligned} \tag{2.75}$$

Let us suppose that the collision angle α is small and that the connecting string segment forms along the x-direction. Then, for $t > 0$, we will have

$$\mathbf{x}_3(\sigma, t) = (\sigma, 0, 0), \qquad \mathbf{a}_3'(\sigma) = \mathbf{b}_3'(\sigma) = (1, 0, 0). \tag{2.76}$$

From the symmetry of the problem it is obvious that it is sufficient to study either of the two junctions along the x-axis. Choosing the positive one and using (2.73), we find $s_1 = s_2 = -(\mu_3/2\mu_1)s_3$. The vertex will be moving along the x-axis with uniform velocity $\dot{s}_3$ and position $\mathbf{X}(t) = (s_3(t), 0, 0)$. For the c_{ij} of (2.71) we find

$$c_{12} = \mathbf{b}_1' \cdot \mathbf{b}_2' = -\gamma^{-2}\cos 2\alpha - v^2, \qquad c_{13} = \mathbf{b}_1' \cdot \mathbf{b}_3' = -\gamma^{-1}\cos\alpha = c_{23}. \tag{2.77}$$

Substituting into (2.72) we get

$$\dot{s}_3 = \frac{2\mu_1\gamma^{-1}\cos\alpha - \mu_3}{2\mu_1 - \mu_3\gamma^{-1}\cos\alpha}, \qquad \dot{s}_1 = \dot{s}_2 = -\frac{\mu_3}{2\mu_1}\dot{s}_3. \tag{2.78}$$

Requiring the string 3 to grow means $\dot{s}_3 > 0$. Thus, we get the constraint

$$\alpha < \arccos\left(\frac{\mu_3\gamma}{2\mu_1}\right) \qquad (x\text{−axis}). \tag{2.79}$$

This is consistent with our initial assumption that the connecting string would form on the x-axis for small collision angle α. Similarly, for a string along the y-axis (α closer to $\pi/2$) one finds

$$\alpha > \arcsin\left(\frac{\mu_3\gamma}{2\mu_1}\right) \qquad (y\text{−axis}). \tag{2.80}$$

From the triangle inequalities, we deduce that a junction cannot be formed if $\mu_3 > 2\mu_1$. Also, we find that there is an upper bound on the velocity the strings can have in order to form a junction:

$$\gamma < \frac{2\mu_1}{\mu_3}. \tag{2.81}$$

This means that very fast Abelian strings will simply pass through one another. For non-Abelian strings, there are two possibilities: they can either become joined by a string in the z-direction, or form a locked X configuration.

Following the treatment of strings with equal tension, CKS extended their study to the case of colliding strings with unequal tensions [52]. They first define

$$\mu_+ \equiv \mu_1 + \mu_2, \ \mu_- \equiv \mu_1 - \mu_2. \tag{2.82}$$

Then, from the triangle inequalities, it follows that μ_3 is in the range

$$\mu_- \leq \mu_3 \leq \mu_+. \tag{2.83}$$

Because the tensions of the colliding strings are not the same, the symmetry of the equal tension case is lost. Now, suppose that at $t = 0$ the strings bind forming a x-link, where the new string is at an angle θ to the x-axis, and moves along the z-direction with velocity u (see Fig. 2.7). That is,

$$\mathbf{x}_3(\sigma, t) = (\gamma_u^{-1}\sigma\cos\theta, \gamma_u^{-1}\sigma\sin\theta, ut). \tag{2.84}$$

After quite a bit of algebra, they found that the equation for the bridge velocity u is

$$\mu_-^2(\sin^2\alpha)u^4 + [\mu_3^2(1-v^2) + \mu_-^2(v^2\cos^2\alpha - \sin^2\alpha)]u^2 - \mu_-^2 v^2\cos^2\alpha = 0. \tag{2.85}$$

This equation always has one positive root for u^2, and also $u^2 < v^2$. After u is found, the angle θ can be determined by the equation

$$\frac{\tan\theta}{\tan\alpha} = \frac{u}{v}. \tag{2.86}$$

In [111], the authors showed that the above kinematic constraints, which were derived for Nambu-Goto strings, are essentially the same if one considers collisions of

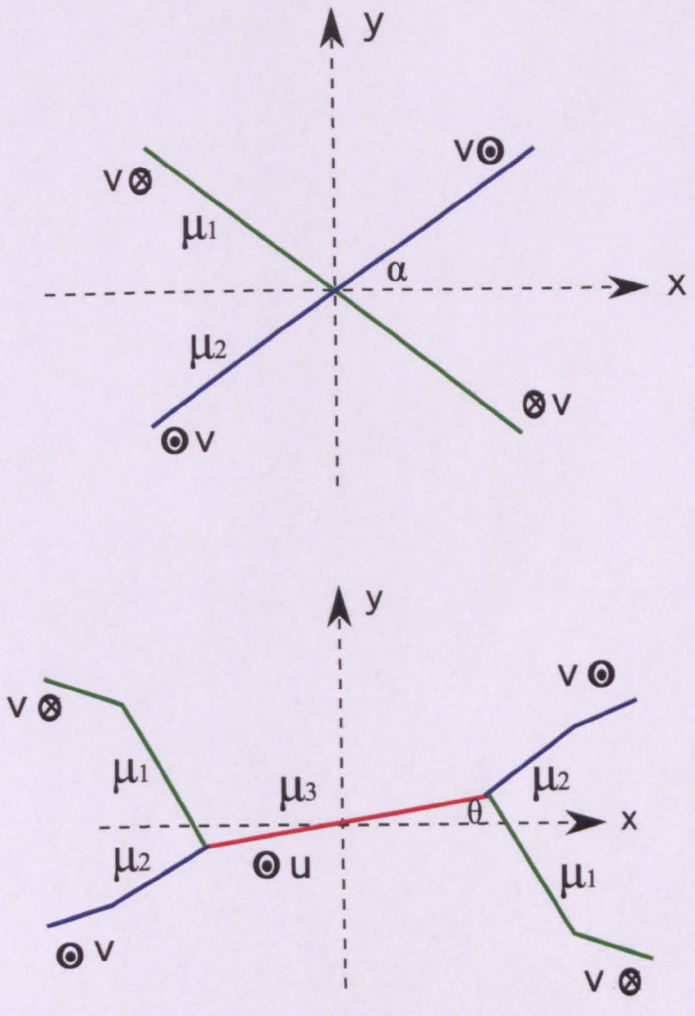

Figure 2.7: Two strings with different tensions μ_1 and μ_2 collide and become joined by a third string μ_3, forming a x-link.

(p, q)-cosmic superstrings with tensions

$$\bar{\mu}_i = \sqrt{p_i^2 + \frac{q_i^2}{g_s^2}}. \tag{2.87}$$

The condition for junction formation is

$$\dot{s}_3 > 0. \tag{2.88}$$

Then, the expression for $\dot{s}_3$ is found to be [111]

$$\dot{s}_3 = \frac{G\bar{\mu}_+ - \bar{\mu}_3}{\bar{\mu}_+ - G\bar{\mu}_3}, \tag{2.89}$$

with

$$G = \frac{\gamma^{-1}\cos\alpha}{\gamma_u^{-1}\cos\theta} = \sqrt{\frac{(1-v^2)(v^2\cos^2\alpha + u^2\sin^2\alpha)}{v^2(1-u^2)}} \tag{2.90}$$

This implies important kinematic constraints on the (v, α) parameter space for a x-link formation, which we will now derive following [111].

From the inequality $u^2 < v^2$, we deduce that $G < 1$. Furthermore, the denominator of (2.89) is always positive, respecting the triangle inequalities. We therefore have

$$G > \frac{\bar{\mu}_3}{\bar{\mu}_+} \tag{2.91}$$

which can be written as

$$f(\gamma^{-1}) \equiv A_1\gamma^{-4} + A_2\gamma^{-2} + A_3 < 0, \tag{2.92}$$

where

$$A_1 = \bar{\mu}_+^2 \cos^2\alpha[\bar{\mu}_3^2 - \bar{\mu}_+^2 \sin^2\alpha - \bar{\mu}_-^2 \cos^2\alpha], \tag{2.93}$$

$$A_2 = 2\bar{\mu}_+^2\bar{\mu}_-^2 \cos^2\alpha - \bar{\mu}_3^2 - (2\cos^2\alpha - 1)\bar{\mu}_+^2\bar{\mu}_3^2, \tag{2.94}$$

$$A_3 = \bar{\mu}_3^4 - \bar{\mu}_+^2\bar{\mu}_-^2. \tag{2.95}$$

The condition (2.92) depends on the collision angle α, the collision velocity v and the tensions of the three strings. It can be solved to obtain constraint on the values of v for which a junction can form:

$$0 \leq v^2 < v_c^2(\alpha), \tag{2.96}$$

where the critical velocity, v_c, depends on $\bar{\mu}_1$ and $\bar{\mu}_2$. The authors showed that $v_c^{max} \leq 1$ only if

$$\bar{\mu}_3^2 \geq \bar{\mu}_+|\bar{\mu}_-| = |\bar{\mu}_1^2 - \bar{\mu}_2^2|. \tag{2.97}$$

If this condition is satisfied, then the two colliding strings will simply pass through one another without forming a junction, for $v > v_c^{max}$.

Let us now illustrate the effect of these constraints using a simple example. Taking $\bar{\mu_1} = \bar{\mu_2}$, the constraint (2.91) can be written as [111]

$$\sqrt{1-v^2}\cos\alpha > \frac{\bar{\mu_3}}{2\bar{\mu_1}}. \tag{2.98}$$

For the collision of an F with a D string forming an FD string and $g_s = 1$, we find [111]

$$\sqrt{1-v^2}\cos\alpha > \frac{1}{\sqrt{2}} \text{ and } u \sim \theta \sim 0. \tag{2.99}$$

Using (2.99), we plot the allowed (v, α) parameter space for the formation of a x-link (Fig. 2.8).

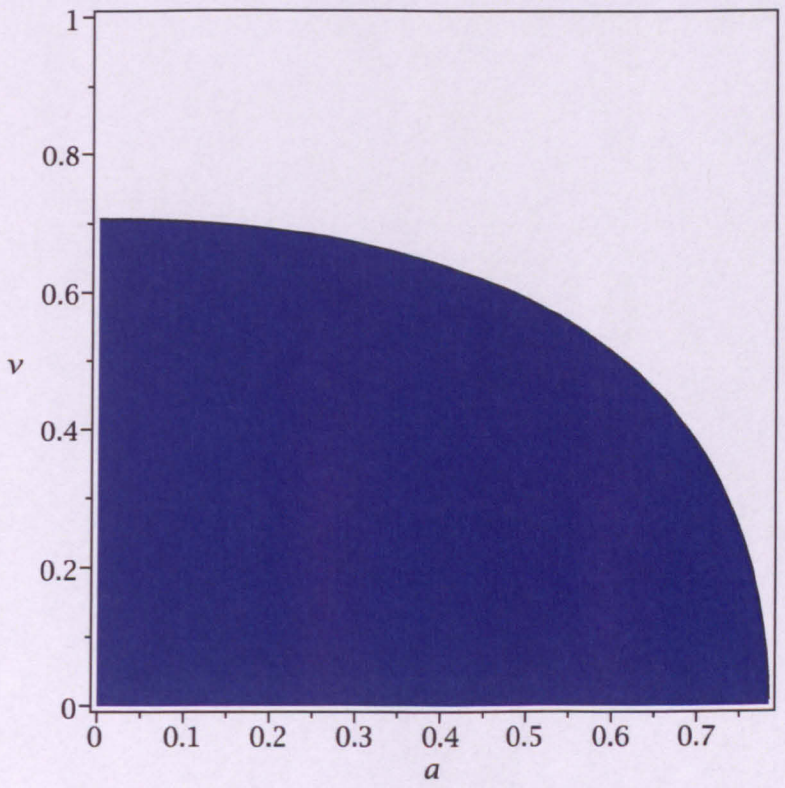

Figure 2.8: The allowed parameter range in (v, α) space for the collision of an F string with a D string to form an FD string (x-link) is shown in blue for $g_s = 1$.

The CKS predictions for the kinematic constraints governing junction formation are derived using the Nambu-Goto approximation. One might wonder how successful they

are when compared with field theory simulations, where the zero-width approximation is not valid anymore. This comparison was performed in [112, 113], finding very good agreement.

2.8 Cosmic Strings with Junctions in an FLRW universe

We will now study the evolution of cosmic strings with junctions in an expanding universe (see [114] for a nice study of cosmic string loops in FLRW spacetimes, and [115] for a thorough investigation of cosmic string collisions in cosmological backgrounds). In addition, we will present an exact solution for a loop with junctions in a de Sitter background.

For three strings forming a junction in an FLRW spacetime, the action can be written as

$$S = -\sum_j \mu_j \int d\tau \int d\sigma\, \Theta(s_j(\tau)-\sigma) a^2(\tau)\sqrt{\mathbf{x}'^2(1-\dot{\mathbf{x}}^2)} + \sum_j \int d\tau\, a^2(\tau)\mathbf{f}_j(\tau)\cdot[\mathbf{x}_j(s_j(\tau),\tau)-\mathbf{X}(\tau)], \tag{2.100}$$

where τ is the conformal time. Varying $\mathbf{x}_j$ yields the usual equation of motion for a string in an expanding universe

$$\ddot{\mathbf{x}}_j + 2\frac{\dot{a}}{a}\dot{\mathbf{x}}_j(1-\dot{\mathbf{x}}_j^2) = \frac{1}{\epsilon_j}\left(\frac{\mathbf{x}'_j}{\epsilon_j}\right)', \tag{2.101}$$

where $\mathbf{x}' = \partial_\sigma \mathbf{x}$, $\dot{\mathbf{x}} = \partial_\tau \mathbf{x}$ and $\epsilon_j = \sqrt{\frac{\mathbf{x}'^2_j}{1-\dot{\mathbf{x}}^2_j}}$. There are also boundary terms which give us the boundary conditions

$$\mu_j\left(\frac{\mathbf{x}'_j}{\epsilon_j} + \epsilon_j \dot{s}_j \dot{\mathbf{x}}_j\right) = \mathbf{f}_j \tag{2.102}$$

where the functions are evaluated at $(s_j(\tau), \tau)$. Varying $\mathbf{X}$ provides the constraint

$$\sum_j \mathbf{f_j} = 0 \tag{2.103}$$

so we can write the boundary conditions as one equation

$$\sum_j \mu_j \left(\frac{\mathbf{x}'_j}{\epsilon_j} + \epsilon_j \dot{s}_j \dot{\mathbf{x}}_j \right) = 0 \tag{2.104}$$

By considering a circular loop

$$\mathbf{x} = r(\tau)(\cos\sigma, \sin\sigma, 0)$$

we find using eq. (2.101) that $r(\tau)$ must satisfy

$$\ddot{r} + 2\frac{\dot{a}}{a}(1 - \dot{r}^2)\dot{r} = \frac{\dot{r}^2 - 1}{r}. \tag{2.105}$$

Now, let us consider a de Sitter universe, with $a(t) = e^{Ht}$, $H = \text{const}$. Using

$$\frac{\dot{a}}{a} = -\frac{1}{\tau}, \tag{2.106}$$

we find a solution to eq. (2.105). That is

$$r = \frac{-1}{\sqrt{2}}\tau = \frac{1}{\sqrt{2}H}e^{-Ht}. \tag{2.107}$$

We can generalise this solution to a configuration comprising three semicircular arcs symmetrically arranged around a common diameter:

$$\begin{aligned}
\mathbf{x}_1(t,\sigma) &= \frac{1}{\sqrt{2}H}e^{-Ht}(\cos\sigma, 0, \sin\sigma) \\
\mathbf{x}_2(t,\sigma) &= \frac{1}{\sqrt{2}H}e^{-Ht}(-\frac{1}{2}\cos\sigma, \frac{\sqrt{3}}{2}\cos\sigma, \sin\sigma) \\
\mathbf{x}_3(t,\sigma) &= \frac{1}{\sqrt{2}H}e^{-Ht}(-\frac{1}{2}\cos\sigma, -\frac{\sqrt{3}}{2}\cos\sigma, \sin\sigma)
\end{aligned}$$

with $|\sigma| < \pi/2$. Each one of them will satisfy the equation of motion and, if we choose $\mu_1 = \mu_2 = \mu_3$ we can check that the boundary condition (2.104) is satisfied with $\dot{s}_1 = \dot{s}_2 = \dot{s}_3 = 0$, so that $s_j(t) = \pi/2$ for all t.

This solution can be thought of as a generalisation of a circular cosmic string loop solution found in [116]. The physical radius is

$$R(t) = ar = \frac{1}{\sqrt{2}H}. \tag{2.108}$$

As the authors note, *this solution appears to be static but it is only stationary - it is a contracting loop standing still against the Hubble expansion.*

2.9 Discussion

In this chapter we presented an overview of the most important features of cosmic string dynamics in the Nambu-Goto approximation. In Minkowski spacetime, we studied the equations of motion and presented some representative exact loop solutions. We identified special points on the string, namely cusps and kinks. Their appearance is generic, and they are important sources of gravitational radiation, as we will see in Chapter 4. We also studied the dynamics of strings in an FLRW spacetime. The Hubble expansion damps the motion of the strings, with long wavelengths being conformally stretched as the Universe expands. For short wavelengths and small loops of string the Hubble damping is negligible, so the equations of motion are almost equivalent to those in flat spacetime. We saw that a great deal of analytical and numerical work has been devoted in network evolution. The 'one-scale' model takes into account the expansion of the universe and the long string interactions with associated loop formation. The network evolves towards a scaling regime, where the characteristic length of the long string network is constant relative to the horizon, in agreement with numerics. The VOS model is a more sophisticated analytic model that introduces a dynamical velocity component to the equations — it has also been tested, quite successfully, against

numerical simulations.

The theoretical prediction of cosmic superstrings gave a new boost to the cosmic string research community. The prospect of linking string theory with cosmology, i.e. with observations, is very challenging. We saw that cosmic superstrings can bind together, forming an entangled three-string configuration. We presented an extensive overview of the studies of cosmic strings with junctions in the Nambu-Goto approximation, with particular attention on the kinematic constraints for the formation of junctions. We ended our discussion by deriving the equations of motion for strings with junctions in an expanding spacetime. An exact solution was found for a de Sitter background.

In the next chapter, we will study the evolution and stability of cosmic string loops with Y-junctions using the CKS approach and a field theory U(1)×U(1) model [117]. In addition, the aforementioned kinematic constraints will be of crucial importance when we study the evolution and cosmological implications of multi-tension cosmic superstring networks in Chapter 5.

Chapter 3

Evolution and Stability of cosmic string loops with Y-junctions

3.1 Introduction

The realisation that cosmic superstrings can arise in superstring/M-theory as products of brane inflation [42, 43, 44, 45, 46] has opened up a window on string theory through cosmology, since we might be able to detect them through their imprints in the cosmic microwave background radiation [118, 119, 120, 121, 122, 123], their lensing of distant galaxies [124, 126, 127] and the production of gravitational waves [128, 129, 130].

As we have already mentioned, for standard field-theory strings the intercommuting probability is essentially unity [68, 131, 132, 133, 134]. However, the situation for cosmic superstrings is quite different - the intercommutation probability can be greatly reduced due to the presence of the large extra dimensions, and it depends on the value of the string coupling constant [105, 135, 136, 137]. Furthermore, a network of cosmic

superstrings will look very different from a cosmic string one. As an example, let us imagine a network of F- and D-strings. Inevitably, they will form bound states of p F-strings and q D-strings. Thus, trilinear vertices (Y-junctions) will appear, which is not the case in the Abelian-Higgs cosmic string scenario. This can lead to interesting dynamics following the collision of such strings, and it is natural for one to wonder how the existence of Y-junctions affects the properties of the string network.

However, stable composites can form even in Abelian Higgs models, provided that the gauge coupling is sufficiently high. We also know that junctions are generic in non-Abelian networks. In the following, we use the U(1)×U(1) model [117] of gauge strings that permits junctions, focusing on the particular case of closed planar loops. However, we should note that no known field theory model can give us the rich mass spectrum of bound states for cosmic superstrings. This means that some of the field theory results cannot be extrapolated to the case of cosmic superstrings, for which the U(1)×U(1) field theory is only a toy model.

Our aim is to compare the two different approaches which have been used to describe the dynamics of strings with Y-junctions. The first is the Copeland, Kibble and Steer (CKS) approach [51, 52], which is based on the modification of the Nambu-Goto action. The second is to describe the strings as composite objects in terms of an underlying classical field theory that will allow for the formation of junctions [117] (see also [138, 139, 140, 141, 142, 143, 144]). This comparison has already been done for ordinary cosmic strings with no junctions (for a review see [5, 6]). The results demonstrated that the Nambu-Goto approach is an excellent approximation to describe a cosmic string, provided that the string's curvature is much larger than its width. Recently [113], it has been shown that the late time dynamics of a system of straight

strings colliding and forming Y-junctions can be very accurately described using the CKS method. We would like to know whether this is still the case when considering closed loops consisting of several strings.

Using the Nambu-Goto approximation to study these configurations is profitable for a number of reasons. First of all, the Nambu-Goto simulations are much easier and less numerically costly (for example, only planar loops can be evolved using the field theory code). Furthermore, the CKS approach gives us the freedom to choose the strings' tension, while in the field theory model the spectrum of the tensions is very limited. Additionally, with Nambu-Goto there is more freedom in the choice of the intercommuting probability of cosmic superstrings because, unlike in field theory, it can be dealt by hand and it is not constrained by the equations.

We will compare the field-theory and Nambu-Goto evolution of two initial loop configurations which could be the result of two planar loops colliding. However, we must stress that they are not expected to be representative of loops in a cosmic superstring network. These are very specific configurations, but they still give us the opportunity to explore the properties of Y-junctions, including a new feature, their stability to decomposition into three new junctions, whose separation may grow significantly.

The chapter is organised as follows: In Section 3.2, we discuss the Nambu-Goto method and describe our numerical technique, followed by a brief description of the $U(1)\times U(1)$ field theory model in Section 3.3. In Section 3.4 we compare our results for the two different approaches. We present our conclusions in Section 3.5.

3.2 Nambu-Goto approach

3.2.1 Equations of motion

In this section we set up the Nambu-Goto equations of motion for a string loop with J junctions in Minkowski spacetime, generalising the aforementioned CKS approach that described the dynamics of three straight semi-infinite strings meeting at a junction.

Case of two junctions

As a warm-up, we first set up the equations of motion for a loop with two junctions and three strings. The junctions are labelled by the index $J = (A, B)$, and the position of the ith string ($i = 0, 1, 2$) with tension μ_i is parameterised as

$$x_i^\mu(\tau, \sigma_i), \tag{3.1}$$

where τ and σ_i are the world-sheet coordinates (note that τ is chosen to be the same for all three strings). The induced metric on the world-sheet for string i is

$$\gamma_{ab}^i = \frac{\partial x_i^\mu}{\partial \sigma^a}\frac{\partial x_i^\nu}{\partial \sigma^b}\eta_{\mu\nu}, \tag{3.2}$$

where $a, b = (\tau, \sigma_i)$ and $\eta_{\mu\nu}$ is the 4-dimensional Minkowski metric. Below, a dot/dash denotes a derivative with respect to τ/σ_i respectively. The values of the world-sheet coordinate σ at the junction are denoted by s_i^J and since we are not expecting s_i^J to be constant, they are generally τ dependent. In the case of two junctions, we have the freedom to take σ to increase (or decrease) to a given junction for all three strings. Hence we can choose σ to increase from junction A to junction B so that

$$s_i^A(\tau) \leq \sigma_i \leq s_i^B(\tau). \tag{3.3}$$

The positions of the junctions are

$$X^{\mu}_{J}(\tau) = x^{\mu}_{i}(\tau, s^{J}_{i}(\tau)) \qquad \text{for all } i. \tag{3.4}$$

In the absence of background fluxes and after dilaton stabilisation, the dynamics of a *single infinite* (p,q)-string in flat spacetime is given by the Dirac Born Infeld (DBI) action [111]

$$S_{\rm DBI} = -\bar{\mu}\int {\rm d}\tau {\rm d}\sigma \sqrt{-|\gamma_{ab} + \lambda F_{ab}|}, \tag{3.5}$$

where $\bar{\mu} = |q|/(g_s\lambda)$ is the tension of q coincident D-strings, $\lambda = 2\pi\alpha'$, with α' the Regge-slope parameter, and g_s is the perturbative string coupling. F_{ab} is the electromagnetic tensor on the string world-sheet, and the electric flux density is the momentum conjugate to the electric field $p = \partial L_{\rm DBI}/\partial F_{\tau\sigma}$. The dynamics of *three semi-infinite* (p,q)-strings meeting at a junction was discussed in [111] where it was shown that the resulting equations of motion are exactly equivalent to those obtained by using the Nambu-Goto action for each string, *provided* the ith string tension in the Nambu-Goto action is taken to be given by

$$\mu_i = \sqrt{p_i^2 + \left(\frac{q_i}{g_s}\right)^2}, \tag{3.6}$$

and one imposes charge conservation at the junction

$$\sum_i p_i = 0 \qquad \sum_i q_i = 0. \tag{3.7}$$

Hence, we may assume that the dynamics of each individual segment of string is determined by the Nambu-Goto action.

In the conformal gauge

$$\gamma^{i}_{\tau\tau} + \gamma^{i}_{\sigma_i\sigma_i} = 0\,; \qquad \gamma^{i}_{\tau\sigma_i} = 0, \tag{3.8}$$

the Nambu-Goto action for the three strings of tensions μ_i joined by two junctions is

$$\begin{aligned} S &= -\sum_i \mu_i \int d\tau \int d\sigma_i \left[\Theta(s_i^B(\tau)-\sigma_i)\Theta(-s_i^A(\tau)+\sigma_i)\right. \\ &\qquad \left. \times\sqrt{-x_i'^2\,\dot{x}_i^2}\right] \\ &+ \sum_{J=(A,B)} \sum_i \int d\tau\, f_{i\mu}^J \cdot [x_i^\mu(\tau, s_i^J(\tau)) - X_J^\mu(\tau)], \end{aligned} \tag{3.9}$$

where μ_i is given in equation (3.6) and the four-vector Lagrange multipliers $f_{i\mu}^J(\tau)$ impose the constraints given in Eq. (3.4).

Varying the action (3.9) with respect to x_i^μ yields the usual equation of motion for a string in Minkowski space-time (away from the junction), namely the wave equation

$$\ddot{x}_i^\mu - x_i^{\mu\prime\prime} = 0 \implies x_i^\mu = \frac{1}{2}\left[a_i^\mu(u_i) + b_i^\mu(v_i)\right], \tag{3.10}$$

where

$$u_i = \sigma_i + \tau\,; \qquad v_i = \sigma_i - \tau. \tag{3.11}$$

From the conformal gauge conditions (3.8) the "left" and "right" movers satisfy

$$a_i'^2 = 0\,, \qquad b_i'^2 = 0. \tag{3.12}$$

Furthermore, varying the action with respect to X_J^μ, imposing the temporal gauge and using the boundary conditions gives the energy conservation equation at each junction:

$$\mu_1 \dot{s}_1^J + \mu_2 \dot{s}_2^J + \mu_3 \dot{s}_3^J = 0. \tag{3.13}$$

As the junction is moving, some of the strings will have $\dot{s}_i^J > 0$ while others $\dot{s}_i^J < 0$. These represent growing/shrinking of the string not only in σ-space, but also in real space. The rate of creation of one string must balance the disappearance of other(s).

In order to study the evolution of the whole configuration, we need to determine the dynamics of the two junctions. It is important to note that, unless the configuration is

highly symmetric, we cannot determine its evolution using analytical methods, except at early times. That is because, once an outgoing wave from one junction has reached another junction, then the incoming waves cannot be taken directly from the initial conditions and the problem becomes non-linear. In general, numerical methods will be needed in order to solve the full system.

Let us first consider junction B. The algebraic procedure to determine the outgoing waves $a_i'^{\mu}$ as a function of the incoming waves $b_i'^{\mu}$ at junction B is very similar to the one used in the case where three semi-infinite strings meet at a junction. The basic difference is that the strings are now finite, hence the incoming waves at junction B are the outgoing waves from junction A and vice versa. We can therefore write (for the outgoing waves of junction B)

$$(\dot{s}_i^B + 1)a_i'^{\mu} = b_i'^{\mu}(1 - \dot{s}_i^B) - \frac{2}{\sum_k \mu_k} \sum_j \mu_j (1 - \dot{s}_j^B) b_j'^{\mu}, \tag{3.14}$$

while the evolution of $\dot{s}_i^B$ is determined by

$$1 - \dot{s}_i^B(t) = \frac{\left(\sum_j \mu_j\right) M_i (1 - c_i^B(t))}{\mu_i \sum_k M_k (1 - c_k^B(t))}, \tag{3.15}$$

where

$$c_1^B(t) = \mathbf{b}_2'(v_2^B(t)) \cdot \mathbf{b}_3'(v_3^B(t)), \tag{3.16}$$

$$M_1 = \mu_1^2 - (\mu_2 - \mu_3)^2, \tag{3.17}$$

and cyclic permutations. At vertex A the procedure is similar, though the incoming waves are now given by the $a_i'^{\mu}$.

Multiple Junctions

When three semi-infinite strings meet at a junction, we can always arrange the coordinates σ_i such that they increase toward the junction on all three strings. However, this cannot be done generally, and it is essential to generalise the above equations for the case where there is a different orientation between the three strings at a junction.

To do so we associate a further parameter δ_i^J with the 3 strings meeting at junction J. If $\delta_i^J = +1$ then on string i, σ_i increases into the junction J. If, on the other hand, $\delta_i^J = -1$ for string i then σ_i decreases into the junction. Note that if junctions J and K are connected by string i then $\delta_i^J = -\delta_i^K$. This sign difference introduces a slight complication in the governing equations.

Let us work initially in the conformal gauge, without imposing the temporal gauge. This will enable us to derive the energy conservation equation directly from the action. The action for the whole string configuration can be written as

$$S = -\sum_i \Bigg[\mu_i \int \mathrm{d}\tau \int \mathrm{d}\sigma_i \sqrt{-x_i'^2\, \dot{x}_i^2} \prod_{J(i)} \Theta\big(\delta_i^J \{s_i^J(\tau) - \sigma_i\}\big) + \sum_{J(i)} \int \mathrm{d}\tau\, f_\mu^{J,i} \left\{ x_i^\mu(\tau, s_i^J(\tau)) - X_J^\mu(\tau) \right\} \Bigg]$$

where $J(i)$ implies that J takes on the values of the junctions at either end of string i (for semi-infinite strings it would take on just one value). The presence of the Θ terms ensures contributions only for the allowed range of σ values while the Lagrange multipliers $f_\mu^{J,i}$ ensure that the strings are coincident at the junction locations X_J^μ.

Varying the action with respect to X_J^μ for a single junction gives:

$$\sum_{i(J)} f_\mu^{J,i} = 0, \tag{3.18}$$

where now $i(J)$ implies that i takes on the indices of the strings that meet at junction J (in the $J > 2$ case, different strings will meet at different junctions, while for $J = 2$, the same three strings were meeting at both junctions). Then, varying the action with respect x_i^μ for a single string yields, in general, $\ddot{x}_i^\mu = x_i^{\mu\prime\prime}$, but at the junctions this becomes:

$$\mu_i \delta_i^J \left(x_i^{\mu\prime} + \dot{s}_i^J \dot{x}_i^\mu\right) = f_{i,J}^\mu. \tag{3.19}$$

We now set the more restrictive gauge condition $\gamma_{00} = 1$ (giving $\tau = t$ and σ as invariant length) while combining equations (3.18) and (3.19). This yields immediately the energy conservation expression as the $\mu = 0$ equation:

$$\delta_i^J \mu_i \dot{s}_i^J + \delta_j^J \mu_j \dot{s}_j^J + \delta_k^J \mu_k \dot{s}_k^J = 0 \tag{3.20}$$

where i, j, k are the indices of the three strings meeting at junction J. Consider, for example, the simple case with three strings and two junctions, where we can always choose $\delta_1^J = \delta_2^J = \delta_3^J = +1$. Now change the orientation of string 3. Then $\dot{s}_3$ picks up a minus sign but so does δ_3^J, so the energy conservation equation is unchanged.

Another effect of the sign change relates to the identification of the waves along the string as "incoming" or "outgoing" from a junction. Away from any junction, the strings satisfy the usual wave equation

$$\ddot{\mathbf{x}}_i = \mathbf{x}_i'' \tag{3.21}$$

with general solution

$$\mathbf{x}_i(t, \sigma_i) = \frac{1}{2}\left[\mathbf{a}_i(u_i) + \mathbf{b}_i(v_i)\right]. \tag{3.22}$$

where $u_i = \sigma_i + t$, $v_i = \sigma_i - t$ and the gauge conditions impose $|\mathbf{a}_i'| = |\mathbf{b}_i'| = 1$. While in CKS σ_i always increased towards the junctions and the incoming waves were

always given by $\mathbf{b}_i$, in the multi-junction case outgoing waves at junction J become incoming waves at the junctions to which it is connected.

In the new gauge and using the general solution of the wave equation in terms of right and left movers, the spatial equations become

$$\sum_{i(J)} \mu_i \delta_i^J \left[(1+\dot{s}_i)\mathbf{a}_i' + (1-\dot{s}_i)\mathbf{b}_i'\right] = 0. \tag{3.23}$$

Defining

$$\mathbf{Z}_i = \begin{cases} +\mathbf{b}_i'(s_i - t) & \text{if } \delta_i^J = +1 \\ -\mathbf{a}_i'(s_i + t) & \text{if } \delta_i^J = -1. \end{cases} \tag{3.24}$$

and

$$\mathbf{Y}_i = \begin{cases} +\mathbf{a}_i'(s_i + t) & \text{if } \delta_i^J = +1 \\ -\mathbf{b}_i'(s_i - t) & \text{if } \delta_i^J = -1. \end{cases} \tag{3.25}$$

we can rewrite this as

$$\sum_{i(J)} \mu_i \left[(1+\delta_i^J \dot{s}_i)\mathbf{Y}_i + (1-\delta_i^J \dot{s}_i)\mathbf{Z}_i\right] = 0. \tag{3.26}$$

In addition the constraint that the three strings meet at the junction becomes:

$$2\dot{\mathbf{X}}^J = (1+\delta_i^J \dot{s}_i^J)\mathbf{Y}_i - (1-\delta_i^J \dot{s}_i)\mathbf{Z}_i. \tag{3.27}$$

Eliminating the outgoing waves $\mathbf{Y}_i$ we find:

$$\mu \dot{\mathbf{X}}^J = -\sum_{i(J)} \mu_i (1-\delta_i^J \dot{s}_i^J)\mathbf{Z}_i. \tag{3.28}$$

Furthermore, eliminating $\dot{\mathbf{X}}^J$ from equations (3.27) and (3.28) we can solve for the unknown outgoing waves:

$$(1+\delta_i^J \dot{s}_i^J)\mathbf{Y}_i = \mathbf{Z}_i(1-\delta_i^J \dot{s}_i^J) - \frac{2}{\mu}\sum_h \mu_h (1-\delta_h^J \dot{s}_h^J)\mathbf{Z}_h. \tag{3.29}$$

Squaring these equations and using the gauge condition that $|\mathbf{Y}_i| = |\mathbf{Z}_i| = 1$, the equation for the time evolution of $\dot{s}_i^J$ as a function of the incoming waves (along strings i, j and k) at junction J becomes

$$1 - \delta_i^J \dot{s}_i^J(t) = \frac{\mu M_i[1 - c_i^J(t)]}{\mu_i \sum_h M_h[1 - c_h^J(t)]}, \tag{3.30}$$

where h takes values (i, j, k) and the incoming waves are combined via:

$$c_i^J(t) = \mathbf{Z}_j \cdot \mathbf{Z}_k, \tag{3.31}$$

plus cyclic permutations, and we have the definitions: $\mu \equiv \mu_i + \mu_j + \mu_k$ and $M_i \equiv \mu_i^2 - (\mu_j - \mu_k)^2$, plus cyclic permutations. Note that causality ($|\dot{\mathbf{X}}^J| \leq 1$) implies the triangle inequalities $M_j \geq 0$.

3.2.2 Numerical Method

Given an arbitrary initial configuration $(\mathbf{x}_i(0, \sigma_i), \dot{\mathbf{x}}_i(0, \sigma_i))$, we aim to solve for the full loop evolution and hence $(\mathbf{x}_i(t, \sigma_i), \dot{\mathbf{x}}_i(t, \sigma_i))$ for all $t > 0$. As we have already discussed, this calculation is often analytically intractable, except at early times. Thus, we will generally have to employ numerical methods. The numerical procedure is as follows: For every string i connecting two junctions, we work entirely with $\mathbf{a}'$ and $\mathbf{b}'$, reconstructing the closed string position $\mathbf{x}(t, \sigma_i)$ and velocity $\dot{\mathbf{x}}(t, \sigma_i)$ only a few times in the lifetime of the loop. The initial conditions fix $\mathbf{a}_i'(\sigma_i)$ and $\mathbf{b}_i'(\sigma_i)$ between all the junctions. First we calculate the $c_i^J(t = 0)$, from which $\dot{s}_i^J(t = 0)$ is determined using equation (3.30). Then at time δt, $s_i^J(\delta t)$, $u_i^J(\delta t)$ and $v_i^J(\delta t)$ can be calculated. The last step is to extend the domain of definition of $\mathbf{a}_i'(u)$ and $\mathbf{b}_i'(v)$, which can be done with equation (3.29). The time loop then continues.

We will first study (both analytically and numerically) an initially static loop with three strings and two junctions, having a butterfly shape (see Fig. 3.1). Our simulation ends whenever the length of one string goes to zero, and hence when two junctions meet. The outcome of such a collision is not well understood for cosmic superstrings, and in any case is not included in the Nambu-Goto description described above. However, the field theory simulations discussed in Section 3.3 can of course continue beyond this time.

3.3 Field Theory Approach

While the Nambu-Goto formalism is quite easy to analyze numerically, it does not necessarily give a complete description of Y-junctions. For example, one might expect important interactions between the strings close to and at the junctions, and these are not included in the Nambu-Goto action. Thus, we also study the butterfly configuration using a field theory approach, which guarantees a more complete description of the physics of Y-junctions. We will use the U(1)×U(1) model of gauge strings [117]. This involves two Abelian Higgs models having Lagrangian density:

$$\begin{aligned}\mathcal{L} &= -\frac{1}{4}F_{\mu\nu}F^{\mu\nu} - (D_\mu\phi)^*(D^\mu\phi) - \frac{\lambda_1}{4}\left(|\phi|^2-\eta^2\right)^2 \\ &\quad -\frac{1}{4}\mathcal{F}_{\mu\nu}\mathcal{F}^{\mu\nu} - (\mathcal{D}_\mu\psi)^*(\mathcal{D}^\mu\psi) - \frac{\lambda_2}{4}\left(|\psi|^2-\nu^2\right)^2 \\ &\quad +\kappa\left(|\phi|^2-\eta^2\right)\left(|\psi|^2-\nu^2\right). \end{aligned} \tag{3.32}$$

The two Abelian Higgs models are only coupled via the potential term of equation (3.32). The model gives composite stable solutions (i.e. stable junctions) for a specific range of values of the parameter κ, which we discuss below. We follow the conventions

of [113, 117] and define the gauge covariant derivatives as:

$$D_\mu\phi = \partial_\mu\phi - ieA_\mu\phi, \tag{3.33}$$

$$\mathcal{D}_\mu\psi = \partial_\mu\psi - igB_\mu\psi, \tag{3.34}$$

while the anti-symmetric field strength tensors are given by:

$$F_{\mu\nu} = \partial_\mu A_\nu - \partial_\nu A_\mu, \tag{3.35}$$

$$\mathcal{F}_{\mu\nu} = \partial_\mu B_\nu - \partial_\nu B_\mu. \tag{3.36}$$

Finally, η and ν are constants that set the energy-scales of the two halves of the model while λ_i and κ are dimensionless coupling constants.

For $\kappa = 0$, the two U(1)'s are uncoupled and each half of the model admits string solutions, which are characterised by the phase of ϕ (ψ) having an integer winding $2\pi m$ ($2\pi n$). When $\kappa \neq 0$ the U(1)'s are coupled and, as shown in [117], for $0 < \kappa < \frac{1}{2}\sqrt{\lambda_1\lambda_2}$, two parallel strings from each U(1) can bind to a composite string, reducing their energy. Hence one can have Y-junctions in this theory and their formation as a result of the collision of two infinite straight strings was studied in [113]. The numerical approach employed for the field-theory simulations follows [113], but with a very different set of initial conditions, namely the ones required for the butterfly configuration. These are described in Appendix A.

3.4 Results

3.4.1 Analytic Nambu-Goto result for the butterfly configuration with two vertices

Let us start by introducing the butterfly configuration with two junctions. The initial conditions are a straight string with tension μ_0 (lying on the y axis) and two arcs of unit circles with equal tensions $\mu_1 = \mu_2$ in the $x - y$ plane. The strings are initially

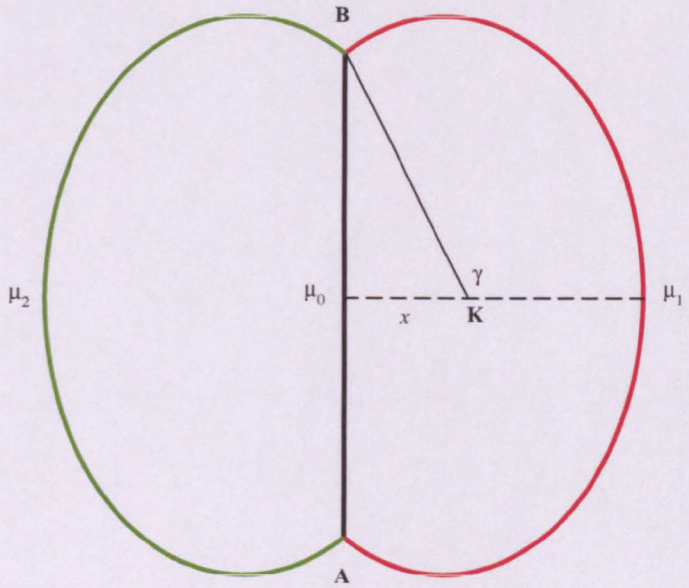

Figure 3.1: The butterfly loop.

static: this means $\dot{s}_j = 0$ or equivalently that the vector sum of tensions at the junction J vanishes

$$\sum_j \mu_j \delta_j^J \frac{\mathbf{x}_j'}{|\mathbf{x}_j'|} = 0. \tag{3.37}$$

It is useful to introduce the angle γ, and we find that for an initially static loop, it is $\cos\gamma = -R, R = \mu_0/(2\mu_1) = x$, where x is the distance of the wings' centres from

the straight string. We then have:

$$\begin{aligned}
\mathbf{x}_0(t=0,\sigma_0) &= (0,\sigma_0,0), \qquad |\sigma_0| < \sin\gamma, \\
\mathbf{x}_1(t=0,\sigma_1) &= (-\cos\gamma + \cos\sigma_1, \sin\sigma_1, 0)\,, \quad |\sigma_1| < \gamma, \\
\mathbf{x}_2(t=0,\sigma_2) &= (\cos\gamma - \cos\sigma_2, \sin\sigma_2, 0)\,, \quad |\sigma_2| < \gamma.
\end{aligned} \tag{3.38}$$

Following our conventions, we label the lower vertex as A and the upper one as B, so that σ_i increases towards junction B for all strings. Because of symmetry, it is sufficient to study one junction, say B. At $t = 0$ we find

$$\begin{aligned}
\mathbf{a}_0' = \mathbf{b}'_0 &= (0,1,0), \\
\mathbf{a}_1' = \mathbf{b}'_1 &= (-\sin\sigma_1, \cos\sigma_1, 0), \\
\mathbf{a}_2' = \mathbf{b}'_2 &= (\sin\sigma_2, \cos\sigma_2, 0).
\end{aligned} \tag{3.39}$$

The energy conservation equation (3.13) implies that $R\dot{s}_0^B = -\dot{s}_1^B$ and hence after integration we have:

$$s_0^B(t) = \sin\gamma - \frac{1}{R}\left(s_1^B(t) - \gamma\right). \tag{3.40}$$

Thus, we only need to determine $s_1^B(t)$. We have $c_1 = c_2 = \cos(s_1^B - t)$ and $c_0 = 2\cos^2(s_1^B - t) - 1$ and, letting $\Delta = t - s_1^B$ and using equation (3.30), we find

$$\dot{\Delta} = \frac{1 - R^2}{1 + R\cos\Delta}. \tag{3.41}$$

Integrating the above equation, we get

$$t\sin^2\gamma = -\cos\gamma\sin\Delta + \Delta - \cos\gamma\sin\gamma + \gamma. \tag{3.42}$$

Together with the definition of Δ and equation (3.40), we now have t, s_0^B and s_1^B specified as functions of the variable Δ.

It is useful to note that, since the string 0 is simply stationary and on the y axis for all times, then the above $t = 0$ result is valid for all t and the ordinarily difficult to handle emitted waves are simply the waves set by the initial conditions.

3.4.2 Direct comparison of field theory and Nambu-Goto strings

We wish to compare the field-theory and Nambu-Goto evolution of two initial loop configurations, which are variants of the butterfly loop. More specifically, we will consider two closely related but different initial conditions (see Fig. 3.2). The first is

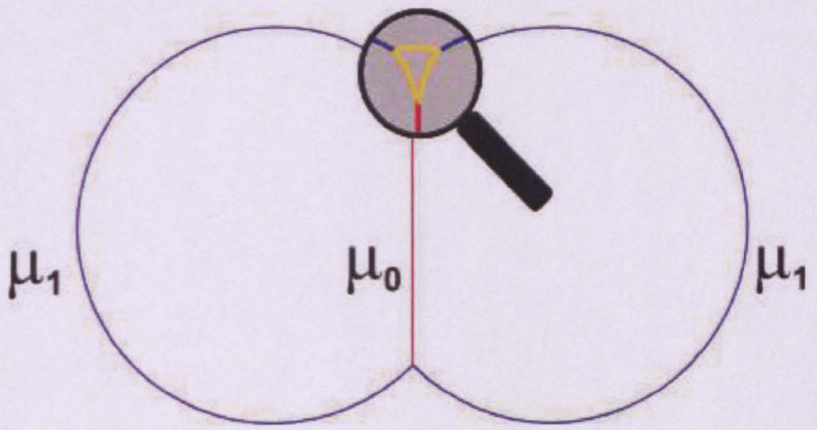

Figure 3.2: An example of a loop configuration with multiple junctions: the butterfly configuration with a central string of tension μ_0 and two arc strings of tension μ_1. The basic butterfly configuration has just two junctions, but we find that under certain situations these can decompose, as indicated by the magnified region, with a single junction splitting into three junctions that then continue to separate.

the butterfly configuration studied above, consisting of three strings and two junctions. For both the Nambu-Goto and field-theory simulations, we use circular arcs with unit radius. For the field-theory case, we follow the standard parameter choice $2 = \lambda_1 = \lambda_2 = 2e^2 = 2g^2$ and $0 < \kappa < 1$ in order for bound-states and Y-junctions to exist. We additionally set $\eta = \nu$ so that there is complete symmetry between the two halves of the model.

For the field-theory simulations, we consider two cases:

- *Case 1:* a $(1,0)$ and a $(0,1)$ string forming the "wings", with a $(1,1)$ bound state string as the central segment.

- *Case 2:* a $(1,-1)$ and a $(1,1)$ string form the "wings", so that a $(2,0)$ bound state string forms the central segment (Fig. 3.3).

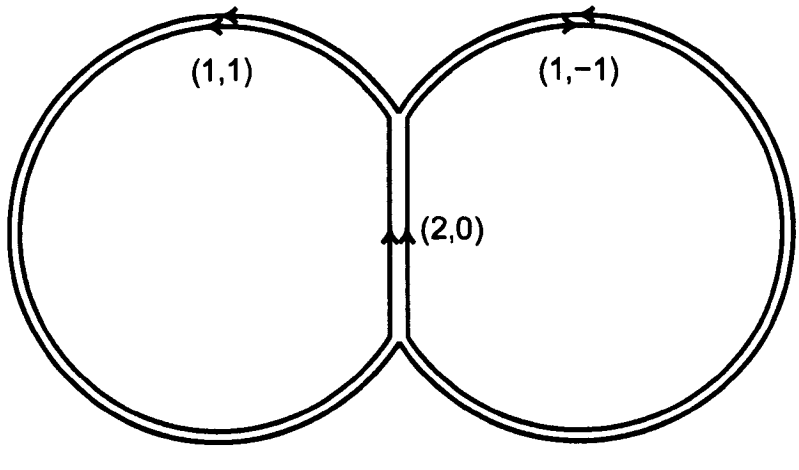

Figure 3.3: The ϕ and ψ fluxes present in the butterfly configuration for field theory simulations of case 2: $(1,1)+(1,-1) \rightarrow (2,0)$.

In the Nambu-Goto simulations, we defined the tension of the wings to be μ_1 and the tension of the central straight segment to be μ_0. This choice greatly simplifies matters, especially when it comes to constructing initially static configurations of loops with junctions, which is a difficult task for both the Nambu-Goto and the field theory approach. When it comes to long straight strings which collide to form a junction, the situation is much simpler, and the study of such collisions of strings with equal and unequal tensions has shown good agreement between the field theory and CKS dynamics after junction formation [113]. In the field theory simulations, the string tensions are calculated [117] for a given coupling κ and cannot be set by hand. Thus, in order to compare Nambu-Goto and field theory simulations, we first calculate the tensions for the field theory, and then we use the results as inputs in the Nambu-Goto code. Table 3.1 gives the string tensions for infinite straight strings (calculated via the

method of [117]) for $\kappa = 0.8$ and 0.95. From the definition of $R = \frac{\mu_0}{2\mu_1}$, the relevant numerical values are also given in table 3.1 and we see that smaller R corresponds to more stable junction. In case 1, R is never very small since most of the energy stems from the covariant derivative term, which cannot be greatly reduced even by increasing κ to its maximum value. A large binding energy exists in case 2 since it involves the cancellation of fluxes. Indeed, we see that for $\kappa = 0.95$, $R = 0.56$, meaning that a $(2,0)$ string is just slightly heavier than a $(1,\pm 1)$ string.

κ	0.80	0.95
$\mu_{(1,0)}/2\pi\eta^2$	0.864	0.728
$\mu_{(1,1)}/2\pi\eta^2$	1.452	1.133
$\mu_{(2,0)}/2\pi\eta^2$	1.622	1.271
$R[(1,0)+(0,1)\rightarrow(1,1)]$	0.840	0.778
$R[(1,1)+(1,-1)\rightarrow(2,0)]$	0.559	0.561

Table 3.1: The energy per unit length and the corresponding R values for $\kappa = 0.8$ and $\kappa = 0.95$.

We start by presenting our Nambu-Goto results for the initial condition given by case 1 with $\kappa = 0.8$ (Fig. 3.4 left) and for the case of $R = 0.5$, hence $\mu_0 = \mu_1$ (Fig. 3.4 right). Before discussing these results, it is useful to recall the initially static circular Nambu-Goto loop of unit radius in Minkowski space-time (see Section 2.3.2). As we know, such a loop collapses to a point after a time $t = \frac{\pi}{2}$ — this is also the collapse time for those regions of the circular arcs on the butterfly wings that remain causally disconnected from the junctions. In the buttefly case, the wings are parts of unit circles and their length is determined by the initial conditions as $2(\pi - \cos^{-1}(R))$. Now, the wave equation tells us that information travels along the strings at the speed of light. This means that, by the collapse time, information about the presence of the junction will have travelled a length of $\pi/2$ along the arcs. Hence, a length $\pi - 2\cos^{-1}(R)$ will remain unaffected by the presence of the junction, i.e. it will behave like a circular

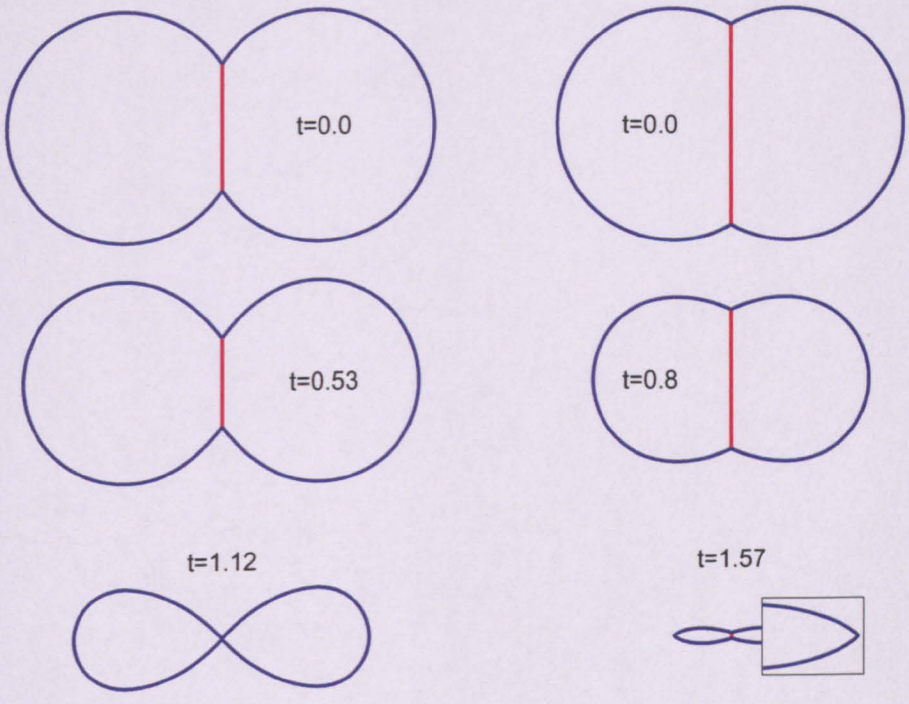

Figure 3.4: Results using the Nambu-Goto method with tensions set to match a field theory $(1,0)+(0,1) \rightarrow (1,1)$ case with $\kappa = 0.8$ (left plot), and all tensions equal (right plot). The later case corresponds to $R = 0.5$ and includes a magnified region showing a kink.

loop. We are therefore expecting that a fraction of the arcs will collapse to a point, reaching the speed of light, and yield a sharp kink in the string. Indeed, in the right panel of Fig. 3.4 the collapse time is $t = 1.57 \gtrsim \pi/2$ and a kink is formed when parts of the wings instantaneously collapse to a point.

A direct comparison of field theory and Nambu-Goto results for the case 1 with $\kappa = 0.8$ is shown in Fig. 3.5, while that for case 2 with $\kappa = 0.95$ is shown in Fig. 3.6. As we can immediately see, the agreement is excellent. This allows us to extend the results for straight strings with kinks to strings with curvature.

In order to perform a more detailed comparison, we plot in Fig. 3.7 the length of the central straight string as a function of time for the Nambu-Goto and field theory simulations. In the NG case, the length is just the difference between $s_0(t)$ at the two junctions and, as we showed earlier, it can also be obtained analytically. Our results confirm that the agreement is excellent until the collapse time. In case 2 we observe

an initial departure, which is basically due to the $(0,1)$ string trying to follow a less kinked route across the junction and therefore moving outwards from it, but then going too far and so undergoing a few low-level oscillations.

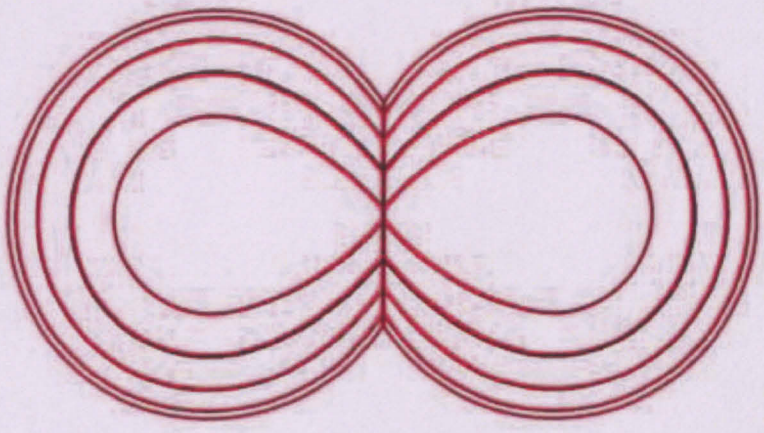

Figure 3.5: The evolution of the butterfly configuration $(1,0)+(0,1) \rightarrow (1,1)$ with $\kappa = 0.8$, shown at equally spaced time intervals: $t = 0.000, 0.267, 0.533, 0.800, 1.067$, with larger configurations corresponding to earlier times. The field theory solution is shown as a bitmap, representing the cumulative projection of its energy density onto the plane, while the Nambu-Goto solution is shown as a solid black line.

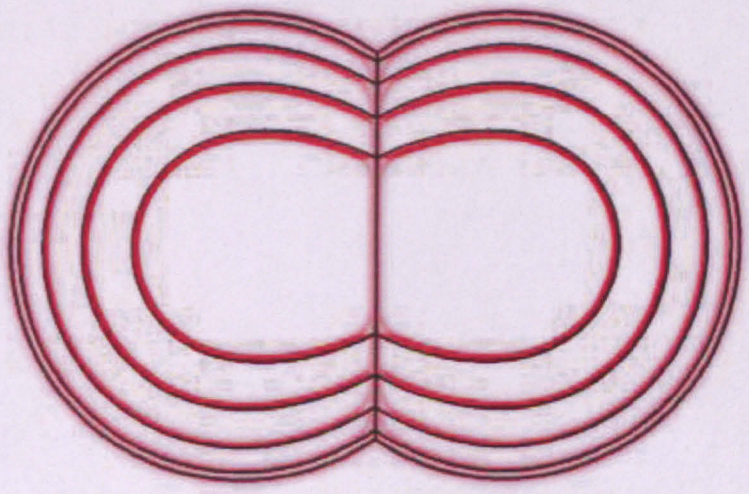

Figure 3.6: As in Fig. 3.5 but for $\kappa = 0.95$ and $(1,1)+(1,-1) \rightarrow (2,0)$.

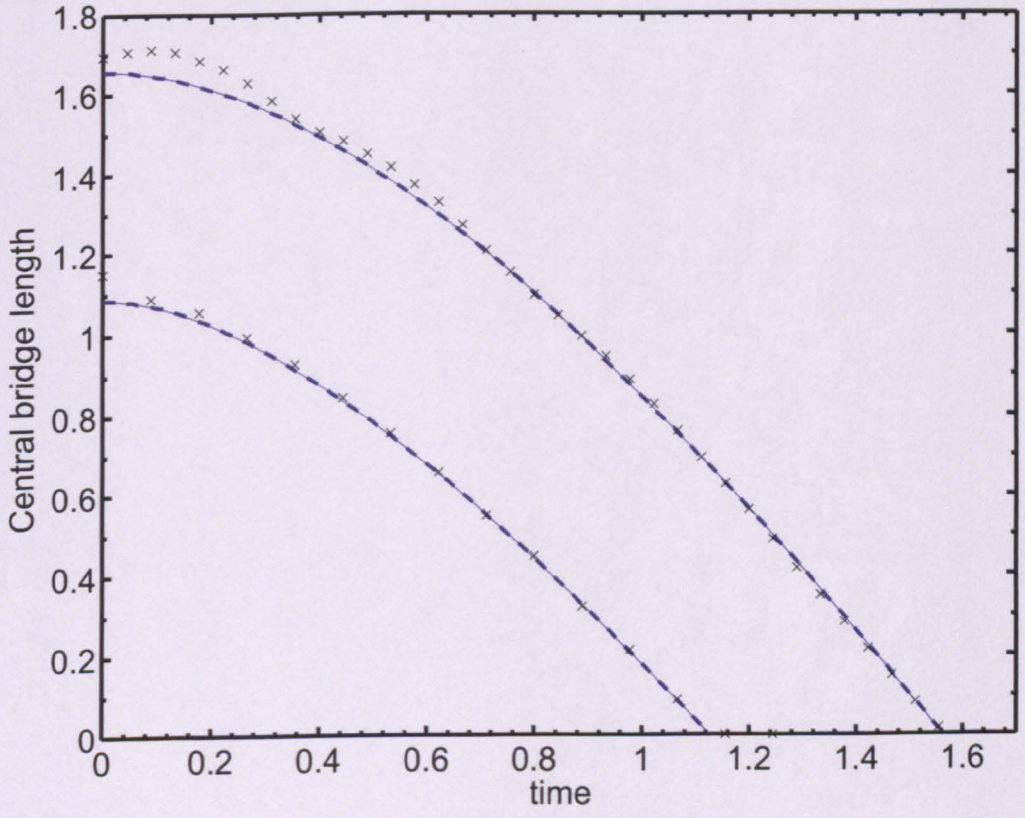

Figure 3.7: The length of the central bridge string as a function of time for the analytic Nambu-Goto solution (thin), the numerical Nambu-Goto results (thick, dashed) and the field theoretic results (crosses). The collection of data with lower bridge lengths is for the $(1,0)+(0,1) \rightarrow (1,1)$ case with $\kappa = 0.8$ while higher bridge values correspond to $(1,1) + (1,-1) \rightarrow (2,0)$ with $\kappa = 0.95$.

3.4.3 Stability of Y-junctions

When the initial butterfly configuration consists of the case 2 scenario of $(1,1)+(1,-1) \rightarrow (2,0)$, the field theory simulations show that the Y-junction can decompose, as illustrated in Fig. 3.8.

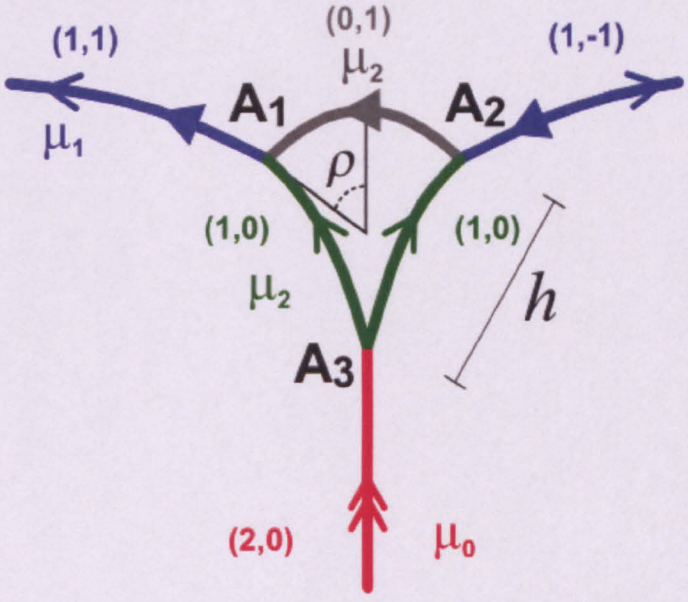

Figure 3.8: The decomposition of a $(1,1)+(1,-1) \rightarrow (2,0)$ junction into three separate Y-junctions.

Let us first try to explain why this decomposition occurs. As we know, the central $(2,0)$ string is a bound state of a $(1,1)$ and a $(1,-1)$ string. However, it can also be constructed from two $(1,0)$ strings. Whether this decomposition will take place depends on the parameters of our U(1)×U(1) system. For our parameter choice $\kappa = 0.8$ and $\kappa = 0.95$, the ratio $R = \frac{\mu_0}{2\mu_1}$ is approximately constant (see table 3.1, $R \approx 0.56$). On the other hand, the ratio $\mathcal{R} = \frac{\mu_1}{2\mu_2}$ (where μ_2 is defined to be the tension of the $(1,0)$ string) decreases from 0.86 to 0.78 with increasing κ across that range. This means that, as κ increases, μ_2 becomes larger relative to both μ_0 and μ_1, which stay in proportion to each other (as the R ratio stays constant). Hence, for the lower value of $\kappa = 0.8$ this decomposition involves a small μ_2 and, as we see in Fig. 3.9, the $(1,0)$

strings are formed and then grow in the time-scale of the simulation.

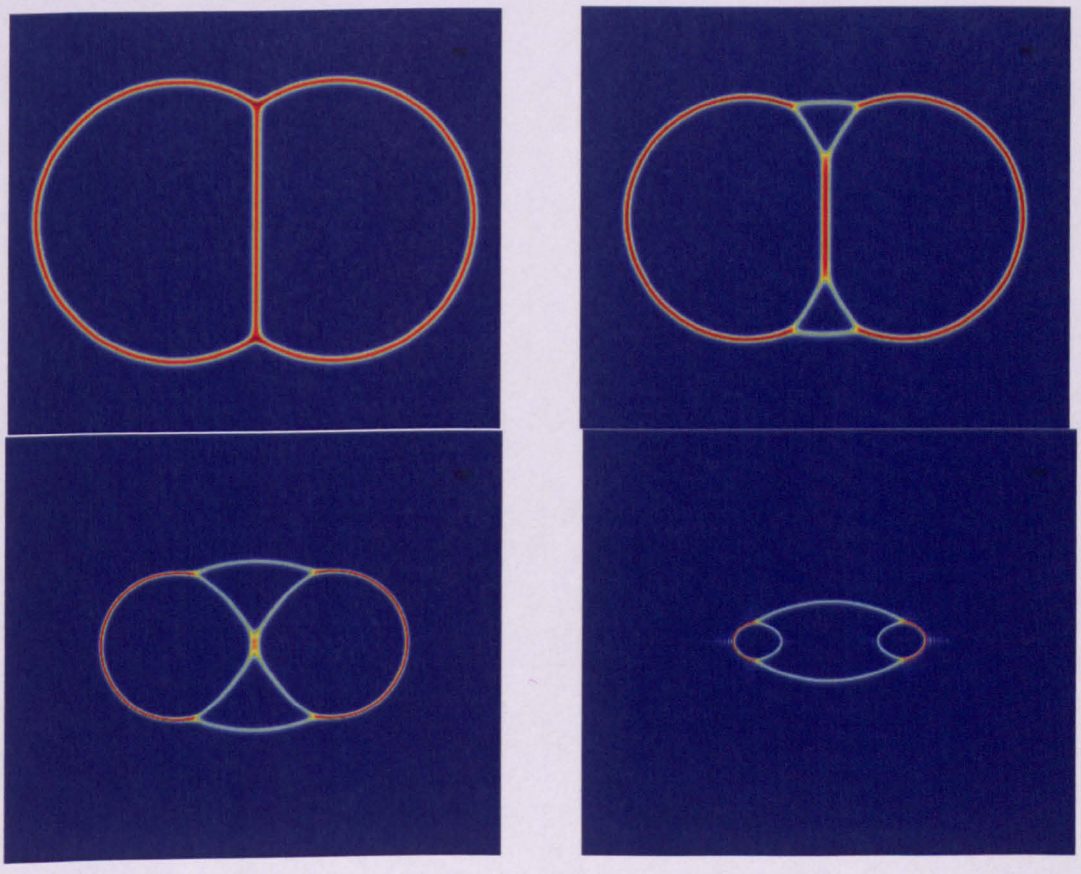

Figure 3.9: The decomposition of the Y-junction as seen in the field theory simulations for $(1,1)+(1,-1) \rightarrow (2,0)$ with $\kappa = 0.8$.

The results for $\kappa = 0.95$ have already been presented in Fig. 3.6. In that case, the $(1,0)$ strings do again form - the difference is that they do not grow, so the loop's evolution is identical to the one of the original butterfly loop. As we can see from Fig. 3.9, the final state for the $\kappa = 0.8$ case is very different: the central bridge has decomposed and peeled open.

The question is if we can reproduce this phenomenon using the Nambu-Goto simulations - the answer is yes, but there is an important constraint: there is no way to get the decomposition dynamically using the NG approach. We have to start with appropriate initial conditions. This is the second set of initial conditions shown in Fig. 3.2, that is adding an initial perturbation consisting of three strings with tension μ_2, which

are all taken to be arcs of circles of size h, effectively the distance between the junctions (note that the free parameter h does not affect the general physical behaviour, if initially small — we will therefore use $h = 0.01$). The Nambu-Goto evolution corresponding to the $\kappa = 0.8$ field theory case 2 is shown in Fig. 3.10 (note that the three-string perturbation is so small at $t = 0$ that it cannot be resolved by eye). However, the snapshot at $t = 0.5$ clearly shows the perturbation which is growing until the end of the simulation, where the central bridge collapses. In Fig. 3.11 we present a

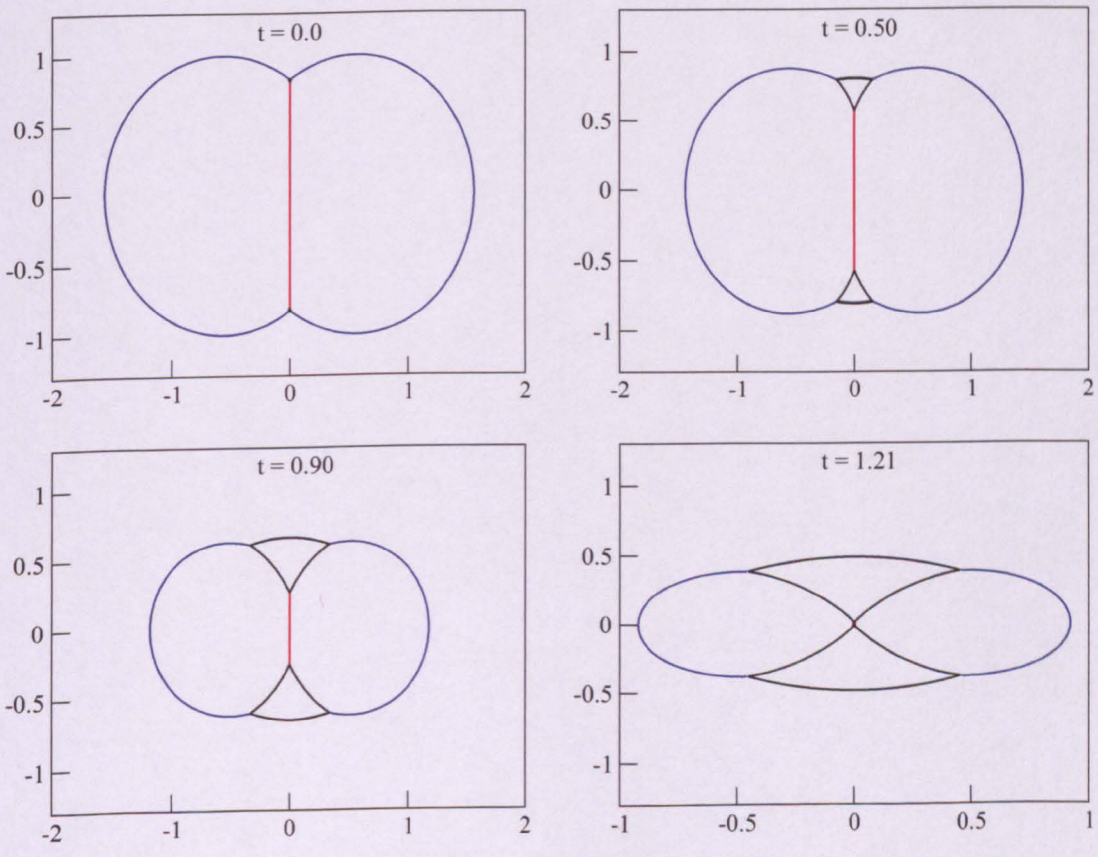

Figure 3.10: Nambu-Goto evolution of the perturbed butterfly loop corresponding to the $\kappa = 0.8$ field theory case of Fig. 3.9, using a perturbation parameter $h = 0.01$ - the instability grows and the loop is unstable.

direct comparison between our Nambu-Goto and field theory results for the unstable configuration. The agreement is again very good throughout the evolution, and we can explain the small departures we see using very simple arguments. At very small times, we see that the field theory perturbation grows more quickly than the Nambu-

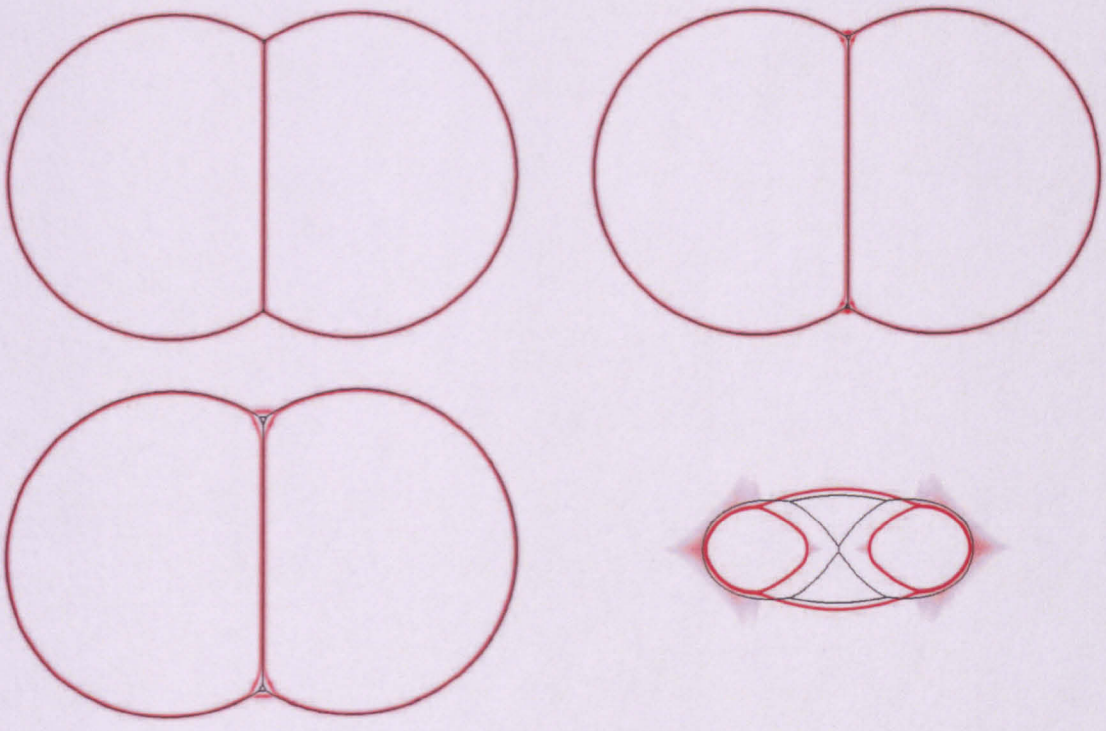

Figure 3.11: Comparison between Nambu-Goto and field theoretic results for t=0, 0.0667, 0.1333, and 1.31. Field theory results shown as a bitmap are from simulations with $\kappa = 0.8$ while the tensions in the Nambu-Goto case (solid black line) are set to match those derived from corresponding theoretic calculations for straight, infinite strings. [h=0.01]

Goto one. This happens because in the Nambu-Goto case we start with all junctions initially static, while in the field theory case the dynamical break-up happens very fast. Additionally, in the Nambu-Goto case we use circular arcs[1] to construct the initial perturbation, which is not expected to be a true represantion of the actual situation. However, with this choice we manage to model the physical string-junction system using the Nambu-Goto approach, which cannot account for junction formation without additional input that mimics the field-theory case just after string collision has occured. At the very end of the simulations (close to the collapse time) we also see a small disagreement. The field theory loop decays quicker and radiates strongly, which is of course expected, since the Nambu-Goto approach cannot account for the interactions between the strings. A similar Nambu-Goto evolution for $\kappa = 0.95$ shows that the

[1]This choice is not unique. For example, we can also construct an initially static perturbation using straight lines.

$(1,1)+(1,-1) \rightarrow (2,0)$ junction is *stable* to the breakup of junctions, again agreeing with the results from field theory.

The approximate matching of the critical value for κ at which the growing decomposition occurs can be considered a success for the less computationally demanding Nambu-Goto approach. As we will show below, it also allows us to make a prediction based purely on the Nambu-Goto results as to when a junction will and will not be unstable to decomposition into multiple junctions.

3.4.4 Stability of Y-junctions in the Nambu-Goto approach

We will now study analytically the stability of the initial perturbation for small times. We will work with junction A_1 in Fig. 3.8, however the same analysis can be applied to any other junction. Let us start by introducing the initial equilibrium conditions for junction A_1, which are defined in terms of the tensions μ_0, μ_1 and μ_2. The position of junction A_1 in σ-space is

$$\begin{aligned} s_1^{A_1}(0) &= \gamma = \pi - \cos^{-1}\left(\frac{\mu_0}{2\mu_1} - h\right), \\ s_2^{A_1}(0) &= \eta = \pi - \gamma - \alpha, \\ s_3^{A_1}(0) &= \rho = \gamma - \alpha - \frac{\pi}{2}. \end{aligned} \tag{3.43}$$

where $\alpha = \cos^{-1}\frac{\mu_1}{2\mu_2}$ and h is the distance between junction A_1 (or A_2) and junction A_3 in Fig. 3.8. As we will demonstrate, the behaviour of the perturbation depends on whether the angle

$$\rho = \frac{\pi}{2} - \cos^{-1}(\mathcal{R}) - \cos^{-1}(R-h) \tag{3.44}$$

is positive or negative. As we will show below, for a given pair of tensions μ_0 and μ_1 there is a critical tension $\mu_2 = \mu_{crit}$, for a small fixed perturbation size h, for which

$\rho = 0$. Above and below this critical limit, we have two distinct regimes: one in which the perturbation grows, and one in which it collapses. We will now consider the two cases separately (note that we drop the index A_1 for simplicity).

Case I: $\rho < 0$

The initial configuration comprises of three strings with tensions μ_1, μ_2 and

$$\begin{aligned} \mathbf{b'}_1(t=0,\sigma_1) &= (\sin\sigma_1, \cos\sigma_1, 0), \\ \mathbf{b'}_2(t=0,\sigma_2) &= (-\sin\sigma_2, \cos\sigma_2, 0), \\ \mathbf{b'}_3(t=0,\sigma_3) &= (-\cos\sigma_3, \sin\sigma_3, 0). \end{aligned} \tag{3.45}$$

At a later time t the incoming waves at junction A are

$$\begin{aligned} \mathbf{b'}_1(t,s_1(t)) &= (\sin(s_1(t)-t), \cos(s_1(t)-t), 0), \\ \mathbf{b'}_2(t,s_2(t)) &= (-\sin(s_2(t)-t), \cos(s_2(t)-t), 0), \\ \mathbf{b'}_3(t,s_3(t)) &= (-\cos(s_3(t)-t), \sin(s_3(t)-t), 0). \end{aligned} \tag{3.46}$$

Using a Taylor expansion around $t = 0$ for s_i we get $s_i(t) = s_i(0)+\lambda_i t^2+...$ (remember $\dot{s}_i = 0$ initially), and using the relations between the angles we find (to first order in t)

$$\begin{aligned} c_1 &= \cos(2\alpha + 2t), \\ c_2 &= -\cos\alpha, \\ c_3 &= -\cos(\alpha + 2t). \end{aligned} \tag{3.47}$$

Using equation (3.30), linearising in t and with $\mathcal{R} = \cos\alpha = \frac{\mu_1}{2\mu_2}$ (which is always less than unity due to the triangle inequalities) we find

$$\dot{s}_1 = -\dot{s}_3 = -\frac{1}{\sqrt{1-\mathcal{R}^2}}t, \qquad \dot{s}_2 = \left(\frac{2\mathcal{R}-1}{1-\mathcal{R}^2}\right)t. \tag{3.48}$$

Case II: $\rho > 0$

The initial conditions can be written as

$$\begin{aligned} \mathbf{b'}_1(t=0,\sigma_1) &= (\sin\sigma_1, \cos\sigma_1, 0), \\ \mathbf{b'}_2(t=0,\sigma_2) &= (-\sin\sigma_2, \cos\sigma_2, 0), \\ \mathbf{b'}_3(t=0,\sigma_3) &= (-\cos\sigma_3, -\sin\sigma_3, 0). \end{aligned} \tag{3.49}$$

Following the same procedure we find

$$\dot{s}_1 = 0, \qquad \dot{s}_2 = -\dot{s}_3 = -\frac{2\sqrt{1-\mathcal{R}^2}}{1+\mathcal{R}}t. \tag{3.50}$$

Having the analytic expressions for $\dot{s}_i$ for both cases, we can use equations (3.23) and (3.27) to obtain the corresponding expression for $\dot{\mathbf{X}}$:

$$\dot{\mathbf{X}} = -\frac{1}{\sum_j \mu_j}\sum_j \mu_j(1-\dot{s}_j)\mathbf{b'}_j. \tag{3.51}$$

In order to study the motion of the vertex in real space, we define the angle

$$\tan(\varphi) = \left(\frac{\dot{X}_y}{\dot{X}_x}\right). \tag{3.52}$$

Since the expression for this angle is very complicated, one can take the limit in which the perturbation size h tends to zero, and also consider small deviations from the $\rho = 0$ case, either with positive or negative ρ. The critical tension μ_2 which leads to $\rho = 0$ is obtained by setting (3.44) to zero and solving for μ_2, resulting in

$$\mu_{crit} = \frac{\mu_1}{2\cos\left(\cos^{-1}(R-h) - \pi/2\right)}. \tag{3.53}$$

Therefore, in the limit $h \to 0$ and $\mu_2 = \mu_{crit}$ equation (3.51) reduces to

$$\frac{\dot{X}_y}{\dot{X}_x} = -\frac{R}{1+\sqrt{1-R^2}} + \frac{-1+3R^2+\sqrt{1-R^2}}{R^2(1+\sqrt{1-R^2}-2R^2\sqrt{1-R^2})}t \tag{3.54}$$

for $\rho < 0$, and

$$\frac{\dot{X}_y}{\dot{X}_x} = \frac{\sqrt{1-R^2}}{R} - \frac{2+R^2-2\sqrt{1-R^2}}{2R^4}t \tag{3.55}$$

for $\rho > 0$. Notice that, as one should expect, in the critical tension limit $\mathcal{R}$ drops out from the expressions, and only $R = \frac{\mu_0}{2\mu_1}$ appears. For both cases ($\rho > 0$ and $\rho < 0$), $\dot{X}_x$ is initially positive, so it is the y direction which changes. For $\rho > 0$, the vertex A_1 moves with an initial angle of

$$\varphi = \pi + \tan^{-1}\left(\frac{\sqrt{1-R^2}}{R}\right) \tag{3.56}$$

in the critical limit ($\mu_2 = \mu_{crit}$), and bigger angles for $\mu_2 > \mu_{crit}$; therefore the perturbation does not grow. In contrast, for $\rho < 0$, the vertex A_1 moves away from the y-axis, with an initial angle of

$$\varphi = \pi - \tan^{-1}\left(\frac{R}{1+\sqrt{1-R^2}}\right), \tag{3.57}$$

which is practically along the butterfly wing. In this case, the junctions separate initially from each other and the butterfly configuration is unstable.

It is insightful to visualise our results by plotting the evolution of the angle ϕ (Fig. 3.12). The main result is the discontinuity in ϕ when going from $\rho > 0$ to $\rho < 0$. Negative ρ corresponds to the arc A_1A_2 in Fig. 3.8 going from concave, as shown, to convex. Equivalently, the center of the circle from which the arc is formed moves from below the arc, as in the figure, to above it. This shows how the evolution of the splitting of the Y-junction in the original butterfly depends mainly on the *initial local curvature* of the strings involved. When $\rho > 0$ (see Fig. 3.8), strings 2 and 3 are "competing"in σ-space while the butterfly wing (string 1) is not contributing much (note that for small times $\dot{s}_1 = 0$ to first order in t). After some time and in real space,

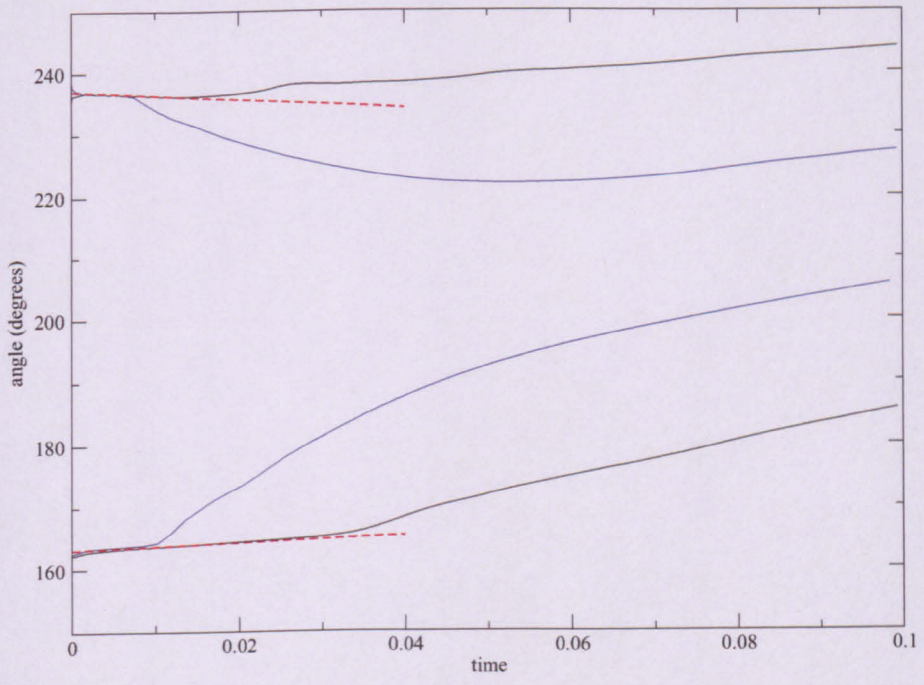

Figure 3.12: Numerical (solid lines) and analytic (dashed red lines) evolution of the angle φ, for junction A1, for two cases with $\rho > 0$ and two with $\rho < 0$; all close to the critical value $\rho = 0$ (blue lines are closer to the critical value). For $\rho < 0$ (bottom curves) the Y-junction is said to be unstable, since vertex A moves along the butterfly wing until it reaches 180°, and then it starts moving towards the centre of the big arc, as shown in Fig. 3.10. For $\rho > 0$ (top curves), vertex A moves downwards, leading to a stable Y-junction. The analytic approximations are calculated using $R = 0.561$ and equations (3.54) and (3.55), which are linear truncations (in time), and only hold for small times since $\ell_{\min}^{A_1}(t) \sim h$. We choose $h = 0.01$.

the vertex A_1 moves downwards with an initial angle of $\varphi \geq \pi + \tan^{-1}(\sqrt{1-R^2}/R)$ (with the equality in the limit of $\rho \to 0$) from the x-axis, as can be seen in Fig. 3.12. In this case the perturbation does not grow and, for a tension μ_2 big enough, it may even collapse faster than the central bridge does. However, for $\rho < 0$ the local curvature is such that the strings of the triangular perturbation grow in σ-space. In real space, vertex A_1 initially moves rapidly away from the y-axis and almost along the butterfly wing (string 1), which corresponds to an initial angle of $\varphi \leq \pi - \tan^{-1}(R/(1-\sqrt{1-R^2})$ from the x-axis. In figures 3.10 and 3.12, one can see this initial evolution. Later in the evolution (when the angle φ reaches π), the segment A_1A_2 changes from convex to concave, and the vertex A_1 evolves like any other point on the big arc segment, hence moving towards the centre of the butterfly wing, as one can see in the last two plots of Fig. 3.10. Therefore, for $\rho < 0$ the perturbation grows for some time (which depends

on how negative ρ initially is), implying the original butterfly Y-junction is unstable, leading to the criterion for stability based on simply obtaining the value for ρ.

3.5 Discussion

In this chapter, we have extended previous studies on the dynamics of cosmic strings to include the description of the situations one expects in cosmic superstring networks, namely, the formation of junctions when strings of different kind form bound states.

We concentrated on a specific configuration and we centered our attention on the comparison of Nambu-Goto and field theory numerical simulations. The advantage of the Nambu-Goto approach is its simplicity, both analytical and numerical. The reduction in the degrees of freedom compared to field theory simulations allows for numerical computations with larger dynamic range. However, we know that the Nambu-Goto description breaks down when two strings cross, loops contract to a point, or when junctions collide. This is well established for the case of usual Abelian cosmic strings, but algorithms have been developed (using feedback from the field theory results) which nevertheless allow the Nambu-Goto approach to be used to model the evolution of a cosmic string network. Establishing similar confidence for the case of cosmic strings with junctions is of crucial importance. In this work, we have been able to explore some aspects of the relationship between the two approaches.

We saw that, when it comes to the general dynamics, the Nambu-Goto action models very well the evolution of a configuration of strings with junctions. However, the field theory approach unravelled a new phenomenon, a new instability that could not be possibly seen using solely the Nambu-Goto method. We saw that a junction can in

fact break into three new junctions, hence the composite string unzips, changing completely the dynamics and evolution of the loop. Studying our field theory model, we realized that for weakly-bound composites the junctions can cause the strings to unzip, causing the aforementioned instability. We also discovered that we can in fact model this using Nambu-Goto dynamics, provided that we use appropriate initial conditions, i.e. introducing a perturbation consisting of three initially tiny strings with equal tensions and letting the loop evolve. Remarkably, we could then predict when a junction would unzip or not, depending on a single parameter, the angle ρ. With this done the agreement between the two methods is remarkably good.

Our chosen configuration is not, of course, representative of a cosmological network of cosmic superstrings. The key point here is that, given the feedback from field theory, we were able to understand and model the instability using the Nambu-Goto method. As we have already mentioned, the kinematic constraints derived using the NG approach have been checked with field theory results and the agreement is (generally) good [112, 113, 144, 145]. We therefore believe it will again be possible to perform large-scale cosmological simulations of cosmic superstrings using the modified Nambu-Goto approach, in the same manner that it is possible to perform simulations of ordinary strings using the Nambu-Goto equations.

Chapter 4

Observational Signatures of Cosmic Strings

4.1 Introduction

In this chapter, we will attempt to review the most important observational consequences of cosmic strings [5, 6]. We concentrate on strings whose interactions are primarily gravitational, determined by the value of $G\mu$. We will present results and constraints from lensing, gravitational radiation, CMB and pulsar timing.

When possible, we will extrapolate these results to cosmic superstrings. However, most of the work on the subject of cosmic superstrings has been more qualitative than quantitative, since the rich features of cosmic superstring networks cannot be fully implemented in the calculations. Recently, however, more systematic efforts to quantify the cosmological effects of cosmic superstrings have appeared in the literature — we will highlight them where appropriate.

4.2 Lensing

Let us start by studying the gravitational properties of a straight string lying along the z-axis [5]. The Poisson equation for the Newtonian gravitational potential ϕ is

$$\nabla^2\phi = 4\pi G(\rho + p_x + p_y + p_z). \tag{4.1}$$

The string under consideration has an equation of state $p_z = -\rho, p_x = p_y = 0$. This gives $\nabla^2\phi = 0$. As a result, straight strings do not exert a gravitational force on any surrounding matter. This unusual property is a result of the string's tension, which acts as a negative gravitational source cancelling out the effect of the string's mass.

Taking the zero-width approximation and assuming that the gravitational field of the string is sufficiently weak, we can linearise the Einstein equations and derive the space-time metric of a straight static string. We find [36]

$$ds^2 = dt^2 - dz^2 - dr^2 - r^2 d\theta^2 \tag{4.2}$$

in cylindrical coordinates (r, θ, z). The metric has a Minkowskian form, which means that the spatial geometry around the string is locally Euclidean. However, this is not true globally, since the angle θ does not vary in the full range $0 \leq \theta \leq 2\pi$, but in the smaller range

$$0 \leq \theta \leq 2\pi(1 - 4G\mu). \tag{4.3}$$

The geometry is actually conical, with a global deficit angle

$$\Delta = 8\pi G\mu. \tag{4.4}$$

For a GUT string, we expect that $G\mu$ is of order $10^{-6} - 10^{-7}$, and the deficit angle is a few seconds of arc.

The string acts as a cylindrical lens (Fig. 4.1). If a light source (e.g. a galaxy) is behind it, the result of the string's conical geometry is to create double images with a typical angular separation of order Δ, similar magnitude, and no distortion [146, 147]. This feature is quite unique, as most classical lenses (ordinary compact matter) produce odd numbers of images with distortion. The presice formula for the angular separation $\delta\alpha$ of the images is [146, 147]

$$\delta\alpha = \frac{D_{ls}}{D_s}\Delta \sin\theta, \tag{4.5}$$

where D_{ls} is the normal distance of the source from the lens (the cosmic string), D_s is the normal distance between the source and the observer, and θ is the angle between the line of sight and the tangent to the string. Furthermore, observing in the vicinity of

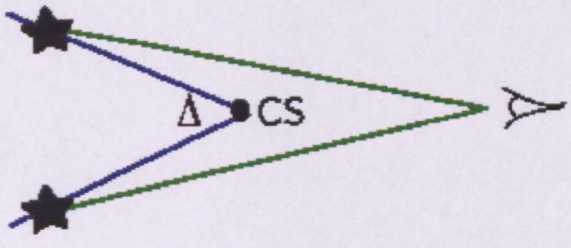

Figure 4.1: The lensing of a distant light source by a cosmic string (CS).

a lensing effect due to a cosmic string should reveal an array of additional lensed pairs [148].

Our previous analysis is only valid for a straight, static string. In fact, as we have already discussed, there is a great deal of small scale structure (wiggliness) on the strings. An observer will not be able to resolve the small scale structure, but its effect can be quantified by an effective energy per unit length, U, which is larger than μ. On the contrary, the effective tension T is reduced. Overall, we will have a $UT = \mu^2$ equation of state [149, 150]. Hence, there is a non-zero gravitational acceleration towards the string, proportional to $U - T$. In that case, the expression for the angular

separation becomes [151]

$$\delta\alpha = \frac{D_{ls}}{D_s} 8\pi G U \sin\theta. \tag{4.6}$$

For straight strings with velocity $\mathbf{v}$, the corresponding formula is [125, 126]

$$\delta\alpha = 8\pi G\mu\sqrt{\gamma^2(1+\hat{\mathbf{n}}\cdot\mathbf{v})^2 - \cos^2\theta}\,\frac{D_{ls}}{D_s}, \tag{4.7}$$

where $\hat{\mathbf{n}}$ is the unit vector along the line of sight. The lensing effect of a string is *enhanced* by its motion.

An observation suspected to be a signature of cosmic string lensing was reported in [152]. Unfortunately, further investigation proved that the observed object was actually a pair of interacting giant elliptical galaxies [124]. A recent paper [153] investigated possible cosmic-string lensing candidates using imaging surveys. Their non-detection placed un upper limit on the cosmic string tension, $G\mu < 6.5 \cdot 10^{-7}$.

Other suggested ways to detect cosmic strings are via microlensing or weak lensing. Microlensing occurs when the lens and the source are in relative motion. This leads to a measurable change of the apparent luminosity of the source over time, making microlensing a very useful method of detection when the image splitting is too small for astronomical measurements to resolve (i.e. when the lens mass is too low). A recent study [127] investigated the possibility of detecting gravitational microlensing of distant quasars by cosmic strings. Their calculation showed that the expected event rate from long strings is very small, and the lensing time-scale too long. Furthermore, the small loops contributions do not seem to enhance the detectability. Even when the more optimistic estimations are made, CMB constraints significantly reduce the available parameter space. The weak lensing properties of cosmic strings were recently studied in [154]. The authors found that no signal exists for straight strings, and a

small, difficult to detect signal is produced from strings with small scale-structure.

Finally, the lensing effects due to strings binding together to form Y-shaped junctions were studied in [126, 155]. In the case of a static junction of three coplanar strings, it was shown that an observer looking at a light source located behind the plane of the strings will see three identical images. In fact, the force balance condition at the junction, $\sum \vec{\mu}_i = 0$, leads to a similar balance condition for the angular separations, $\sum \delta\vec{\alpha}_i = 0$, allowing for the relative tensions of the strings to be determined.

4.3 Gravitational Radiation

4.3.1 The weak-field approximation

We will briefly review the weak-field treatment of a gravitating cosmic string [5, 49]. For strings with energy scale $\eta \ll m_{pl}$, the weak-field treatment is generally applicable, excluding the small regions around cusps and kinks.

Using the weak-field approximation, the spacetime metric can be written as a small perturbation away from flat Minkowski space. That is

$$g_{\mu\nu} = \eta_{\mu\nu} + h_{\mu\nu}, \quad |h_{\mu\nu} \ll 1|. \tag{4.8}$$

Linearizing in $h_{\mu\nu}$ and using the harmonic gauge conditions

$$\partial_\nu \left(h^\nu_\mu - \frac{1}{2}\delta^\nu_\mu h^\sigma_\sigma \right) = 0,$$

the Einstein equations take the form

$$\Box h_{\mu\nu} = -16\pi G S_{\mu\nu}, \tag{4.9}$$

with $\Box \equiv \partial_t^2 - \nabla^2$ the flat space d'Alembertian and $S_{\mu\nu} = T_{\mu\nu} - \frac{1}{2}\eta_{\mu\nu}T^{\sigma}_{\sigma}$.

The standard retarded solution to equation (4.9) is

$$h_{\mu\nu} = -4G \int \frac{S_{\mu\nu}(t', \mathbf{x}')}{|\mathbf{x} - \mathbf{x}'|} d^3x', \tag{4.10}$$

where t' is the retarded time $t - |\mathbf{x} - \mathbf{x}'|$. This means that the source points $(t', \mathbf{x}')$ cover all points on the past light cone of the field point $(t, \mathbf{x})$ for which $S_{\mu\nu} \neq 0$ [49]. Using equation (2.14) for the string's energy momentum tensor we find [58]

$$h_{\mu\nu}(t, \mathbf{x}) = -4G\mu \int \frac{F_{\mu\nu}(\tau, \sigma)}{|\mathbf{x} - \mathbf{r}(\tau, \sigma)|} [1 - \mathbf{n} \cdot \dot{\mathbf{r}}(\tau, \sigma)]^{-1} d\sigma, \tag{4.11}$$

where $F_{\mu\nu} = \dot{x}_\mu \dot{x}_\nu - x'_\mu x'_\nu + \eta_{\mu\nu} x'^{\sigma} x'_{\sigma}$, $\mathbf{n} = (\mathbf{x} - \mathbf{r}(\tau, \sigma))/|\mathbf{x} - \mathbf{r}(\tau, \sigma)|$ is the unit vector from the source point $\mathbf{r}$ to the field point $\mathbf{x}$ and $\tau = t - |\mathbf{x} - \mathbf{r}(\tau, \sigma)|$. If the source is a periodic loop with period T and length L, the time average of $h_{\mu\nu}$ over one oscillation is [58]

$$\langle h_{\mu\nu}(\mathbf{x}) \rangle = -\frac{4G\mu}{T} \int_0^T \int_0^L \frac{F_{\mu\nu}(\tau, \sigma)}{|\mathbf{x} - \mathbf{r}(\tau, \sigma)|} d\sigma d\tau. \tag{4.12}$$

Note that equation (4.11) diverges if the string contains a cusp, where $|\dot{\mathbf{r}}| = 1$, so that a cusp emits a thin pulse of gravitational energy in the direction of its motion. We will futher analyse the gravitational bursts from cusps (and kinks) in Section 4.3.4. Also note that, in most cases, the approximation $\mathbf{n} = \mathbf{x}/|\mathbf{x}|, r = |\mathbf{x}|$ is used, since we are interested in the energy transmitted at large distances from the source.

4.3.2 Gravitational Radiation from cosmic string loops

We have already discussed that gravitational wave emission is the main energy loss mechanism for an oscillating macroscopic string loop. The gravitational radiation

power for an isolated string loop of length L can be estimated using the quadrapole formula [15]

$$P \propto G\left(\frac{d^3D}{dt^3}\right)^2, \tag{4.13}$$

where D is the quadrupole moment. With $D \sim ML^2$, where $M \sim \mu L$ is the mass of the loop, and $\omega \sim L^{-1}$ the characteristic frequency, we find

$$P = \Gamma G\mu^2, \tag{4.14}$$

where Γ, the radiative efficiency coefficient, is a constant to be determined. Note that the power is independent of the size L of the loop. Then, the lifetime of the loop is given by

$$\tau \sim \frac{M}{P} \sim \frac{L}{\Gamma G\mu}. \tag{4.15}$$

However, the quadrupole formula cannot be trusted for relativistic sources, so we need to use the full relativistic formalism [5, 6].

In the weak-field approximation, the power from an isolated periodic source can be calculated as [15]

$$P = \dot{E} = \sum_n P_n = \sum_n \int d\Omega \frac{dP_n}{d\Omega}, \tag{4.16}$$

where

$$\frac{dP_n}{d\Omega} = \frac{G\omega_n^2}{\pi}\left[T^*_{\mu\nu}(\omega_n, \mathbf{k})T^{\mu\nu}(\omega_n, \mathbf{k}) - \frac{1}{2}|T^\nu_\nu(\omega_n, \mathbf{k})|^2\right] \tag{4.17}$$

is the radiation power per unit solid angle at frequency $\omega_n = 2\pi n/T$ in the $\mathbf{k}$-direction, $|\mathbf{k}| = \omega_n$, T the oscillation period and

$$T^{\mu\nu}(\omega_n, \mathbf{k}) = \frac{1}{T}\int_0^T dt e^{i\omega_n t}\int d^3x e^{-i\mathbf{k}\cdot\mathbf{x}}T^{\mu\nu}(\mathbf{x}, t) \tag{4.18}$$

is the Fourier transform of the energy-momentum tensor.

The first studies of the radiated power from simple loops using the above formalism were performed in [83] and [61]. In [83], the authors studied the gravitational radiation emission from the Kibble-Turok family of loop solutions, while [61] was devoted to the Burden solutions (see Section 2.3.2), for which the angular distribution of radiated power $dP_n/d\Omega$ can be expressed analytically in terms of Bessel functions. Both studies found $\Gamma \sim 100$. A similar study, but for the cuspless kinked loops [59], found $\Gamma \sim 50 - 100$. Note that, in some special cases, the power diverges due to the presence of persistent cusps.

A more thorough numerical investigation was performed in [156]. The authors studied the gravitational radiation power from cosmic string loops produced in a flat space numerical simulation of loop fragmentation. The gravitational radiation was found to be strongly peaked in the region $\Gamma = 40 - 60$. A numerical treatment in an expanding universe [74] produced very similar results, with $\langle\Gamma\rangle \approx 65$. In Fig. 4.2 we present our

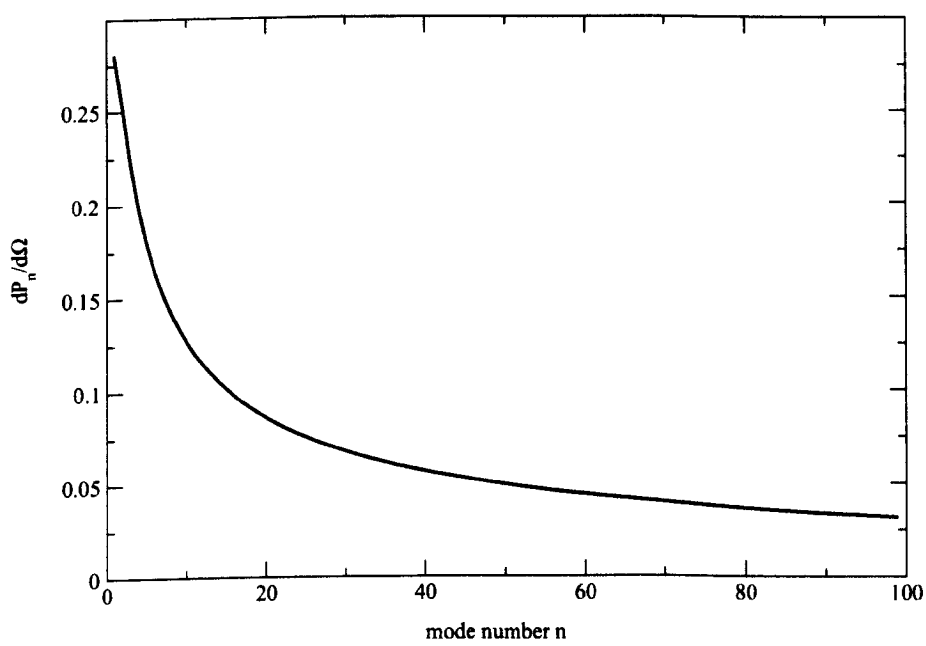

Figure 4.2: $dP_n/d\Omega$ in the equatorial plane for the planar circular loop. The radiation falls slowly with increasing mode number n (c.f. with Fig.3 in [74]).

results for the gravitational emission $dP_n/d\Omega$ in the equatorial plane direction from an idealised[1] planar circular loop using a simple numerical algorithm. Our discrete circular loop consists of 1000 points, and the numerical result is indistinguishable from the analytics (c.f. with Fig. 3 in [74]). Finally, analytical and numerical work in [158, 159, 160] improved the previous results and showed the possible existence of a lower bound in the radiative efficiency of cosmic string loops, $\Gamma_{min} \simeq 39$ [160].

4.3.3 Gravitational Radiation from wiggly strings

Using the weak field formalism, we can also estimate the power radiated from wiggly strings. In [161], the gravitational radiation from a helical string was studied. Letting $u = \sigma + t$, $v = \sigma - t$, the string's trajectory has the form $x^\mu = [t, \frac{1}{2}(\mathbf{a} + \mathbf{b})]$, with

$$\mathbf{a}(u) = \left[\frac{\epsilon}{\Omega}\cos(\Omega u), \frac{\epsilon}{\Omega}\sin(\Omega u), \sqrt{1-\epsilon^2}u\right], \tag{4.19}$$

$$\mathbf{b}(v) = \left[\frac{\epsilon}{\Omega}\cos(\Omega v), \frac{\epsilon}{\Omega}\sin(\Omega v), \sqrt{1-\epsilon^2}v\right], \tag{4.20}$$

where Ω is the breathing frequency of the helix and the parameter ϵ is its winding number per unit length ($0 \leq \epsilon < 1$). In the limit $\epsilon \to 0$, the trajectory is just a straight line across the z-axis. The energy-momentum tensor for this trajectory is periodic in time with period $2\pi\Omega^{-1}$, and also periodic in z with period $2\pi\Omega^{-1}\sqrt{1-\epsilon^2}$. Due to the symmetry of the problem, it is convenient to study the radiated power through a cylinder centered on the source and having a radius much larger than the size of the source. Then, the expression for the radiated power per unit angle per unit length

[1] As we have already mentioned, a realistic circular loop would collapse to form a black hole [60]. For the calculation of the radiated power per unit solid angle in this situation, see [157].

becomes [161]

$$\frac{dP}{dzd\theta} = 2G\sum_{\omega}\sum_{k_z}\omega\left[T^{*}_{\mu\nu}(\omega_n,\mathbf{k})T^{\mu\nu}(\omega_n,\mathbf{k}) - \frac{1}{2}|T^{\nu}_{\nu}(\omega_n,\mathbf{k})|^2\right], \tag{4.21}$$

where $\omega = |\mathbf{k}|$, $\mathbf{k} = (\mathbf{k}_\perp, k_z)$ and the energy flux is calculated in the $\mathbf{k}_\perp$ direction. Since there is no explicit dependence on the angle θ, the total power per unit length in the z-direction is found by multiplying the RHS of equation (4.21) with 2π. The energy per unit length $\hat{E}$ along the z-axis can be written as [161]

$$\hat{E} = \frac{\mu}{\sqrt{1-\epsilon^2}}. \tag{4.22}$$

For this reason, the radiated power diverges as $\epsilon \longrightarrow 1$. On the other hand, in the limit $\epsilon \longrightarrow 0$ the power vanishes, since the trajectory reduces to that of a static straight string. In [161], the radiated power as a function of ϵ was calculated numerically, finding an increasing power with increasing ϵ. The radiated power for a given ϵ decreases with increasing frequency ω, while the contribution from odd frequencies becomes less important with increasing ϵ. For small ϵ, almost all the power is emitted at the lowest even mode. Finally, the gravitational damping of the oscillations was found to be efficient for large-amplitude waves ($\epsilon \sim 1$).

This work was later generalised in [162, 163]. The general case can be treated as a straight string with small-amplitude transverse perturbations. The most important result is that both right- and left-moving modes are required to produce gravitational radiation. If all the travelling waves on the string move along one direction, the radiation power vanishes.

It is interesting to note that, in a recent treatment of GW emission from strings at a stationary junction [164], it was found that a purely left-moving wave, generated on one string leg, is partly reflected and transferred from the junction, resulting in the

necessary mixing of left- and right-moving modes.

4.3.4 Gravitational Radiation from cusps and kinks

The gravitational wave bursts (GWB) from cosmic string cusps and kinks were studied in detail in [128, 165]. The scope of these papers was to assess whether conventional cosmic strings could be detectable from gravitational wave detectors such as LIGO/Advanced LIGO and LISA.

The authors of [128, 165] first calculate the logarithmic cusp waveform for a closed loop of length L:

$$h^{cusp}(f,\mathbf{n}) \sim \frac{G\mu L}{r(|f|L)^{1/3}}\Theta(\theta_m(f)-\theta). \tag{4.23}$$

Here, $f = \omega_m/2\pi = 2m/L$ is the frequency, $\Theta(x)$ is the step function (1 if $x > 0$; 0 if $x < 0$), θ is the angle between the wave vector $\mathbf{n}$ and the cusp vector $\mathbf{n}^c$, and $\theta_m \simeq (2/L|f|)^{1/3}$ gives the opening angle of the cone where the GWB from the cusp is concentrated. As we can see, there is a very slow decay with the mode number $|m|^{-1/3}$. The analogous calculation for a *kink* revealed a $|m|^{-2/3}$ dependence, so we expect stronger signals from cusps.

In order to sum the individual contributions from a network of cosmic string loops in the Universe, the authors of [128, 165] consider the one-scale model, where the typical length and number density of loops are given by

$$L \sim \alpha t, \;\; n_L(t) \sim \alpha^{-1}t^{-3}, \tag{4.24}$$

where $\alpha \sim \Gamma G\mu$, with $\Gamma \sim 50$. The number of cusp events per unit spacetime volume

is then given by

$$\nu(t) \sim \frac{cn_L(t)}{PT_L} \sim 2cP^{-1}\alpha^{-2}t^{-4}, \tag{4.25}$$

where P is the intercommuting probability (equal to unity for the usual cosmic strings in consideration), while c is the average number of cusps per loop period $T_L = L/2 \sim \alpha t/2$. The waveform frequency is redshifted as $f \rightarrow (1+z)f$ in an expanding universe, and also r must be transformed to the physical distance $a_0 r = (1+z)D_A(z)$, where $D_A(z)$ is the angular diameter distance at redshift z. The estimate for the rate of GWB's observed around frequency f coming from the spacetime volume in redshift interval dz is [165]

$$d\dot{N} \sim \frac{\nu(z)}{(1+z)} \frac{\pi\theta_m^2(z)D_A(z)^2}{(1+z)H(z)} dz. \tag{4.26}$$

The analogous result for kinks depends, of course, on the average number of kinks per loop and has a θ_m dependence, since the burst from kinks is emitted in a fan of directions of solid angle $\sim \theta_m$ instead of a cone of solid angle $\sim \theta_m^2$ (cusps).

Allowing for $G\mu$ to vary with an upper bound of 10^{-6}, the authors of [128, 165] found that, even if only 10% of the loops in a network have cusps (i.e. $c = 0.1$), their GW bursts could be detectable from GW detectors such as LIGO/VIRGO and LISA, for a wide range of tensions $10^{-13} < G\mu < 10^{-6}$. Even if the cusp events are very few, LISA could potentially detect GW bursts from kinks.

In a later paper [166], the authors generalised the above treatment to include cosmic superstrings, i.e. strings with lower intercommuting probability P. Considering the range $10^{-3} \leq P \leq 1$ and taking $c = 1$, they found that the signal is enhanced with decreasing p, going above the noise levels of LIGO/Advanced LIGO, and well above the noise levels of LISA, for a $10^{-13} < G\mu < 10^{-6}$ range of tensions. Also allowing

the fractional loop-length parameter $\alpha/\Gamma G\mu$ to vary as $10^{-12} < \alpha/\Gamma G\mu < 1$, they find that their previous results are quite robust, as long as $\alpha/\Gamma G\mu \geq 10^{-11}$ ($\alpha/\Gamma G\mu \geq 10^{-7}$) in the case of LIGO (LISA). The general point is that a smaller reconnection probability *enhances* the detectability of cosmic superstrings (for a detailed analysis including the effects of late time acceleration and different loop distributions, see [129, 167]).

The average number of cusps and kinks on cosmic string loops is still an open question, and their significance for GW emission has generated a fair amount of interest for the case of cosmic superstrings. In [168], it was shown that pairs of FD-string junctions, such as may form after F-D intercommutation in a cosmic superstring network born at the end of brane inflation, generically contain cusps. More importantly, their properties may allow for extra channels of energy loss, in addition to the usual GW background. In [169, 170, 171], the authors studied cosmic string loops containing junctions, finding a much bigger number of large amplitude kinks than the one expected for standard loops (kink 'proliferation'). For strings with small tensions ($G\mu \lesssim 10^{-12}$), a large number of kinks is allowed and the incoherent superposition of bursts emitted at kink-kink encounters leads to a GW background that is bigger than the usual individual bursts from cusps and kinks.

In [172, 173], the effect of extra dimensions on the GW signal from cusps was thoroughly investigated. The main feature arising due to the motion of cosmic superstrings in the extra dimensions is the avoidance of an exact cusp, since the unit curves $\mathrm{a}' = \mathrm{b}'$ will miss each other in the higher dimensional Kibble-Turok sphere. The authors generalise the exact cusp to a "near cusp event". The beaming cone is narrowed, resulting in a decreased θ_m value. The most important result is that the gravitational radiation

signal is *suppressed* — the kinematics have a larger effect than the reduced intercommutation probability. Thus the bounds found in [166] are relaxed. In a subsequent publication [174], the effect of extra dimensions on the kink signal was studied. The main result is that the damping of the kink signal is not as significant, and the GWB's from kinks on cosmic superstrings are more likely to be detected by LIGO or LISA.

4.4 Signatures and Constraints from CMB and pulsar timing

4.4.1 The Cosmic Microwave Background and Inflation

As we saw in Chapter 1, when the temperature of the Universe cooled down to about 1 eV, electrons and nuclei joined to form neutral atoms and the Universe became transparent. The CMB photons that were emitted after that era scattered freely, and they are observed today as a blackbody spectrum with $T = 2.725 \pm 0.001$ K (1σ) [23]. In the following, we will sketch the physics of the CMB , and see how today's observables are connected with the inflationary paradigm (see [175, 176, 177, 178, 179, 180] and references therein).

Along a direction (line of sight) $\mathbf{n} = (\theta, \phi)$ on the sky, the temperature fluctuation can be expressed as an expansion in spherical harmonics

$$T(\mathbf{n}) = \sum_{\ell m} a_{\ell m} Y_{\ell m}(\mathbf{n}), \tag{4.27}$$

where the index ℓ gives us the angular scale, with $\theta \sim \pi/\ell$ (i.e. large multipole moments represent small angular scales). The coefficients $a_{\ell m}$ give us the size of the

irregularities on different scales, with the power spectrum defined by

$$\langle a_{\ell m} a^*_{\ell' m'} \rangle = C_\ell \delta_{\ell \ell'} \delta_{m m'}, \tag{4.28}$$

with isotropy implying that all m's are equivalent. We usually plot the quantity $(\Delta T)^2 = \ell(\ell+1)C_\ell/2\pi$, which represents the power per logarithmic interval in ℓ.

The temperature of the CMB is astonishingly uniform across the sky, exhibiting only minute fluctuations at the 10^{-5} level, which have been analysed by the COBE [181] and WMAP [14] satellites. In Fig. 4.3, we show the latest temperature power spectrum as measured by WMAP. Because the fluctuations are so small, we can use

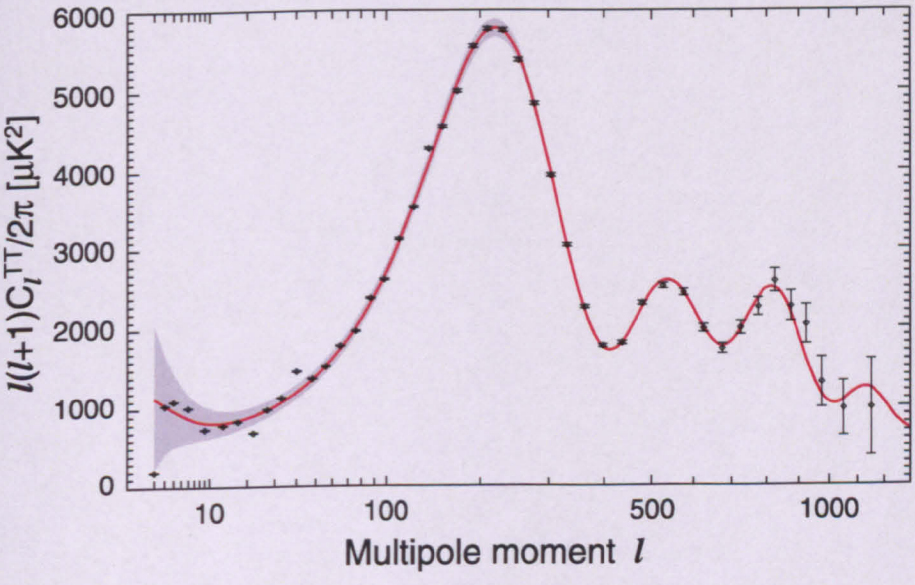

Figure 4.3: The 7-year temperature (TT) power spectrum from WMAP. The curve is the ΛCDM model best fit.

linear perturbation theory to describe them. Considering a spatially flat background metric with linear scalar, vector and tensor perturbations, we can use the decomposition theorem to treat them separately. Without a source term, the vector perturbations decay in an expanding background and can be neglected. For the scalar and tensor perturbations, we can write

$$ds^2 = a^2(\tau)\{(1+2\Psi)d\tau^2 - [(1-2\Phi)\delta_{ij} + h_{ij}]dx^i dx^j\}, \tag{4.29}$$

where the Newtonian-like potentials Ψ and Φ represent the density (scalar) perturbations, while the tranverse and trace-free h_{ij} describes the tensor perturbations (gravitational waves). For an isotropic energy-momentum tensor, we have $\Phi = \Psi$. We can now see how inflation comes into the picture — during the period of accelerated expansion, we have a generation of quantum fluctuations which are getting stretced to become classical superhorizon density perturbations. They can be expressed as spatially varying quantum perturbations around the homogeneous background of the inflaton field. That is

$$\phi(t, \mathbf{x}) = \phi_0(t) + \delta\phi(t, \mathbf{x}). \tag{4.30}$$

After horizon re-entry, these fluctuations source the density perturbations which form the large-scale structure of the Universe via gravitational collapse. The variance of these fluctuations results in a power spectrum in Fourier space. Within the slow-roll approximation, we get [182]

$$P_S(k) \approx A_s(k/k_0)^{n_s - 1} \tag{4.31}$$

for the scalar modes, and

$$P_T(k) \approx A_t(k/k_0)^{n_t} \tag{4.32}$$

for the tensor modes, where k_0 is some pivot wavenumber. The amplitudes are given by $A_s = \frac{8\pi G H^2}{\pi\epsilon}$, $A_t \equiv r A_s = 16\epsilon A_s$, and the "spectral indices" are $n_s - 1 = -4\epsilon + 2\eta$, $n_t = -2\epsilon$. Note that H is the Hubble parameter during inflation evaluated when $k_0 = aH$, i.e. when the mode with physical wavenumber k_0/a exits the horizon H^{-1}. Through the ϵ and η dependence, we deduce that the inflationary predictions for the power spectra basically rely upon the inflationary potential $V(\phi)$ and its derivatives. It

is then evident that CMB observations of high precision are our best tool to constrain inflationary physics.

At this point, let us just state the basic predictions of the inflationary paradigm, which established it as the primary candidate for the generation of the primordial inhomogeneities. The simplest inflationary models predict a *flat* geometry — we have already seen that this has been tested to a very high accuracy, 1%, by measuring the position of the first peak in the CMB [16]. They also predict *Gaussianity* and near *scale-invariance*, namely $n_s \simeq 1$, $n_t \simeq 0$ to first approximation. To be more precise, small deviations from scale invariance are predicted by the vast majority of inflationary models. The 7-year WMAP data give $n_s = 0.9603 \pm 0.014$ [12]. In addition, inflation predicts *primordial gravitational waves*, the yet unobserved tensor modes. Denoting by r the ratio of the tensor to scalar spectra at some ℓ, different inflationary models will lead to different predictions — this is again due to the $V(\phi)$ dependence. The value of r is still difficult to constrain, but an upper limit combining WMAP5 and other data is found to be $r < 0.22$ [183].

For completeness, we will now sketch the underlying physics behind the CMB spectra we observe today. Before and around recombination, which is our time of interest, we can approximate the photon-baryon plasma as a tightly coupled fluid. There is also dark matter, which of course interacts only gravitationally, and its perturbations grow as the Universe expands. For the photon-baryon fluid, there is a competition between gravitationally driven collapse, and a restoring pressure force. More specifically, the equation for the fractional temperature fluctuation Θ in wavenumber space is [184]

$$[(1+B)\dot{\Theta}]^{\cdot} + \frac{k^2}{3}\Theta = -\frac{k^2}{3}(1+B)\Psi - [(1+B)\dot{\Phi}]^{\cdot}, \tag{4.33}$$

where $c_s^2 = 1/3(1+B)$ is the photon-baryon sound speed and $B = \frac{\rho_b + p_b}{\rho_\gamma + p_\gamma}$ is the baryon inertia. Deconstructing this equation gives us almost all the information we need to understand the general form of the TT spectrum (4.3).

Let us first ignore the effect of baryon inertia (i.e. take $B = 0$) and consider constant gravitational potentials. This gives

$$\ddot{\Theta} + c_s^2 k^2 \Theta = 0, \tag{4.34}$$

which is the simplest harmonic oscillator equation, with $c_s^2 = 1/3$ for the photon-dominated fluid. With the initial conditions $\Theta(0)$ and $\dot{\Theta}_0$, the solution to equation (4.34) can be written as

$$\Theta(\tau) = \Theta(0)\cos(ks) + \frac{\dot{\Theta}(0)}{kc_s}\sin(ks), \tag{4.35}$$

where $s \equiv \int c_s d\tau$ gives us the sound horizon. Using adiabatic initial conditions, which is the case for inflation, we have $\dot{\Theta}_0 = 0$ and at recombination time τ_* we have

$$\Theta(\tau_*) = \Theta(0)\cos(ks_*). \tag{4.36}$$

We see that all wavelengths share the same starting phase — they are *temporally coherent*. However, different k will result in different oscillation periods. Hence, at the last scattering surface different wavelengths will be "caught" at different phases. For example, for very large modes $ks \ll 1$, the perturbation is frozen into its initial conditions. On smaller scales, we will have oscillations caught at their maxima or minima at recombination, resulting to peaks in the power at $k_n = n\pi/s_*$, where n is an integer. In addition, we will have modes which peak before reaching the recombination time — their amplitude will be very small at τ_* and they will correspond to power spectrum troughs.

Now let us include gravity. We have

$$\ddot{\Theta} + c_s^2 k^2 \Theta = -\frac{k^2}{3}\Psi - \ddot{\Phi}. \tag{4.37}$$

In a flat Universe and in the absense of pressure, Φ and Ψ are constant. Continuing neglecting the baryons, we can write $c_s^2 = 1/3$ and the new solution is

$$[\Theta + \Psi](\tau) = [\Theta + \Psi](0)\cos(ks). \tag{4.38}$$

Hence, $(\Theta + \Psi)$ is the effective temperature fluctuation we observe, with Ψ accounting for the energy loss of the photons when they overcome the gravitational potentials. In the large scale limit of equation (4.37) at recombination, we find

$$(\Theta + \Psi)(\tau_{rec}) = \frac{1}{3}\Psi(\tau_{rec}), \tag{4.39}$$

which is the so-called Sachs-Wolfe effect [185]. The shape of the CMB TT power spectrum at these scales is approximately flat and is known as the Sachs-Wolfe plateau.

Adding baryons, we finally get the full version of equation (4.33). Considering the case of $B = \text{const}$, we can write

$$[\Theta + \Psi](\tau_*) = [\Theta + (1 + B)\Psi](0)\cos(ks) - B\Psi, \tag{4.40}$$

where $s = \tau_*/\sqrt{3(1 + B)}$. We thus get an increase in the amplitude, a shift of the zero-point and a frequency decrease. The baryons drag the fluid deeper into the potential wells. The zero point shift breaks the symmetry of the oscillations, and the baryons enhance only the compressional phase, i.e. every other peak (first, third etc.). This general result is valid also for a time-variable B, but with an additional adiabatic damping effect. The specific peak positions and heights reflect the exact matter content of the Universe. The latest measurements give $\Omega_b h^2 = 0.02258$, $\Omega_c h^2 = 0.1109$ and $\Omega_\Lambda = 0.73$ [12], and the ΛCDM model is a perfect fit to the data (see Fig. 4.3).

After recombination, there is an additional contribution from the integrated Sachs-Wolfe effect taking into account the varying of the gravitational potentials. This contribution is a line integral of the form $\int_{rec}^{0} \dot{\Phi} d\tau$. At the smallest scales, the oscillations are heavily damped due to photon diffusion. This process is known as Silk damping [186]. Furthermore, the last scattering surface has a thickness, and averaging through it washes out anisotropy from small-scale fluctuations. Note that, in order to get an accurate description for the CMB spectra, we need to solve the Einstein equations simultaneously with the Boltzmann equations for all radiation and matter particles present. This can be done numerically using publicly available codes, like CMBFAST [187] or CAMB [188].

Another CMB observable which is becoming increasingly more important is CMB polarization. This is generated by Thomson scattering of photons by electrons, resulting to a scattered polarized light that reaches the observer. We can decompose the linear polarization pattern into a divergence part, the E-mode, and a curl part, the B-mode. We thus get 3 additional spectra, namely $C_\ell^{TE}, C_\ell^{EE}, C_\ell^{BB}$. Note that the B-mode spectrum can be sourced only by vector or tensor modes. This is extremely important: scalar modes only source E-modes, so the observation of a B-mode signal is a direct way of probing gravitational waves.

4.4.2 CMB anisotropy from cosmic strings

Now that we have a feel of the general features of the CMB spectra and their connection to the inflationary paradigm, let us return to cosmic strings. First, a historical note. Before the CMB data became available, strings were thought of as candidates

for generating the energy density inhomogeneities responsible for structure formation [58]. More specifically, the ratio $\delta\rho/\rho$ for GUT strings is

$$\frac{\delta\rho}{\rho} \sim G\mu \sim 10^{-6}, \tag{4.41}$$

which has the correct order of magnitude for seeding galaxy formation. Unfortunately, the data from WMAP showed an angular spectrum consisting of a series of peaks, while cosmic strings predict a pretty flat spectrum with a single, broad peak — note that this is hardly surprising, since the cosmic string generated fluctuations are not temporally coherent.

However, a contribution from cosmic strings cannot be excluded, but is limited to less than 10% of the total CMB temperature anisotropy [121, 189, 190, 191, 192, 193, 194, 195]. Although a network of cosmic strings cannot source the majority of the observed CMB TT spectrum, the CMB can be used to provide a distinctive signature of their existence through the B-mode polarization spectrum. That is because cosmic strings actively source scalar, tensor *and* vector perturbations, with the scalar and vector ones being of similar magnitude (see [196, 197, 198, 199, 200, 201, 202, 203] for work on the subject).

The effect of a moving string on the CMB anisotropy was first studied in [204]. The authors showed that a moving string will produce a line discontinuity in the temperature anisotropy maps. This anisotropy is given by

$$\frac{\delta T}{T} = G\mu\gamma(v)v, \tag{4.42}$$

where v is the transverse string velocity and $\gamma(v)$ the corresponding Lorentz factor. The so-called Kaiser-Stebbins effect is due to the conical spacetime around the string. Photons passing from the two sides of the string will be Doppler shifted, producing a

discontinuity separating a cold from a hot spot. However, this effect is quite difficult to detect — for a recent study, see [205].

As we already stated, the most promising way to detect cosmic strings is via the B-mode polarization spectrum. To evaluate CMB temperature and polarization spectra sourced by cosmic string networks, we can use the publicly available code CMBACT [206, 207], which is a modification of CMBFAST [187] to include anisotropies from *active* sources.

In CMBACT, the string network is represented as a collection of uncorrelated string segments, an approximation proposed in [208] and adapted for calculation of CMB spectra in [118, 206, 209]. In the unconnected segment model (USM), straight segments of strings are produced at some early time and given random/uncorrelated orientations and velocities. At later times, a certain fraction of the number of segments decays in such a way as to match the number density given by a scaling model. The initial positions and orientations of the segments are drawn from uniform distributions, and the direction of the velocity is taken to be uniformly distributed in the plane perpendicular to the string orientation (longitudinal velocities are neglected).

In the default version of CMBACT, the key parameters of the segments — namely their length, rms velocity and number density — are modelled using the VOS equations described in Section 2.4. The USM does not explicitly follow the loop distribution, however the energy in the loops is effectively included as part of the covariant conservation of the energy momentum of the scaling network. On their own, the straight string segments with open ends violate the energy conservation. To remedy this, CMBACT enforces energy conservation by calculating the components T_{00} and T_{ij} (with $i \neq j$) of the energy momentum tensor and then using the covariant conservation equa-

tion $\nabla^{\mu}T_{\mu\nu} = 0$ to calculate T_{0i} and T_{ii}. Finally, the Einstein and Boltzmann codes are integrated simulataneously. In Fig. 4.4 we show a typical CMB TT spectrum produced using CMBACT. The procedure one can follow to normalise to 10% of the total contri-

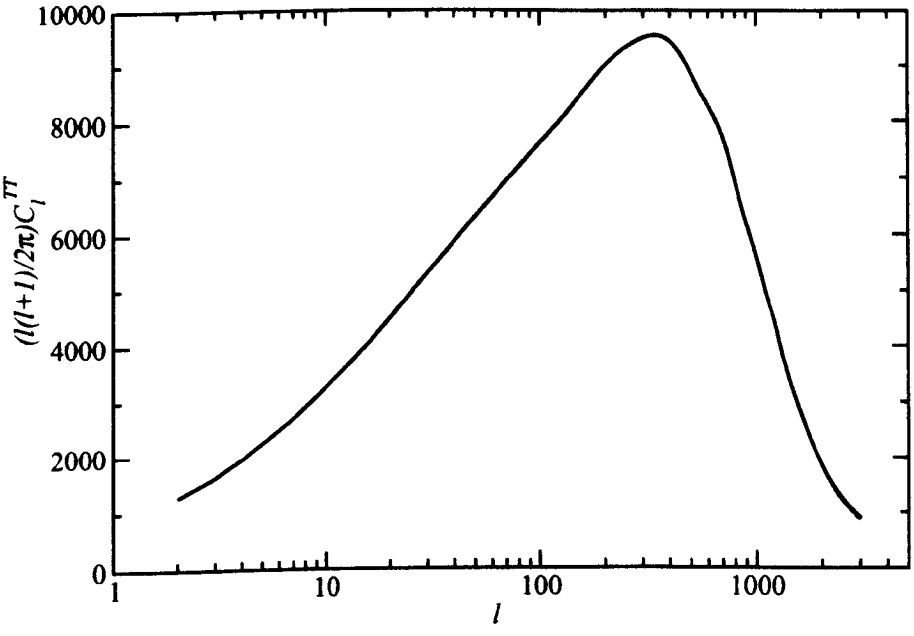

Figure 4.4: A typical CMB TT power spectrum induced by a cosmic string network using CMBACT.

bution is very simple [200]. First note that the overall amplitude of the CMB angular spectra C_ℓ is approximately determined by

$$C_\ell^{strings} \propto \left(\frac{G\mu}{\xi}\right)^2 . \tag{4.43}$$

Thus, we can define

$$C^{TT} \equiv \sum_{\ell=2}^{2000}(2\ell+1)C_\ell^{TT} \tag{4.44}$$

and adjust the free parameter of the code, namely $G\mu$, to satisfy

$$f_s = C^{TT}_{strings}/C^{TT}_{total} = 0.1 . \tag{4.45}$$

Then, the adjusted value of $G\mu$ can be used to study the properties of the B-mode spectrum. In [200], this approach was used to investigate how the macroscopic properties

of a cosmic string network affect the B-mode induced spectra. The correlation length and the rms velocity of the main string type set the dominant momentum modes in the strings stress-energy, which determine the position of the main peak. Larger string correlation lengths will move the peaks in the TT and BB spectra to lower ℓ. In addition, the rms velocity also controls the position of the peak, although the dependence is non linear. The positions of the TT and BB peaks move to higher multipoles (smaller scales) for low and moderate velocities, but move to larger scales (lower ℓ) for higher velocities. This non-trivial behaviour is a manifestation of the non-linear dependence of the string stress energy on string velocities. Also, larger values of v decrease the amount of BB power relative to TT power. The most important point is that, even with a marginal contribution to the TT spectrum (of the order of 1%), strings can be a prominent source of B mode polarization — that is, there is a predicted and observable systematic excess of B-mode power over what is expected from inflation [200].

4.4.3 Constraints on $G\mu$ from CMB and pulsar timing

In a very recent publication [195], updated constraints on the cosmic string tension using CMB and pulsar timing were derived. The authors first showed that the USM can successfully describe CMB spectra obtained from Nambu-Goto and Abelian-Higgs simulations, provided that the network parameters obtained from each simulation are used as an input.

They first derive upper bounds on $G\mu$ using the fact that the TT power spectrum produced by the string network must be limited to at most 10% contribution to the

total. For the Nambu-Goto simulations, the authors find

$$G\mu < 2.6 \times 10^{-7}, \tag{4.46}$$

and for the Abelian-Higgs simulations

$$G\mu < 6.4 \times 10^{-7}. \tag{4.47}$$

The gravitational wave emission from a cosmic string network, in particular from loop decay, would result in a stochastic GW background. Pulsar timing experiments place very strong constraints in the amount of this background that can be present in the Universe, using the fact that any gravitational waves which are propagating between us and a pulsar would disturb the photon trajectories causing fluctuations in the expected time of arrival of the observed pulses. In [195], the authors use the formula [210]

$$\Omega_g h^2 = 1.17 \times 10^{-4} G\mu \left(\frac{1 - \langle v_{\rm rad}^2 \rangle}{\xi_{\rm rad}^2 \Omega_{\rm m}} \right) \frac{(1 + 1.4x)^{3/2} - 1}{x}, \tag{4.48}$$

where $\Omega_g h^2$ is the energy density in gravitational waves, $x = \alpha/(\Gamma G\mu)$, α is the loop production size relative to the horizon, and $\Omega_{\rm m}$ is the total matter density relative to the critical density. They use parameters measured from the Nambu simulations to give $\xi_{\rm rad}$, $\langle v_{\rm rad}^2 \rangle$ and set $\Omega_{\rm m} = 0.3$, $\Gamma = 60$. Imposing the limit $\Omega_g h^2 < 2 \times 10^{-8}$ [211], they find

$$G\mu < 7 \times 10^{-7} \tag{4.49}$$

for $\alpha/(\Gamma G\mu \ll 1)$ and

$$G\mu < 5 \times 10^{-11}/\alpha \tag{4.50}$$

for $\alpha/(\Gamma G\mu \gg 1)$. We can easily see that the constraints coming from pulsar timing can potentially be stronger than the ones coming from CMB. However, the uncertainties in the pulsar timing method are large [195].

4.5 Discussion

In this chapter, we gave a fairly representative review of the observational signatures of cosmic strings. Where possible, we also presented results from recent work on the analogous signatures from cosmic strings with junctions and/or cosmic superstrings. We paid special attention on the work on cusp/kink formation and gravitational wave bursts from cosmic superstrings. Further studies on the average number of cusps per loop oscillation and the characteristic loop size would boost this area of research, for both cosmic strings and superstrings.

We also stressed that, arguably, the B-mode polarization is our best chance of probing a cosmic string network. In the next chapter, we will investigate the CMB imprints of a cosmic superstring network. In order to determine the network's evolution, we will make use of the latest string-theory calculations for the intercommuting probabilities of cosmic superstrings, and we will incorporate them to an extension of the VOS model which includes the kinematic constraints for the formation of junctions. We will then use a modified version of CMBACT, in order to include a multi-tension network of different string types.

Chapter 5

Cosmological Implications of multi-tension Cosmic Superstring Networks

5.1 Introduction

Although it has been established that a network of cosmic strings cannot source the majority of the observed cosmic microwave background (CMB) temperature anisotropy [118], the CMB can still provide a distinctive signature of their presence through the specific primordial B-mode polarization spectrum [196, 197, 198, 199, 200, 201, 202, 203]. The spectrum generated by strings is different from the one generically produced from tensor modes arising in inflationary scenarios, and future probes of the B-mode should be able to reveal the presence of cosmic strings, even if strings contribute as little as 0.1% to the CMB temperature anisotropy [199, 200, 201, 202, 203].

Interest in cosmic strings has revived following the realisation that they can arise in superstring theory [45, 46], for example in models of brane inflation [42, 43, 44, 103, 212, 213]. Cosmic superstrings can have small tensions ($10^{-12} \gtrsim G\mu \gtrsim 10^{-7}$ [45, 46, 107]), can be effectively stable over cosmological timescales, and can stretch over cosmological distances [104, 106, 214]. Hence, they can have interesting cosmological implications. Furthermore, their intercommutation probabilities can be significantly less than unity [46, 105, 135, 136] and, because of the charges present on them, they can zip together to form Y-junctions (trilinear vertices), leading to more complicated networks than those usually considered in the case of 'standard' Abelian cosmic strings. Understanding the imprint of such additional network features on observables, such as CMB temperature and polarization, is a step that may lead to interesting new constraints on the basic parameters of the string theory, such as the string coupling g_s and the fundamental string tension μ_F.

Several approaches have been developed to model the evolution of cosmic string networks, and an interesting recent attempt to extend them to cosmic superstring networks – which contain different types of string – is due to Tye, Wasserman and Wyman [215]. Their model, based on the velocity-dependent one-scale model of Martins and Shellard [79, 80], describes the evolution of a multiple tension string network (MTSN) under the assumption that all types of strings have the same correlation length and root-mean-square (RMS) velocity. Studying the evolution of the number density of strings, they find that scaling is achieved when the energy associated to the formation of junctions is assumed to be radiated away. This model has been extended in [216], where the authors assigned a different correlation length and velocity to each string type, and enforced energy conservation at each junction. Scaling is again achieved

(with different number densities), but not as generically as in [215].

In a complementary approach, a number of authors have studied the kinematics of cosmic string collisions [51, 52, 168]. When two Nambu-Goto (NG) strings (of generally different tensions) collide, rather than intercommuting in the standard way, they can form two junctions and a linking string of a third tension. Kinematically this can only occur if the relative orientation, velocity and string tensions lie in certain ranges. In [111], the authors extended their earlier studies to (p, q)-cosmic superstrings by modifying the NG equations to take into account the additional requirements of flux conservation. Once again the kinematic conditions required for the formation of Y-junctions were established, with results very similar to the ones obtained for NG strings. These kinematic constraints have been checked quite extensively with dynamical field theory simulations of strings collisions, and the agreement is (generally) good [112, 113, 144, 145, 217]. In a recent publication [218], they have been incorporated into the model of [216], giving the new conditions required for scaling.

In the following, we will use the model of [218] to study the evolution of a cosmic superstring network for different values of the string coupling g_s and different charges (p, q) on the strings. We find that in all cases the three lightest strings, i. e. the $(1, 0)$, $(0, 1)$ and $(1, 1)$ strings, dominate the string *number* density. When the string coupling is large, $g_s \sim \mathcal{O}(1)$, most of the network *energy* density is in the lightest $(1, 0)$ and $(0, 1)$ strings (respectively F- and D-strings), whose tensions are approximately equal — the contribution from the $(1, 1)$ FD-string is subdominant. At smaller values of $g_s \sim \mathcal{O}(10^{-2})$, the $(1, 0)$ string becomes much lighter than both $(0, 1)$ and $(1, 1)$, and dominates the string *number* density. However, the rarer $(0, 1)$ and $(1, 1)$ strings dominate the *energy* density of the network at small couplings because of their much

larger tension. In either of the two limiting regimes, the *energy* density of the multi-tension network is effectively dominated by strings of one tension.

With the scaling solutions to hand we then focus on the CMB imprints of these networks, using a modified version of the publicly available code CMBACT [206, 207]. In particular, we extend the Unconnected Segment Model (USM), first introduced in [118, 209], to describe the MTSN of [218] and implement it in CMBACT to obtain the CMB temperature and polarization spectra. We find that for sufficiently large values of the parameter w, which is inversely proportional to the effective volume of the compactified dimensions, the two limiting regimes, one with the network energy dominated by light populous strings and the second with it dominated by rare heavy strings, can each produce distinctly different shapes of CMB spectra, especially for the B-mode polarization. In particular, for $w \sim 1$, the position of the peak in the B-mode spectrum is at $\ell \approx 770$ for $g_s = 0.9$ and at $\ell \approx 610$ for $g_s = 0.04$. This allows for the exciting possibility that upcoming observations may not only constrain the overall contribution of strings, but in fact rule out certain values of the string coupling. Namely, the combination of the normalization and the peak position of the B-mode spectrum can point to a particular combination of g_s and the fundamental string tension μ_F.

It is common to report constraints on standard cosmic strings in terms of bounds on the single dimensionless string tension $G\mu$. These bounds have an implicit assumption on the number density of strings corresponding to the usual Abelian Higgs model strings with intercommutation probability $\mathcal{P} = 1$. However, in a more general situation of strings with lower intercommutation probabilities and, as is the case for cosmic superstrings, different tensions, each type of string will in principle have a different number density: the same fraction of CMB anisotropy can be sourced either

with many light strings or with a few heavy ones. In general, each type of observational bound will constrain a different combination of the string tensions and densities (which, for cosmic superstrings, are derived from the fundamental string tension μ_F as well as g_s). In particular CMB and pulsar bounds, which we discuss in Section 5.4, will lead to different shapes of bounding contours in the (μ_F, g_s) parameter plane. We show that combining these two constraints can lead to complementary constraints on properties of superstrings. The position of the peak in the B-mode spectrum can be used to further eliminate a large region of the (μ_F, g_s) parameter space.

In Section 5.2 we summarise the extended VOS model which describes multi-tension networks with junctions. We then present the scaling solutions for cosmic superstrings as a function of the string coupling g_s. In Section 5.3 we determine the temperature and B-mode spectra for these scaling solutions using a generalised version of CMBACT. Finally in Section 5.4 pulsar constraints on gravitational waves from string networks are discussed. We conclude in Section 5.5.

5.2 Scaling of F-D superstring networks

F-D superstrings provide an example of a network of strings with multiple tensions that can join each other at Y-shaped junctions. Letters F and D denote the type of quantized charge carried by strings – the F charge is identified with fundamental strings, while the D charge is carried by D-branes. A general (p, q) string has p quanta of F charge and q quanta of D charge [107, 109, 219].

In the following, we review the model developed in [216, 218], which describes a network of N different types of strings with junctions. We then customize the pa-

rameters of this model for the case of F-D superstrings paying particular attention to their dependence on the string coupling g_s. While the exact values of the parameters are model-dependent, e.g. depend on the choice of the compactification manifold, we are able to identify general trends in their dependence on g_s. These trends, in turn, lead to two different scaling scenarios in the limits of large and small g_s that may be distinguished observationally.

5.2.1 The VOS model for single type string networks

We introduced the VOS model for single type string networks in Section 2.4. The relevant equations are

$$\dot{\rho} = -2\frac{\dot{a}}{a}(1+v^2)\rho - \frac{\tilde{c}\,v\rho}{L}, \tag{5.1}$$

$$\dot{v} = (1-v^2)\left(\frac{k}{L} - 2\frac{\dot{a}}{a}v\right), \tag{5.2}$$

where the constant $\tilde{c}$ represents the efficiency of loop formation, and k is the curvature parameter which indirectly encodes information about the small-scale structure on strings. It can be expressed as a function of the velocity [80];

$$k = \frac{2\sqrt{2}}{\pi}\left(\frac{1-8v^6}{1+8v^6}\right), \tag{5.3}$$

which incorporates the Virial condition $v^2 \leq \frac{1}{2}$, observed in simulations in expanding background. The scaling solutions are

$$\xi^2 = \frac{k(k+\tilde{c})}{4\beta(1-\beta)}, \tag{5.4}$$

$$v^2 = \frac{k(1-\beta)}{\beta(k+\tilde{c})}. \tag{5.5}$$

The relation between intercommutation probability and the loop chopping efficiency parameter $\tilde{c}$ is not fully understood at present. Nambu-Goto simulations of

strings interacting with a microphysical probability $\mathcal{P} < 1$ suggest that $\tilde{c} \simeq \mathcal{P}^{1/3}$ in both the matter and radiation era [137]. A different dependence, $\tilde{c} \simeq \mathcal{P}^{1/2}$, was reported in [220] based on a flat space simulation. In the subsequent sections we will take $\tilde{c}$ to scale as the cubic root of the corresponding intercommutation probability. Such a weak dependence of $\tilde{c}$ on $\mathcal{P}$ can be attributed to the presence of small scale structure on long strings, allowing for multiple chances of intercommutation when two string segments cross [137].

5.2.2 Evolution of multi-tension networks with junctions

In order to describe the evolution of a multi-tention string network (MTSN) with junctions, we adopt the model developed in [216, 218]. In this model, one solves for the energy densities and rms velocities of each string type using the following equations:

$$\dot{\rho}_i = -2\frac{\dot{a}}{a}(1+v_i^2)\rho_i - \frac{c_i v_i \rho_i}{L_i} - \sum_{a,k} \frac{d_{ia}^k \bar{v}_{ia} \mu_i \ell_{ia}^k(t)}{L_a^2 L_i^2} + \sum_{b,\, a\leq b} \frac{d_{ab}^i \bar{v}_{ab} \mu_i \ell_{ab}^i(t)}{L_a^2 L_b^2}\,, \tag{5.6}$$

$$\dot{v}_i = (1-v_i^2)\left[\frac{k_i}{L_i} - 2\frac{\dot{a}}{a}v_i + \sum_{b,\, a\leq b} b_{ab}^i \frac{\bar{v}_{ab}}{v_i}\frac{(\mu_a+\mu_b-\mu_i)}{\mu_i}\frac{\ell_{ab}^i(t) L_i^2}{L_a^2 L_b^2}\right]. \tag{5.7}$$

Here μ_i is the tension of the ith type of string, and, in analogy to networks consisting of a single type of string, one defines a correlation length L_i through

$$\rho_i = \frac{\mu_i}{L_i^2}\,. \tag{5.8}$$

As in the single string case, the coefficients c_i in (5.6) quantify the efficiency with which self-interactions of strings of type i chop off closed loops, removing energy from the long string network of type i. The last two terms in equation (5.6) model the effect of collisions between strings of different types, leading to the formation of

new segments ending on 3-string junctions. More specifically, the penultimate term describes the loss of energy, from network i, due to string segments of type i colliding with segments of type a and forming links of type k. Similarly, the last term models the energy gain in network i through collisions between different strings a and b, leading to the formation of a link of type i. The parameter $d_{ij}^{k} = d_{ji}^{k}$, which we will discuss in more detail below, is essentially the probability with which strings of types i and j interact and produce a type k segment. This parameter captures quantum interaction and volume effects [46, 105], as well as the kinematic constraints discussed in [51, 111, 112, 218]. The average length of the links formed by this process at time t is denoted as $\ell_{ij}^{k}(t)$, whose explicit form will be given below (equation (5.19)). In equation (5.7), the coefficients k_i are curvature parameters which indirectly encode information about the small-scale structure on strings. We will follow [80] and take them to depend on the rms velocities as

$$k_i = \frac{2\sqrt{2}}{\pi}\left(\frac{1-8v_i^6}{1+8v_i^6}\right). \tag{5.9}$$

Finally, the parameters b_{ab}^{i} have been introduced in order to interpolate between the model of [216] (where $b_{ab}^{i} = d_{ab}^{i}$), in which the energy liberated by the formation of junctions is redistributed in the network as kinetic energy, and a model analogous to that in [215] (corresponding to $b_{ab}^{i} = 0$), in which all of this energy is radiated away. The most realistic situation is probably somewhere in between, with $b_{ab}^{i} < d_{ab}^{i}$, so that a fraction of the liberated energy is radiated away and the rest is redistributed. Finally, $\bar{v}_{ab}$ is the magnitude of the relative velocity between strings of type a and b averaged over all directions, that is $\bar{v}_{ab} = \sqrt{v_a^2 + v_b^2}$.

5.2.3 Parameters for F-D cosmic superstring networks

We have already seen that in cosmic superstring networks the tension of each string type is determined by the corresponding charges, (p, q), and the string coupling g_s. In ten flat dimensions and for vanishing RR scalar, the tension of a (p, q) string is given by [107, 109, 219]

$$\mu_i \equiv \mu_{(p_i,q_i)} = \frac{\mu_F}{g_s}\sqrt{p_i^2 g_s^2 + q_i^2}\,, \tag{5.10}$$

where μ_F is the tension of the lightest fundamental string (F-string) carrying charge $(1, 0)$. The D-string has a charge $(0, 1)$, while the strings carrying charges (p, q) with $p, q \geq 1$ can be thought of as bound states between p F-strings and q D-strings. There is an infinite hierarchy of such (p, q) bound states, but, as was found in [215, 216, 218], the cosmological evolution of interacting networks of this type leads to solutions in which only the first few lightest strings dominate, so one can truncate the system at finite N. Here we will take $N = 7$ so we only have seven different types of strings carrying charges $(p_i, q_i) \equiv (p, q)_i$ with

$$\{(p, q)_i\} = \{(1, 0), (0, 1), (1, 1), (2, 1), (1, 2), (3, 1), (1, 3)\}\,, \quad (i = 1, ..., 7)\,. \tag{5.11}$$

The parameters in equations (5.6-5.7) which will determine the scaling patterns of the cosmic superstring networks we consider are the self- and cross- interaction coefficients, c_i and d_{ij}^k respectively. They are averaged network quantities that depend on the microphysical intercommuting probabilities of the corresponding interaction processes, which in turn can be modelled using string theory techniques [105, 135]. Note that the cross-interaction coefficients d_{ij}^k also depend on kinematic constraints on 3-string junctions [51, 111, 112].

We will first consider the microphysical intercommuting probability $\mathcal{P}_{ij}$ for interactions between strings of types i, j. For processes involving at least one F-string, that is F-(p, q) interactions, this probability can be calculated perturbatively in string theory [105, 135]. The result is a function of the string coupling g_s, the relative velocity v and the angle θ of the incoming strings. There is also a model-dependent volume factor which depends on the size of the compact extra dimensions, parameterized by a parameter w, and the amplitude of fluctuations of the string position fields. The latter depends on the string tension and, therefore, on the string coupling g_s. Let us write

$$\mathcal{P}_{ij}(v, \theta, w, g_s) = \mathcal{F}_{ij}(v, \theta, g_s)\, \mathcal{V}_{ij}(w, g_s)\,, \tag{5.12}$$

where $\mathcal{F}_{ij}(v, \theta, g_s)$ is the quantum interaction piece and $\mathcal{V}_{ij}(w, g_s)$ the volume dependence.

Let us discuss the volume-independent piece, $\mathcal{F}_{ij}(v, \theta, g_s)$. As mentioned above, for interactions involving at least one F-string, we can use perturbative methods [105]. On the other hand, for interactions involving only D-strings or heavier composites, the process is non-perturbative and less understood. At present there are at least two approximate results, by Jackson, Jones & Polchinski [105] (hereafter JJP) based on a worldsheet calculation, and by Hanany & Hashimoto [136] (hereafter HH) using a field theory approach. The two calculations are in good qualitative agreement, but there are quantitative differences reflecting the uncertainties arising from the currently incomplete understanding of such non-perturbative processes. Nevertheless, these calculations provide a basis for systematically computing the network coefficients in equations (5.6-5.7), and allow us to study the effect of these uncertainties on the macroscopic evolution of the networks[1]. As the available methods for calculating these processes

[1] We will discuss how network results depend on this and other uncertainties in section 5.2.4.

improve (for recent progress see [135]) such uncertainties will be eventually controlled. Here, we will use the results of JJP for the perturbative processes involving at least one F-string, and the result of HH for the non-perturbative D-D interactions. These have non-trivial dependencies on v and θ and the relevant string charges p and q (for details see [105, 136]), but there are a few key features with respect to their dependence on the string coupling g_s which can be summarised: F-F string interactions scale with g_s^2, F-(p,q) interactions with $q \geq 1$ scale with g_s, and the non-perturbative D-D interactions scale with U^{1/g_s}, where U is a number of order unity. For interactions between heavier composites, i.e. (p,q)-(p',q') with $q,q' > 1$ and $p,p' \geq 1$, the amplitude is not known but it is understood that it is enhanced with respect to the D-D amplitude by the multiplicity qq' of the relevant Chan-Paton states [105]. In addition, for small values of the coupling g_s we can neglect the effect of the light perturbative F-strings so we will approximate the enhanced amplitude as $\mathcal{F}_{(p,q)(p',q')} = 1 - (1 - \mathcal{F}_{\rm DD})^{qq'}$. The detailed form of the factors $\mathcal{F}_{ij}(v,\theta,g_s)$ we assume (including their full v, θ dependence) is shown in table 5.1.

Interaction (ij)	$\mathcal{F}_{\rm ij}$
F-F	$g_s^2 \frac{\left(1-\cos\theta\sqrt{1-v^2}\right)^2}{8\sin\theta\, v\sqrt{1-v^2}}$
F-D	$g_s \frac{v^2+\left(\cos\theta\sqrt{1-v^2}\right)^2}{8\sin\theta\, v\sqrt{1-v^2}}$
F-(p,q) , $q \geq 1$	$\frac{q^2v^2+\left(g_sp-\cos\theta\sqrt{(1-v^2)(g_s^2p^2+q^2)}\right)^2}{8\sin\theta\, v\sqrt{(1-v^2)(g_s^2p^2+q^2)}}$
D-D	$\min\left\{\frac{\sqrt{g_s}}{2\pi^{3/4}\theta^{3/4}}e^{2\sqrt{2/3}(\theta/v)}\exp\left[-\frac{4\sqrt{\pi}\theta^{3/2}}{g_s}e^{-4\sqrt{2/3}(\theta/v)}\right], 1\right\}$
(p,q)-(p',q') , $q,q' \geq 1$	$1-(1-\mathcal{F}_{\rm DD})^{qq'}$

Table 5.1: The coefficients $\mathcal{F}_{ij}$ for different string interactions.

We now turn our attention to the volume factors $\mathcal{V}_{ij}(w,g_s)$. These arise because the strings are moving in a higher-dimensional space so they can miss each other as

they cross, leading to an overall suppression on the amplitude that scales with the inverse of the volume of the extra dimensions. However, it has been argued [105] that this suppression effect may not be as important as originally anticipated [46], because the string position fields are worldsheet scalars – not protected by any symmetry – and should therefore be stabilised at a minimum of a potential well (see however [173, 221]), rather than explore the compact orthogonal dimensions. In this case, there is still a volume effect arising from the fact that strings are quantum objects whose positions fluctuate around the classical minimum, thus giving rise to an effective volume that each string explores, which is, however, a small fraction of the total. The size of the fluctuations is determined by the mass of the string, so this effective volume depends on the type of string and on the coupling g_s (for details see [105]). For F-F interactions, both strings have the same tension and fluctuate by the same amount, but for F-D interactions (and for small g_s) the fluctuation of the heavier D-string can be neglected, leading to a volume which is a factor of $(\sqrt{2})^6 = 8$ smaller[2] than the corresponding F-F volume. Finally, for D-D interactions the volume is approximately a factor $g_s^3 = (\sqrt{g_s})^6$ smaller than the F-F volume [105]. The overall volume suppression factor becomes unity when the effective string volume becomes equal to the minimum "string-scale volume" $V_{\rm min} = (2\pi^2\alpha')^3$. Thus, defining our model-dependent parameter w as

$$w \equiv V_{\rm min}/V_{\rm FF} \in (0, 1]\,, \tag{5.13}$$

we have for the relevant suppression factors $\mathcal{V}_{\rm FF} = w$, $\mathcal{V}_{\rm FD} = \min(8w, 1)$ and $\mathcal{V}_{\rm DD} = \min(wg_s^{-3}, 1)$ as long as $g_s \ll 1$. Here, we generalise these volume factors for (p, q)-strings and for $g_s \lesssim 1$ in a phenomenological way so as to reproduce the above limits.

[2]Note that 6 is the number of extra dimensions.

In particular, we assign a factor of $(p^2 + q^2 g_s^{-2})^{3/4}$ to each (p, q)-string. We show the resulting $\mathcal{V}_{ij}(w, g_s)$ in table 5.2. This is simply a choice we make in order to be able to systematically calculate these suppressions for different string types, but is one which successfully reproduces the results of [105] in the appropriate limits. The dependence of our network scaling results on this choice will be discussed in section 5.2.4. We are thus left with a residual model-dependent variable w that we treat as an external tunable parameter like g_s. Note that the choice $w \simeq 1$ for this parameter (corresponding geometrically to a compactification very close to the string scale) makes $\mathcal{V}_{ij} \simeq 1$ for all strings, so the dependence of the intercommuting probability $\mathcal{P}_{ij}$ on the string type and g_s is determined only by the quantum interaction $\mathcal{F}_{ij}(v, \theta, g_s)$ in this case.

Interaction (ij)	$\mathcal{V}_{ij}$
F-F	w
F-D	$\min(w g_s^{-3/2}, 8w, 1)$
F-(p,q) , $q \geq 1$	$\min\left[(p^2 + q^2 g_s^{-2})^{3/4} w, 8w, 1\right]$
D-D	$\min(w g_s^{-3}, 1)$
(p,q)-(p',q') , $q, q' \geq 1$	$\min\left\{\left[(p^2 + q^2 g_s^{-2})(p'^2 + q'^2 g_s^{-2})\right]^{3/4} w, 1\right\}$

Table 5.2: The coefficients $\mathcal{V}_{ij}$ for different string interactions.

For the macroscopic string networks we are interested in, string collisions happen perpetually as the network evolves, with a range of relative velocities and angles. We therefore average out the velocity and angle dependence of the microphysical probabilities $\mathcal{P}_{ij}(v, \theta, w, g_s) = \mathcal{F}_{ij}(v, \theta, g_s)\, \mathcal{V}_{ij}(w, g_s)$ (see [218]). This yields the probabilities $\mathcal{P}_{ij}(w, g_s)$ which now depend only on our two free parameters w and g_s.

The question now is how these probabilities are related to the network coefficients c_i and d_{ij}^k in the macroscopic evolution equations (5.6-5.7). As we already discussed, for *self-interactions*, numerical simulations of Nambu-Goto string networks with reduced

microphysical probabilities [137], suggest that the effective (loop-chopping efficiency) coefficient $\tilde{c}$ in equation (5.1) scales with the third root of the microphysical probability $\mathcal{P}$. That is

$$c_i = 0.23 \times \mathcal{P}_i^{1/3}, \tag{5.14}$$

where we have denoted $\mathcal{P}_{ii} \equiv \mathcal{P}_i$ and the number 0.23 is chosen so as to reproduce single network results for $\mathcal{P}_i = 1$, $d_{ij}^k = 0$ in the radiation era. In the matter era, the corresponding proportionality constant is 0.18. For the *cross-interactions* (i.e. with $i \neq j$) producing zipped configurations, there are at present no network simulations to compare to (for recent progress towards this direction see [144]) in order to determine the dependence of d_{ij}^k on the microscopic probabilities $\mathcal{P}_{ij}$. However, one may expect this dependence to be similar to the self-interaction case if these cross-interactions are initiated at a point (at which the incoming strings first cross) and then proceed by the zipping of the colliding strings, rather than exchange of partners. If that is the case, then one may expect the effect of small-scale-structure on the strings to enhance the interaction probability by increasing the number of encounters within one crossing time, much like in the case of self-interactions. Let us therefore define:

$$d_{ij}^k = d_{ij} S_{ij}^k, \tag{5.15}$$

with

$$d_{ij} = \kappa \times \mathcal{P}_{ij}^{1/3}, \tag{5.16}$$

where κ is a constant of order unity that we set to 1. Note that the effect of a $\kappa \neq 1$ will still be captured to some extent[3] by our subsequent analysis, because this parameter

[3]Since $w \in (0, 1]$ it cannot account for $\kappa \gtrsim 1$.

is degenerate with w (refer to tables 5.1,5.2 and equation (5.12)), which we will vary as an external parameter. At this point, we stress that the scaling (5.16) with $\mathcal{P}_{ij}$ is an important model-dependent assumption, as it determines the values of the correlation length of the dominant strings in our model. This highlights the need for investigating numerical simulations of strings with junctions.

The final ingredient that enters the systematic computation of the cross-interaction coefficients d_{ij}^k is the factor S_{ij}^k in equation (5.15). This describes the conditional probability that the crossing of strings i and j produces a zipper of type k, given that strings i and j have interacted. The interaction is fully described by an additive and a subtractive channel, so, for each pair $\{i,j\} \equiv \{(p_i,q_i),(p_j,q_j)\}$ there are only two possibilities for k; either $k = (p_i+p_j, q_i+q_j) \equiv +$ or $k = (p_i-p_j, q_i-q_j) \equiv -$. Which channel is followed is determined by energetic considerations based on the balance of string tensions at the 3-string junction. To a first approximation, the conditional probability that the additive or subtractive channel is followed is given by [105]:

$$P_{ij}^k \equiv P^{\pm}_{(p_i,q_i),(p_j,q_j)} = \frac{1}{2}\left(1 \mp \left(\frac{p_i p_j g_s^2 + q_i q_j}{(p_i^2 g_s^2 + q_i^2)^{1/2}\,(p_j^2 g_s^2 + q_j^2)^{1/2}}\right)\right), \qquad (5.17)$$

which add to unity. Note, however, that there are kinematic constraints [51, 52, 111, 112] which must be satisfied for the junction to form. Reference [218] showed how these microphysical constraints can be integrated over a distribution of velocities and angles in a string network to obtain the averaged network coefficients:

$$S_{ij}^k = \frac{2}{\pi}\int_0^1 \int_0^{\pi/2} \Theta(-f_{\vec{\mu}}(v,\theta)) \exp[(v-\bar{v}_{ij})^2/\sigma_v^2]\,\sin(\theta)\,v^2 \mathrm{d}\theta \mathrm{d}v\,, \qquad (5.18)$$

where $\Theta(-f_{\vec{\mu}}(v,\theta))$ is a step function imposing the kinematic constraints $f_{\vec{\mu}}(v,\theta) < 0$ [111] and σ_v^2 is the variance of the velocity distribution, assumed to be Gaussian peaking on the relative scaling velocities $\bar{v}_{ij} = (v_i^2+v_j^2)^{1/2}$. Note the direct dependence

of these coefficients on the string tensions $\vec{\mu}$, and thus on the string coupling g_s. By comparison, the dependence on w is very weak and enters only indirectly through the scaling velocities in $\bar{v}_{ij}$.

In our model, therefore, we shall replace the approximation (5.17) by the coefficients S_{ij}^k in (5.18), which take into account the kinematic constraints. It is important to note that due to the constraints being violated in part of the parameter (v, θ) space, one has $S_{ij}^+ + S_{ij}^- < 1$, in contrast to $P_{ij}^+ + P_{ij}^- = 1$ in (5.17). In table 5.3 we show these suppression coefficients for the three lightest string components (F$\equiv$ 1, D$\equiv$ 2, FD$\equiv$ 3) and for different values of the string coupling g_s in the radiation era[4]. The weak dependence of these coefficients on w practically makes no difference between their values at $w = 0.1$ and $w = 1$.

w	g_s	S_{12}^3	S_{13}^2	S_{23}^1
$w \in [0.1, 1]$	$g_s = 0.04$	0.180	0.293	0.950
	$g_s = 0.05$	0.166	0.293	0.938
	$g_s = 0.1$	0.117	0.302	0.881
	$g_s = 0.2$	0.071	0.312	0.790
	$g_s = 0.3$	0.050	0.325	0.707
	$g_s = 0.5$	0.033	0.354	0.590
	$g_s = 0.7$	0.028	0.388	0.516
	$g_s = 0.9$	0.026	0.424	0.462

Table 5.3: The coefficients S_{ij}^k for the three lightest string components (F$\equiv$ 1, D$\equiv$ 2, FD$\equiv$ 3) for different values of the free parameters g_s and $0.1 \lesssim w \lesssim 1$, in the radiation era.

Putting all these factors together, the resulting coefficients c_i and d_{ij}^k, in the radiation era, for interactions between the lightest string components are shown in table 5.4 for the same values of g_s and w as in table 5.3. In the matter era, the coefficients c_i are a factor 0.78 smaller, while the d_{ij}^k coefficients only change through the velocity

[4]There is a weak dependence of the coefficients S_{ij}^k on the expansion law (matter vs radiation era) due to their dependence on the scaling string velocities.

dependence in equation (5.18). This change does not affect significantly the scaling values of the correlation lengths and velocities of the strings, and we can safely neglect it. The main difference with reference [218] is that, there, the coefficients d_{ij} were chosen independently as free parameters, while now they are systematically computed as described above and they depend only on g_s and w, which are our free parameters here.

w	g_s	c_1	c_2	c_3	d_{12}^3	d_{13}^2	d_{23}^1
$w=1$	$g_s=0.04$	0.02	0.13	0.13	0.05	0.08	0.55
	$g_s=0.1$	0.03	0.16	0.16	0.04	0.11	0.62
	$g_s=0.2$	0.05	0.19	0.19	0.03	0.14	0.63
	$g_s=0.3$	0.07	0.20	0.20	0.03	0.16	0.61
	$g_s=0.5$	0.10	0.21	0.21	0.02	0.21	0.54
	$g_s=0.7$	0.12	0.22	0.22	0.02	0.26	0.49
	$g_s=0.9$	0.15	0.22	0.22	0.02	0.31	0.45
w	g_s	c_1	c_2	c_3	d_{12}^3	d_{13}^2	d_{23}^1
$w=0.1$	$g_s=0.04$	0.01	0.13	0.13	0.05	0.07	0.55
	$g_s=0.1$	0.02	0.16	0.16	0.04	0.10	0.62
	$g_s=0.2$	0.02	0.19	0.19	0.03	0.13	0.63
	$g_s=0.3$	0.03	0.20	0.20	0.02	0.14	0.61
	$g_s=0.5$	0.05	0.20	0.21	0.01	0.15	0.54
	$g_s=0.7$	0.06	0.15	0.22	0.01	0.17	0.39
	$g_s=0.9$	0.07	0.12	0.21	0.01	0.20	0.31

Table 5.4: The coefficients c_i and d_{ij}^k of equations (5.6-5.7) for the three lightest string components (F≡1, D≡2, FD≡3) for different values of the free parameters g_s and w.

The average length $\ell_{ij}^k(t)$ of zippers produced at time t which appears in equations (5.6-5.7) is, in principle, model-dependent. However, for cosmic superstrings, which are not subject to topological conditions like for example in non-Abelian field theory strings, it can be taken to be [216, 218]

$$\ell_{ij}^k = \frac{L_i L_j}{L_i + L_j} \,. \tag{5.19}$$

With this choice we are assuming that the produced zipper has a length which is smaller than – but close to – the smallest of the two correlation lengths of the colliding strings.

For simplicity we set the coefficients b_{ij}^k to zero. In this way we concentrate on the effects coming from the junction terms in equation (5.6) and not from the extra terms in the velocity evolution equations (5.7). Note, however, that setting $b_{ij}^k = d_{ij}^k$ we find that our results are insensitive to this choice, in agreement with [218].

Finally, in order to interpolate between the radiation and matter dominated eras, we follow the approach in [118, 206], accounting for the different probabilities for each string type. That is,

$$c_i = \frac{c_r + gac_m}{1 + ga} \times \mathcal{P}_i^{1/3}, \tag{5.20}$$

with $c_r = 0.23$ (radiation) and $c_m = 0.18$ (matter), $g = 300$ and $a(\tau)$ is normalised so that $a = 1$ today.

5.2.4 Scaling of F-D networks at large and small string couplings

We have solved equations (5.6-5.7) numerically using the parameters computed in section 5.2.3 for different values of our external parameters g_s and w. We find scaling solutions with all network components reaching approximately constant string number densities and rms velocities during radiation and matter eras, as in [215, 216, 218]. The string number density per unit Hubble volume, $\xi_i^{-2} \equiv (t/L_i)^2$, is dominated by the lightest three network components, namely the F, D and FD-strings, while all heavier components are suppressed and end up having negligible number densities. The F, D and FD-strings also dominate the effect on the CMB observables or, more generally, any observable linearly related to the two point function of the string energy momentum tensor. It is useful to introduce the *power spectrum density* M_i given by [198]

$$M_i = \left(\frac{\mu_i}{\xi_i}\right)^2, \tag{5.21}$$

which determines the amplitude of string induced power spectra.

Fig. 5.1 shows the evolution of the rms velocity, number density and the power spectrum density for the three lightest strings for $g_s = 0.04$ and $g_s = 0.9$, with $w = 1$. When g_s is close to unity, the tensions of the F and D strings are comparable. As a result, their densities are similar, as shown in the panels on the right. When g_s is decreased, the lighter F strings become more populous and thus dominate the *number* density of the network. However, the D strings become heavier at smaller g_s and, despite being rare, can actually dominate the power spectrum density. This is evident from the $g_s = 0.04$ case shown in the left panels of Fig. 5.1. We can therefore identify a transition in the power spectrum: At large string couplings, where the tensions of the F, D and FD strings are approximately equal, F strings dominate the power spectrum because they have the smallest correlation length. At small string couplings, the power spectrum is dominated by the heavy rare D strings. This transition appears to be a generic property of FD networks and is one of our key results. Reducing the volume parameter w to 0.1 results in an enhancement of the overall network number density is (since $\mathcal{P}_{ij} \propto \mathcal{V}_{ij} \propto w$), but the dependence of the network scaling patterns on g_s remains the same.

In Fig. 5.2, we plot the number and power spectrum densities of the three relevant strings at the time of last scattering vs g_s for two values of w, in order to visualise the aforementioned transition. Reducing the value of the string coupling from $g_s \approx 1$, initially reduces the contribution of D strings to M_{total} as they become more rare, but this trend quickly changes as we continue reducing g_s and the D-strings become heavy $\mu_{\text{D}} \simeq g_s^{-1}$, eventually dominating M_{total} in the case of $w = 1$. For $w = 0.1$, the power density M_D increases with decreasing g_s, but does not quite catch up with M_F over the

range of string couplings we have studied numerically. Note, however, that the number density of F becomes a few orders of magnitude larger than that of D, meaning that the correlation length of F strings is very small. If their correlation length is smaller than the horizon size at last scattering, the F strings do not contribute significantly to the CMB polarization and, despite their lower power density, the B mode spectrum will in fact be dominated by D strings. We will return to this point in the next section.

Having sketched this interesting trend in the dependence of network scaling patterns on g_s, let us see the way it emerges from the functional forms for MTSN parameters adopted in Section 5.2.3. At *large* string couplings ($g_s \to 1$), the tensions of the F and D strings are comparable ($\mu_{\rm D} = g_s^{-1}\mu_{\rm F} \sim \mu_{\rm F}$), and so are their number and power spectrum densities. In particular, for $w \sim 1$ and $g_s \lesssim 1$, we have $\mathcal{P}_{\rm F} \sim g_s^2 w \lesssim \mathcal{P}_{\rm D} \sim w \sim 1$, so, in effect, one would observe a single effective network of tension $\mu_{\rm F} \sim \mu_{\rm D}$, with a correlation length similar to that of ordinary cosmic strings, but with the extra property of frequently forming 3-string junctions. For small w, the situation would be similar, but with a smaller correlation length, and the appearance of 3-junctions would be more rare since now $\mathcal{P}_{\rm F} \sim g_s^2 w \lesssim w \ll 1$ is somewhat smaller than $\mathcal{P}_{\rm D} \sim w g_s^{-3} > w$, so D-strings would be somewhat more rare. It should be noted, however, that at $g_s \approx 1$ the perturbative methods used to calculate $\mathcal{V}_{\rm FF}$ are not expected to be accurate.

For *small* g_s, the difference between the tensions of F and D strings is large, and so is the difference in the corresponding coefficients c_i, d_{ij}^k (see table 5.4). As a result, the much lighter F strings dominate the network number density. The power spectrum density, however, is dominated by the less populous, but much heavier ($\mu_{\rm D} \propto g_s^{-1}$) D strings which, being very massive, evolve practically independently of the light F-

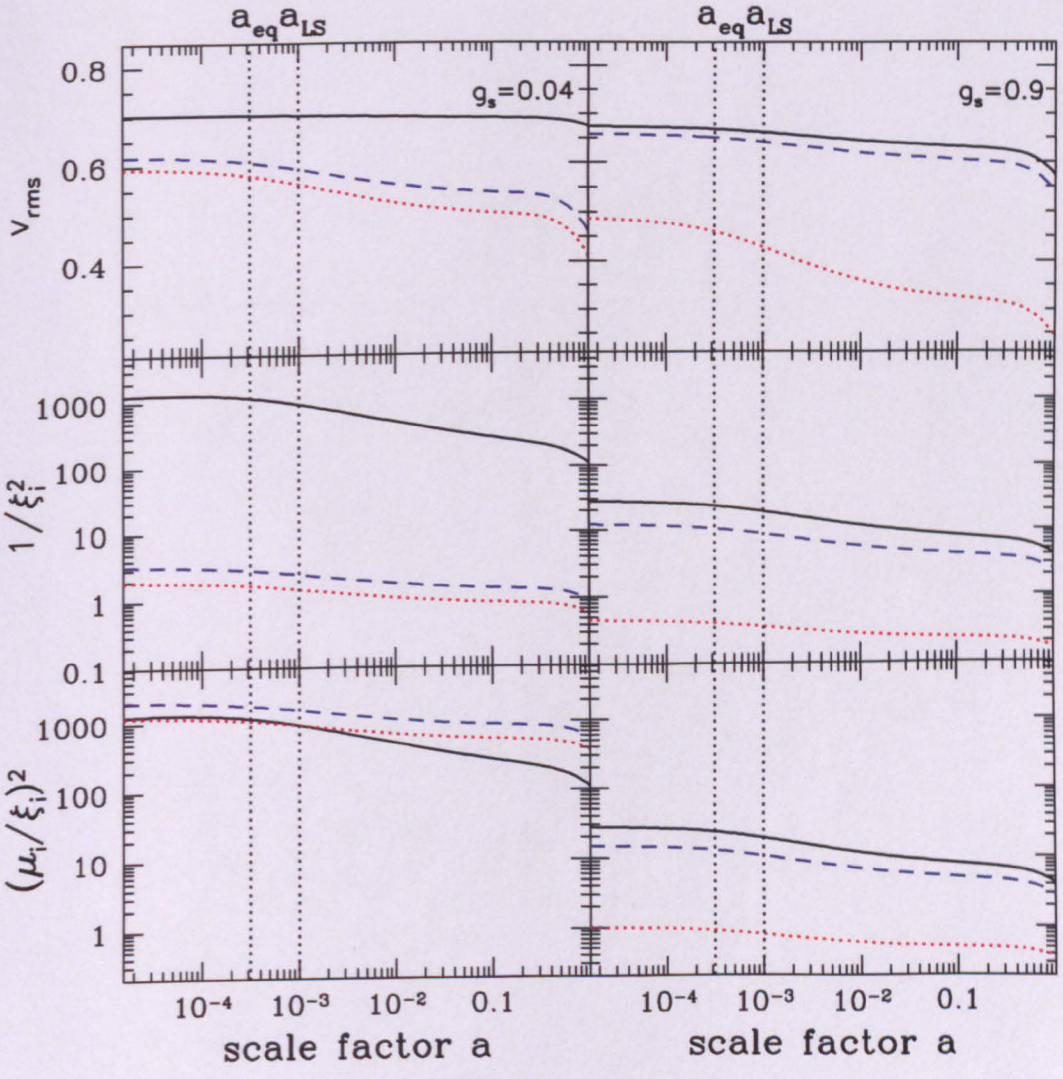

Figure 5.1: Evolution of the rms velocity v_i (top panels), number density $\xi_i^{-2} \equiv (t/L_i)^2$ (middle panels), and the power spectrum density $(\mu_i/\xi_i)^2$ (bottom panels) of the three lightest network components: F-strings (solid black), D-strings (blue dash), and FD (red dot), at two representative values of the string coupling g_s. The panels in the left column are for $g_s = 0.04$, those on the right are for $g_s = 0.9$. All plots are for $w = 1$. For $g_s \to 1$, the tensions of the F and D strings are comparable, as well as their densities. At smaller g_s, the lighter F strings dominate the *number* density, while the heavier and less numerous D strings dominate the power spectrum. The epochs of radiation-matter equality and last scattering are indicated with vertical lines. Of particular relevance for CMB is the correlation length of the string type that dominates the power spectrum density at the time of LS (see also Figs. 5.2 and 5.3).

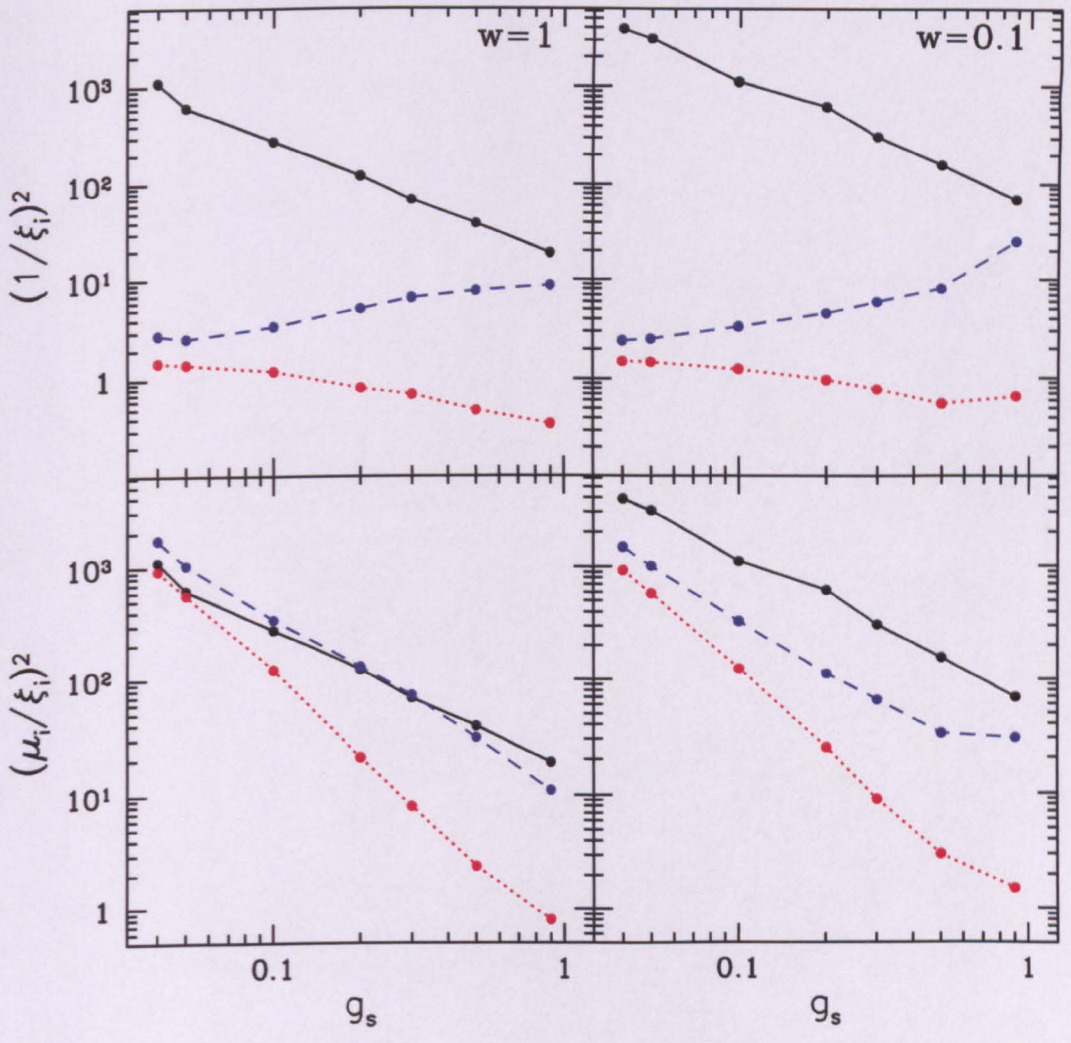

Figure 5.2: Dependence of the string number (top panels) and power spectrum (bottom panels) densities *at the time of last scattering* on the value of the string coupling g_s for $w = 1$ (left) and $w = 0.1$ (right), for the three lightest network components: F-strings (solid black), D-strings (blue dash) and FD-strings (red dot).

string network. In addition, the zipping between F- and D-strings gives rise to FD composites with a tension practically equal to that of the heavy D strings. Again, we effectively have a single network of D-strings dominating the power spectrum, since the F-string component is unobservable due to its low tension. Further, unless $w \ll g_s^3$, the volume factors $\mathcal{V}_{\rm DD} \propto w g_s^{-3}$ in equation (5.12) approach unity while the non-perturbative factor is $\mathcal{F}_{\rm DD} \lesssim 1$. As a result, the network properties are similar to those of an ordinary field theory string network with $\tilde{c} \approx \mathcal{P} \approx 1$.

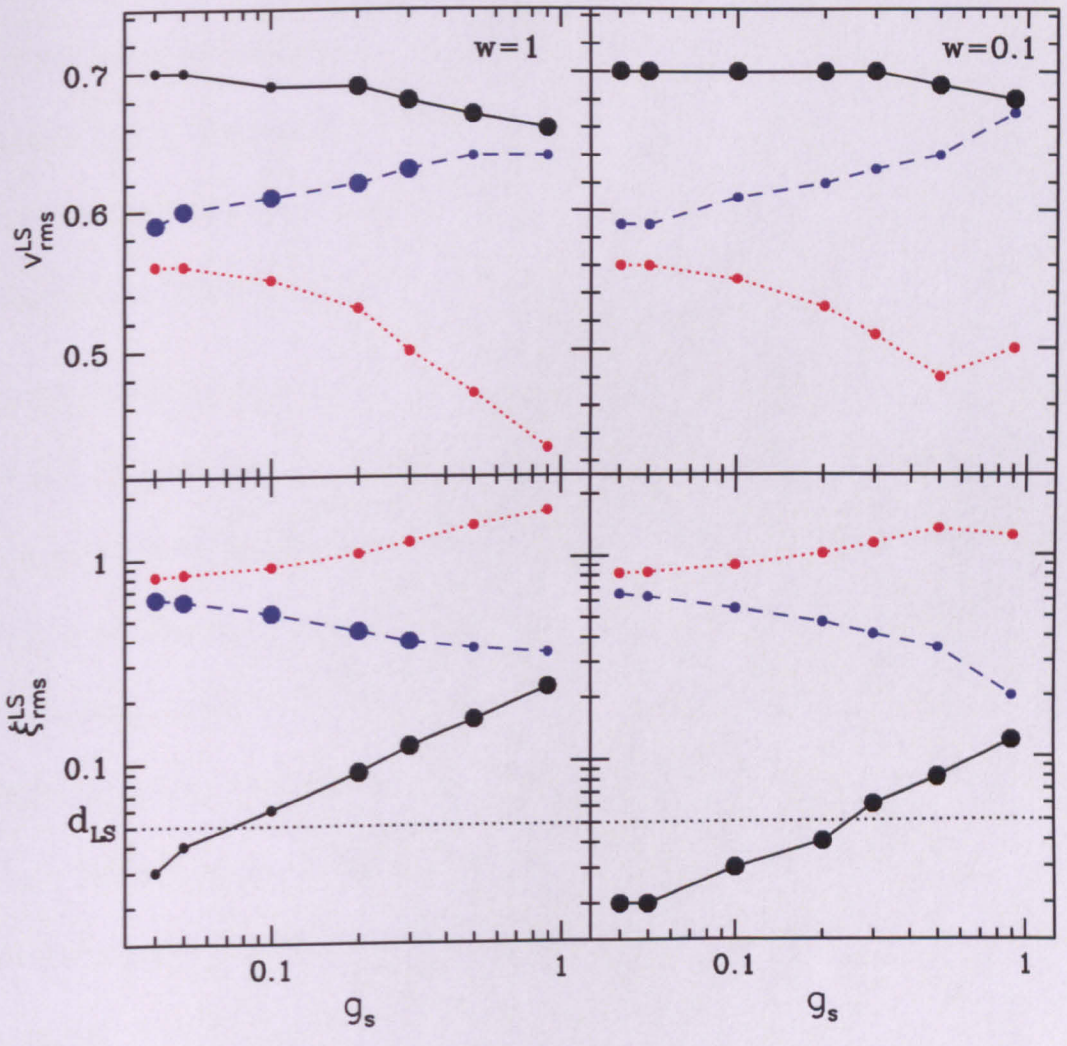

Figure 5.3: The correlation length and the rms velocity *at the time of last scattering* (LS) as a function of the string coupling g_s for $w = 1$ (left) and $w = 0.1$ (right) for the three lightest network components: F-strings (solid black), D-strings (blue dash) and FD-strings (red dot). We show the string type(s) that dominate(s) the power spectrum at LS with oversized points. The horizontal line at $\xi = 0.05$ indicates the thickness of the LS surface.

In the next section we study possible observable signals induced by these networks on the CMBR temperature and polarization power spectra. Before that, let us briefly comment on the importance of the interactions between the different string types for obtaining the above picture. Let us imagine a network of different string types without the junction terms d^k_{ij} in equation (5.6). Naively, one might think that each type of string would evolve independently, following the usual one-scale model, with different c_i's given by equation (5.14). However, we would not be able to truncate such a net-

work to a finite number of string types. The interactions between the strings (p, q) and (p', q') favour the substractive over the additive channel, i.e. the preferred bound state is a $(p - p', q - q')$ segment. This results in the suppression of the heavy string types. For the same reason, the hierarchy in the number density of the surviving three types is always in favour of the lighter species.

The values of the correlation length ($\xi_{\rm LS} = L(t_{\rm LS})/t_{\rm LS}$) and the rms velocity ($v_{\rm LS}$) of the string type that dominates the power spectrum density at the time of last scattering (LS) are particularly important. In Fig. 5.3 we show the dependence of $\xi_{\rm LS}$ and $v_{\rm LS}$ on g_s. The fact that strings of substantially different correlation lengths dominate the spectra at different values of g_s means that their CMB spectra can have distinctly different shapes. This may allow us to use CMB spectra as a discriminant between these different types of limiting behaviour, potentially providing an invaluable tool for constraining the underlying string theory, in particular the string coupling g_s. We also note that, as seen in Fig. 5.3, there is only a minor difference in the values of scaling velocities of the dominant string types at different couplings.

Finally, we comment on the significance of using the one-scale assumption to model the evolution of the network. To test the role of this assumption in setting the hierarchy of densities of different string types we have incorporated a second scale in our model, following the approach of [216], i.e. adding an extra scale $\bar{\xi}$, common to all string types, and modifying appropriately the evolution equations for the correlation length and the velocity. We have concluded that the effect of the second scale is not large – the number densities of the strings do not significantly change and, most importantly, the hierarchy stays the same. Another potential concern, which is of relevance to the CMB predictions, is that the one-scale assumption equates the correlation length along

the strings with the interstring distance. This is only a reasonable approximation for networks with sufficiently large intercommutation probabilities ($\mathcal{P}_i \gtrsim 0.1$). Hence, we do not consider values of w and g_s at which intercommutation probabilities of the dominant strings are too small.

5.3 CMB temperature and B-mode spectra from FD strings

5.3.1 Modelling CMB with CMBACT

To evaluate CMB temperature and polarization spectra sourced by multi-tension string networks (MTSN) we modify the publicly available code CMBACT [206, 207] so as to allow for strings with multiple tensions whose scaling is modelled by equations (5.6) and (5.7).

As we described in Section 4.4.2, CMBACT uses the unconnected segment model (USM) [118, 206, 208, 209] to represent the cosmic string network. The length, rms velocity and number density are modelled using the VOS equations (2.46) and (2.47). We should emphasise that CMBACT is not a means for gaining new insight into the evolution of cosmic string networks. Instead, it is a tool for evaluating CMB spectra for *given* one-scale parameters, such as correlation length and rms velocity. In [195], it was shown that CMB spectra obtained from field theoretical simulations of Abelian-Higgs (AH) strings [120] are reproduced by CMBACT when the one-scale parameters measured in the simulation are used as input. Also, the CMB spectra obtained from the NG simulations of [86, 122] were compared to those from CMBACT with the

one-scale parameters measured in [86], finding a good agreement as well. The default version of CMBACT uses the VOS model with parameters tuned to match NG simulations of [80, 222].

The shapes of the string-induced CMB spectra are mainly determined by the large-scale properties of the string network, such as the correlation length and rms velocity. The overall normalization of the spectrum has a simple dependence on the string tension μ and $\xi = L/t$ [198, 200] given by equation (5.21). The CMB temperature spectra (TT) receive a contribution from the LS surface, for which the relevant scale is ξ at the time of LS. In addition, TT receives roughly equal contributions at each subsequent epoch (which is the mechanism by which strings can produce a scale-invariant TT spectrum on large scales) and hence the value of ξ is approximately the value measured during matter domination. CMB polarization, on the other hand, is sourced at the time of LS and thus the normalization of the B-mode spectrum is given by $\xi_{\rm LS}$.

In this work we generalise CMBACT to include uncorrelated segments of N different types. The lengths and rms velocities of each type are determined from equations (5.6) and (5.7). As in the single-tension case, the T_{0i} and T_{ii} components of the string stress-energy are determined from the the covariant conservation equation, which now takes the form

$$\nabla^{\mu} \sum_{i=1}^{N} T^{i}_{\mu\nu} = 0. \tag{5.22}$$

The overall amplitude of the CMB angular spectra C_ℓ is approximately determined by

$$C_\ell^{strings} \propto M_{\rm total} = \sum_{i=1}^{N} M_i = \sum_{i=1}^{N} \left(\frac{\mu_i}{\xi_i}\right)^2, \tag{5.23}$$

and the shapes of the spectra will be set by the correlation length and the rms velocity of the most dominant population of strings.

We should note that CMBACT has only been tested against simulations of single tension strings with no junctions and with an intercommutation probability of unity. However, as discussed in Section 5.2, the scaling solution of FD networks tends to fall into two categories depending on whether the string coupling is large or small. Namely, the energy density of the network is dominated by light populous strings for large values of g_s, and rare heavy strings at much smaller g_s. In either cases, the bulk of the anisotropy is seeded by a single type of strings. Moreover, the intercommutation probabilities of the dominant string species are 0.1 or larger implying at most a factor of 2 reduction in loop chopping efficiency c_i. This justifies the use of CMBACT for modelling the CMB spectra from FD networks at least in the two limiting cases of large and small string couplings.

5.3.2 The CMB spectra for scaling FD strings

Before proceeding to discuss the CMB spectra sourced by FD strings, let us again stress that cosmic strings cannot contribute more than 10% of the total CMB temperature anisotropy [121, 189, 190, 191, 192, 193, 194, 195]. To comply with this bound [5], we will adjust the fundamental (F-)string tension μ_F to be such that

$$f_s = C_{strings}^{TT}/C_{total}^{TT} = 0.1 \ , \tag{5.24}$$

[5]The current bound on the fraction of string sourced CMB temperature anisotropy is only weakly dependent on the detailed shape of the spectrum, so we can safely use the existing bound in our studies. As an example, let us note that the bound on global strings, which have a rather different form of the CMB spectrum from that of Abelian Higgs strings, is also approximately 10%.

where we follow conventions of [200] to define

$$C^{TT} \equiv \sum_{\ell=2}^{2000} (2\ell+1) C_\ell^{TT}. \tag{5.25}$$

Even with a marginal contribution to the TT spectrum, strings can be a prominent source of B mode polarization. This is because strings, unlike inflation, are actively sourcing vector mode perturbations of magnitude comparable to the scalar perturbations [196, 197, 198, 200, 201, 202].

The dependence of the TT and BB power spectra on the correlation lengths and the rms velocities was extensively studied in [200] and more recently in [195]. The overall amplitude of the spectrum is approximately given by equation (5.23). The correlation length and the rms velocity of the main string type set the dominant momentum modes in the strings stress-energy, which determine the position of the main peak. Larger string correlation lengths will move the peaks in the TT and BB spectra to lower ℓ. In addition, the rms velocity also controls the position of the peak, although the dependence is not linear. The positions of the TT and BB peaks move to higher multipoles (smaller scales) for low and moderate velocities, but move to larger scales (lower ℓ) for higher velocities. This non-trivial behaviour is a manifestation of the non-linear dependence of the string stress energy on string velocities. Also, larger values of v decrease the amount of BB power relative to TT power.

In Fig. 5.4 we show the TT and BB power spectra for two values of the string coupling g_s (solid black line for $g_s = 0.04$, and dashed line for $g_s = 0.9$). In Fig. 5.5 we show the normalised total TT power spectra for $g_s = 0.04$ (upper) and $g_s = 0.9$ (lower), including the individual scalar (S), vector (V) and tensor (T) contributions for each case. The scalar and vector contributions are of similar magnitude, as expected

in the case of cosmic strings. The spectra are normalised to give $f_s = 0.1$ as described earlier, which translates into $G\mu_F = 1.8 \cdot 10^{-8}$ for $g_s = 0.04$, and $G\mu_F = 2.1 \cdot 10^{-7}$ for $g_s = 0.9$.

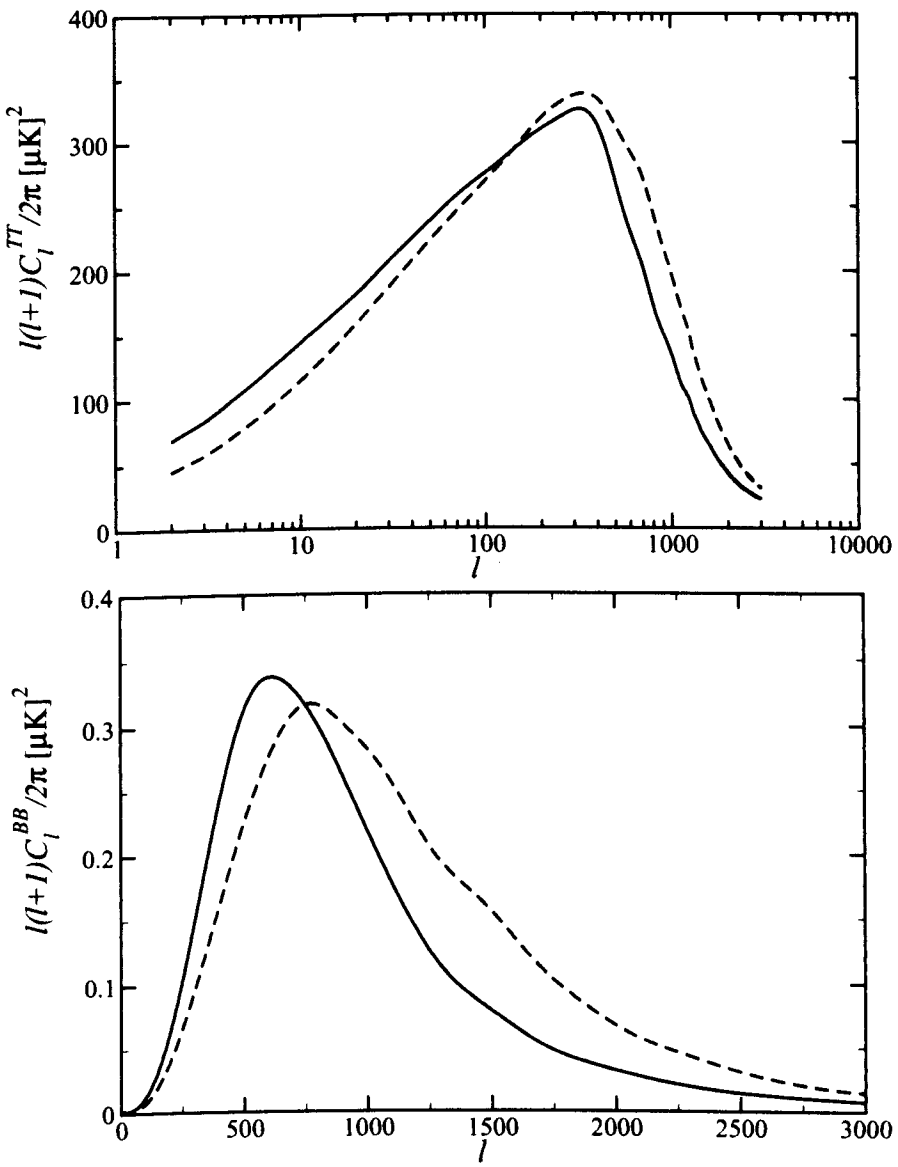

Figure 5.4: The normalised TT (upper) and BB (lower) power spectra for $g_s = 0.04$ (solid) and $g_s = 0.9$ (dash) for $w = 1$, normalised to give $f_s = 0.1$. Note that the smaller string coupling leads to a discernible move in the peak of the BB spectra to smaller ℓ.

We can interpret the CMB spectra at different values of g_s in the context of the scaling behaviour of the different string types discussed in detail in Section 5.2. In the case $g_s = 0.9$, the F and D strings are dominant and most populous, and have almost the

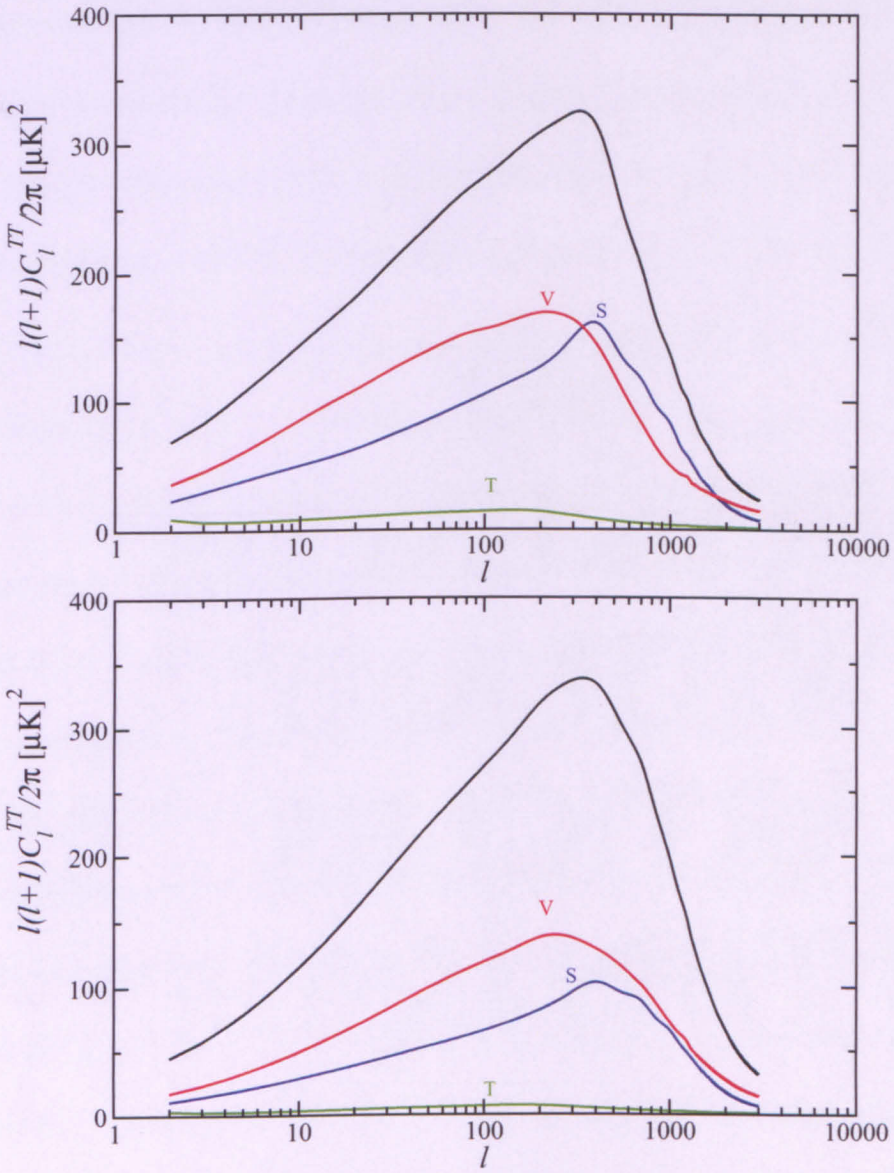

Figure 5.5: The normalised TT power spectra for $g_s = 0.04$ (upper) and $g_s = 0.9$ (lower), including the individual scalar (S), vector (V) and tensor (T) contributions.

same tension. Their correlation lengths and velocities are similar as well, with values close to those of ordinary strings. Hence, their contributions to the CMB spectra are comparable, whereas the contribution from the FD string is not as important. On the other hand, in the $g_s = 0.04$ case, the F string is again light and populous, but the D string is 25 times heavier than the F string, and so is the FD string. Thus, despite being very rare, the D and FD strings dominate the CMB spectra. In addition, there is a small but non-negligible contribution from the heavier $(2, 1)$ string.

The lower panel in Fig. 5.4 clearly shows the impact of the changed hierarchy between the three kinds of strings. The heavy D strings which dominate M_i for $g_s = 0.04$ have a larger correlation length, which translates into a BB peak at smaller ℓ. This offers a tantalising possibility for probing for small string couplings in the CMB.

In Fig. 5.6 we again show the B-type polarization spectrum predicted by our string models for a 10% and a 1% contribution to the total TT. We compare this to the contributions from gravitational lensing of the adiabatic E-mode polarization into B-mode. We see that, especially in the region of high ℓ, there is a possible detection window, where the cosmic string signal would manifest itself as an excess over the expected lensing contribution. The Planck satellite may be able to see the excess if strings contribute at a level currently tolerated by data [223], however, it is likely that Planck's TT, TE, and EE spectra will place tighter bounds on strings even without B-mode measurements. The science goals of the ground based experiments, such as the advanced stages of QUIET [224] and POLARBEAR [225], include accurate measurements of the BB spectrum from lensing. If these science goals are met, they should have the sensitivity to detect the excess due to strings at a level of $f_s \sim 10^{-3}$. If the string contribution is sufficiently large, one may be able to detect the main peak and thus rule out large or small values of g_s based on the position of the peak. More studies are needed to determine the minimum value of f_s for which a particular B-mode experiment will be able to detect the position of peak [203]. In principle, it may be possible to de-lense the B-mode polarization map, taking advantage of the fact that the B-mode due to lensing is a rotation of the E-mode, and hence E and B modes are highly correlated [226, 227]. Some preliminary forecasts of expected constraints on cosmic strings from de-lensed B-modes were reported in [199, 203] but more work is needed to understand feasibility

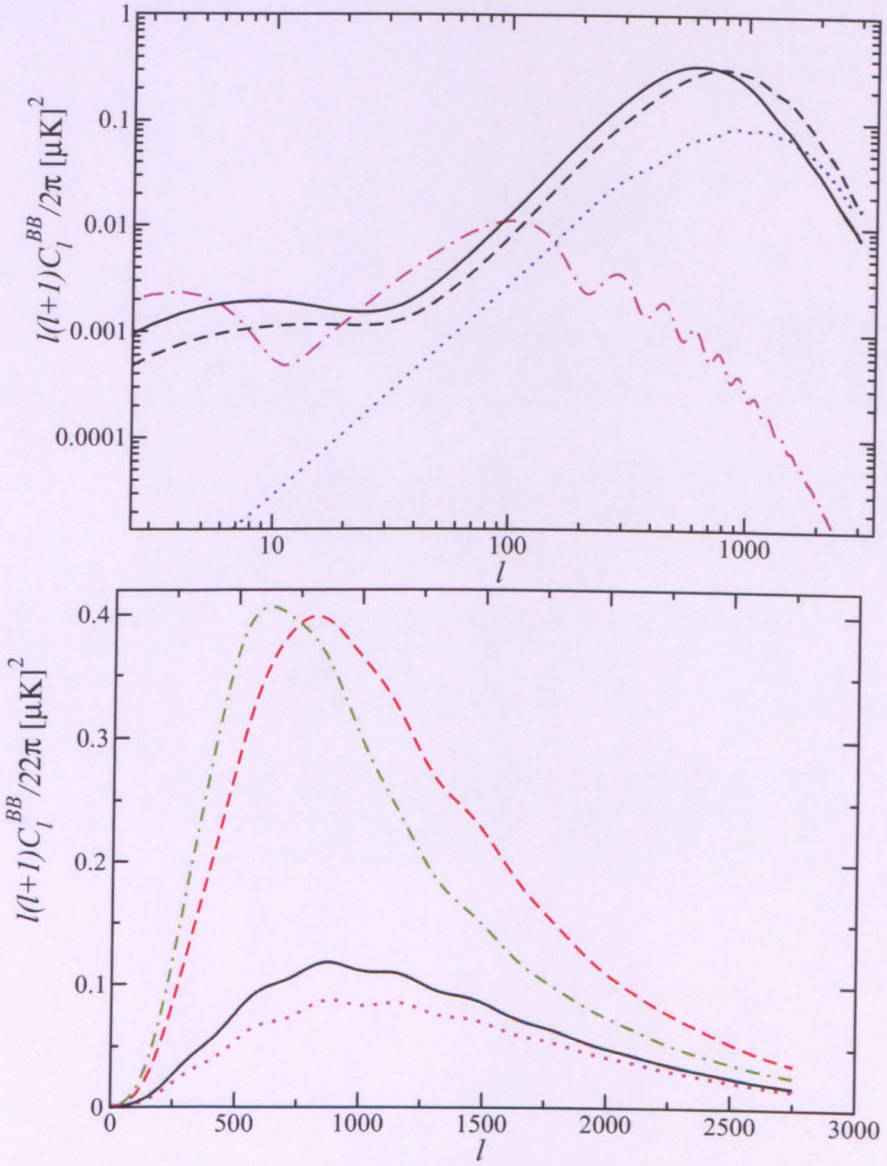

Figure 5.6: *Upper:* The B-type polarization spectra due to cosmic superstrings assuming a 10% contribution ($f_s = 0.1$) are plotted with solid ($g_s = 0.04$) and dashed ($g_s = 0.9$) black lines. The expected C_l^{BB} spectra for E to B lensing (blue dot line) and from primordial gravitational waves assuming a tensor-to-scalar ratio of $r = 0.1$ (magenta-dot-dash line) are shown for comparison. *Lower:* The magenta dot line is the lensing prediction, the black solid line is the sum of the string and lens-sourced B-mode power for $g_s = 0.9$ for $f_s = 0.01$. Strings manifest themselves via the systematic excess power at high-ℓ over the lensing prediction. The sum of strings and lensing contributions is also plotted for $f_s = 0.1$ for $g_s = 0.9$ (red dash) and $g_s = 0.04$ (green dot-dash). By measuring the location of the main peak on can rule out either the small or the large values of g_s.

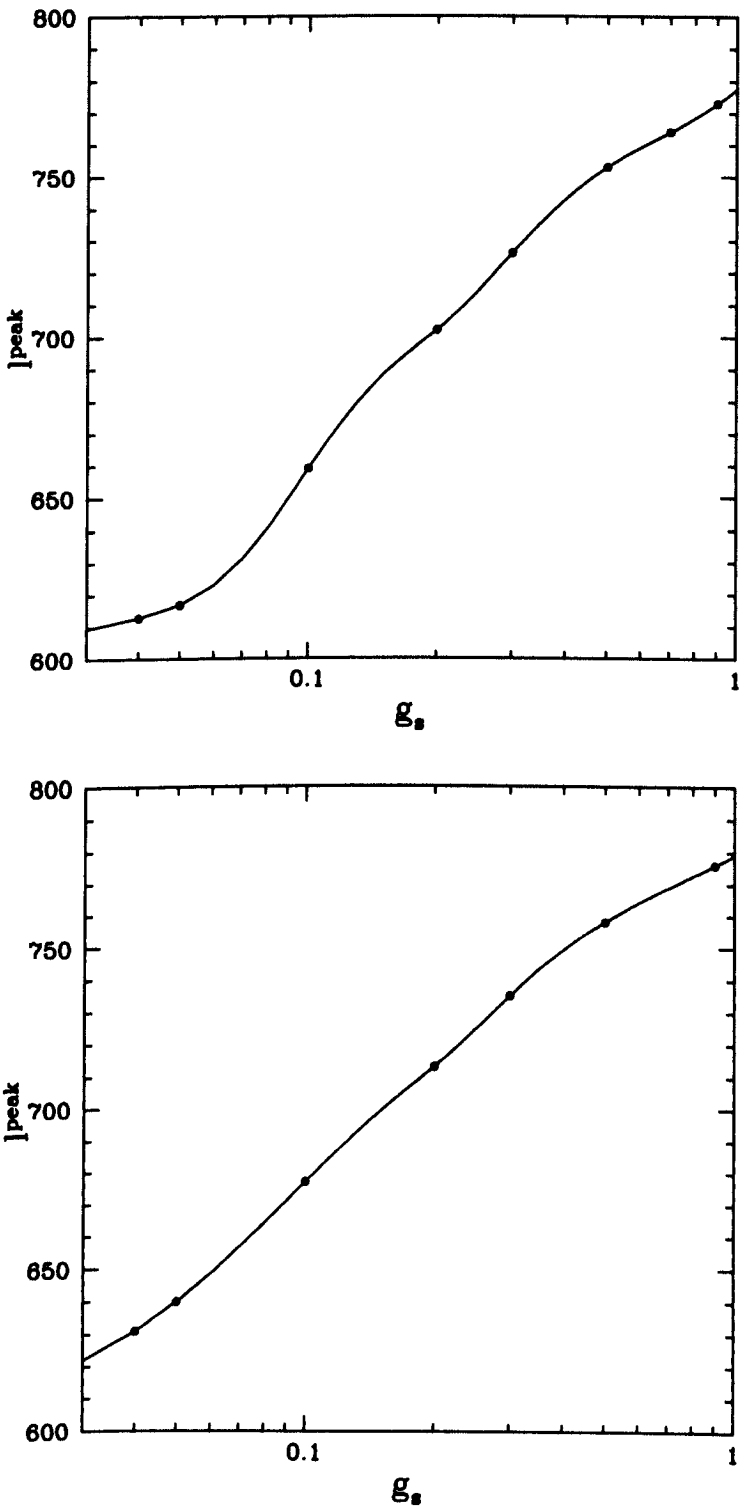

Figure 5.7: The position of the peak of the BB spectrum as a function of the string coupling g_s for $w = 1$ (upper) and $w = 0.1$ (lower).

of measuring the position of the string induced peak from de-lensed polarization maps.

In Fig. 5.7 we show the BB peak location as a function of g_s, ranging from 0.04 to 0.9. For $w = 1$, shown on the upper plot, we see that the position of the BB spectrum as a function of the string coupling g_s is decreasing with decreasing g_s. This is consistent with our earlier discussion for the behaviour of the power spectrum density, which starts being dominated by the F-strings and, after a transition, ends up being dominated by the heavy rare D-strings. Their correlation length increases with decreasing g_s, and the BB peak moves to smaller ℓ.

In the lower plot of Fig. 5.7, which considers the $w = 0.1$ case, we also see that the BB peak position decreases with a decreasing g_s. However, here it happens for somewhat different physical reasons. Namely (see Fig. 5.2), the power spectrum density M_i in the more populous F-strings dominates through the whole range of g_s we have considered. Yet it is again the D-string contribution that dominates the B-mode spectra. One might suggest that the explanation for this lays on the smallness of the ξ_i for the F-strings. For $\xi \lesssim 0.05$, the string correlation length is smaller than the thickness of the LS surface, and thus most of the power in that type of strings does not contribute to the B-mode. Only a small fraction of the total power in F strings contributes, that generated on larger scales, but it is much smaller than the contribution of the D strings. However, the important issue arising here is that when the ξ of the dominant string becomes so small, the one-scale approximation is no longer reliable. This is a well-known problem, and further improvements for accurately calculating the CMB contributions from such strings must be performed in the future.

5.4 Combined constraints on μ_F and g_s from CMB and Pulsar Timing

As mentioned in the previous section, the amplitudes of CMB two-point correlations do not separately constrain the string tensions and their densities. Instead, they constrain a combination of μ_i and ξ_i given by equation (5.23). In particular, they do not differentiate between dense networks of light strings and rare heavy strings. In the case of FD networks, the relative abundances of different types of strings are controlled by the string coupling g_s, with the bound on CMB normalization leading to different values of μ_F for different values of g_s. Thus, the requirement that strings contribute no more than 10% of the total CMB TT power can be translated into a joint constraint on μ_F and g_s shown with a solid black line in Fig. 5.8.

The degeneracy between μ_i and ξ_i, or in the case of FD networks, between μ_F and g_s, can be partially broken if other types of observations become available. One example would be a measurement of the position of the string induced bump in BB. Based on the results in Section 5.3, if a peak is found at $\ell_{\rm peak} \approx 610 \pm 50$, that would rule out $g_s > 0.1$, while $\ell_{\rm peak} \approx 750 \pm 50$ would rule out $g_s < 0.3$. In the future, more sophisticated simulations of CMB from MTSN based on specific compactifications can, in principle, make accurate predictions for the dependence of the BB peak position on g_s.

Another way to reduce the degeneracy between μ_F and g_s is to combine bounds from CMB with the bounds on gravity waves (GW) emitted by strings, such as those coming from pulsar timing experiments and direct GW searches by LIGO. The GW bounds constrain the energy density in strings approximately given by the combination

μ/ξ^2 for each type of strings. The fact that the functional dependences of the GW and CMB bounds on μ_i and ξ_i are different implies that by combining the two probes one can, in principle, reduce the degeneracy between μ_F and g_s.

To illustrate this point, we follow the procedure presented in [195], where the authors calculated the bounds on the cosmic string tension from pulsar timing [211] (note that they are stronger than the ones coming from LIGO). For a network of single type of string, the formula is [210]

$$\Omega_{\rm g}h^2 = 1.17\times 10^{-4} G\mu \left(\frac{1-\langle v_{\rm rad}^2\rangle}{\xi_{\rm rad}^2\Omega_{\rm m}}\right)\frac{(1+1.4x)^{3/2}-1}{x}, \tag{5.26}$$

where $x = \alpha/(\Gamma\, G\mu)$, α is the loop production size, and $\Omega_{\rm m}$ is the total matter density relative to the critical density. They use parameters measured from the Nambu simulations to give $\xi_{\rm rad}$, $\langle v_{\rm rad}^2\rangle$ and set $\Omega_{\rm m} = 0.3$, $\Gamma = 60$. We generalise this formula to include the three types of string that dominate the density of the FD network, namely the $(1,0) = F$, the $(0,1) = D$ and the $(1,1) = FD$ string. Setting $c = 1$ we write

$$\Omega_{\rm g}h^2 = 1.17\times 10^{-4} \sum_{i=1}^{3} G\mu_i \left(\frac{1-\langle v_{\rm rad,i}^2\rangle}{\xi_{\rm rad,i}^2\Omega_{\rm m}}\right)\frac{(1+1.4x_i)^{3/2}-1}{x_i}, \tag{5.27}$$

where $i = 1$ corresponds to the F-string, $i = 2$ to the D-string and $i = 3$ to the FD string. Also, $x_i = \alpha/(\Gamma\, G\mu_i)$, so we take the α and Γ parameters to be the same for all types of string. For a given value of g_s, we use the extended VOS model of Section 5.2 to determine the values of ξ_i. With those in hand, given the bound $\Omega_{\rm g}h^2 < 2\times 10^{-8}$, which is the most reliable published limit [211], we can use the relations $\mu_D = \mu_F/g_s$ and $\mu_{FD} = \mu_F\sqrt{g_s^{-2}+1}$ to find the bound on $G\mu_F$. As in [195] we consider two limiting cases of $x_i \ll 1$ and $x_i \gg 1$.

Case $x_i \ll 1$**:** In this case, eq. (5.27) becomes

$$\Omega_{\rm g}h^2 = \frac{3}{2}\cdot 1.4\cdot 1.17\times 10^{-4}\sum_{i=1}^{3} G\mu_i \left(\frac{1-\langle v^2_{{\rm rad,i}}\rangle}{\xi^2_{{\rm rad,i}}\Omega_{\rm m}}\right), \tag{5.28}$$

so it is independent of α (as in [195]). The corresponding joint constraint on μ_F and g_s is shown with red dotted line in Fig. 5.8.

Case $x_i \gg 1$**:** In this case, eq. (5.27) becomes

$$\Omega_{\rm g}h^2 = 1.4^{3/2}\cdot 1.17\times 10^{-4}\sum_{i=1}^{3} G\mu_i \left(\frac{1-\langle v^2_{{\rm rad,i}}\rangle}{\xi^2_{{\rm rad,i}}\Omega_{\rm m}}\right) x_i^{1/2}. \tag{5.29}$$

As in [195], substituting $x_i = \alpha/(\Gamma G\mu_i)$ results in a $1/\alpha$ dependence of μ_F. The corresponding joint constraint on μ_F and g_s for $\alpha = 0.001$ is shown with a short-dash green line in Fig. 5.8. Note that the chosen value of α gives a bound of $G\mu < 5\cdot 10^{-8}$ for a 'usual' cosmic string with $\xi_{rad} = 0.13$ and $v = 0.65$ [195].

In the limit $x_i \ll 1$, the bounds on μ_F are weaker than the ones coming from CMB. On the other hand, for $x_i \gg 1$ the bounds can be much stronger, because of the $1/\alpha$ dependence. However, the uncertainties in the upper bound on $\Omega_{\rm g}h^2$ in this limit are much more severe [195]. Note that the shapes of the two pulsar bound curves in Fig. 5.8 for the two limits ($x_i \ll 1$ and $x_i \gg 1$) are different because the dependence on μ_i is different.

Future probes of B-mode will be able to constrain cosmic strings down to 0.1% contribution to TT, which translates into an order of magnitude tighter bound on μ_F. In the lower panel of Fig. 5.8 we show the corresponding expected bounds from CMB.

In the context of specific brane inflation scenarios, the cosmic string based constraints on g_s and μ_F would need to be considered in covariance with other predictions of brane inflation, such as the spectral index n_s, the tensor-to scalar ratio r and the

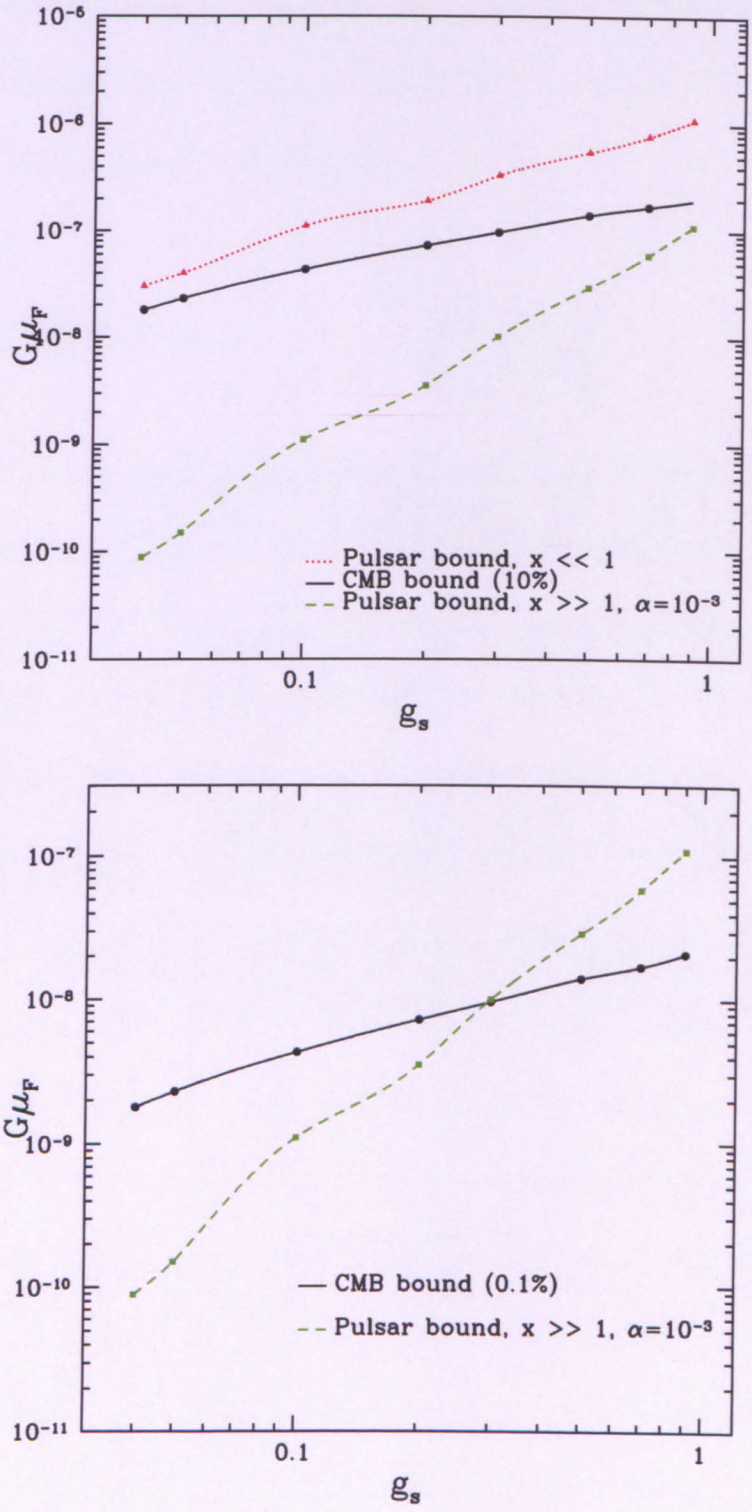

Figure 5.8: *Upper:* current bounds on μ_F and g_s from CMB (solid-black line) and pulsars (short-dash-green and dot-red line). *Lower:* The forecasted bound on μ_F and g_s from CMB based on future BB corresponding to 0.1% in strings (solid-black line) together with the bounds from pulsars for the case $x_i \gg 1$ with $\alpha = 0.001$ (short-dash-green line). Note that a measure peak of BB could exclude a huge region of the diagrams.

tensor index n_T, as well as possible departures from Gaussianity in the distribution of the primordial fluctuations. We expect that such a comprehensive approach can lead to non-trivial constraints on details of brane inflation models, and more generally, the fundamental parameters of string theory.

5.5 Conclusions

Using the MTSN scaling model developed in [218], we have studied the evolution of FD superstring networks, aiming to identify characteristic trends in their scaling properties at different values of the string coupling g_s. Indeed, we demonstrated that the so-called power spectrum density, which controls the amplitude of the two-point function of the string stress-energy, is dominated by populous light F and D strings at $g_s \to 1$, as opposed to rare heavy D strings when g_s is decreased.

Incorporating the MTSN scaling model in CMBACT, we were able to evaluate the contribution of the FD networks to the CMB temperature and polarization spectra. We found that the difference between the scaling patterns at high and low values of g_s is manifested as a different position of the peak in the B-mode spectrum. In the one-scale model, the correlation length is equal to the average inter-string distance, which means that string networks of higher (lower) number density have smaller (larger) correlation lengths. The correlation lengths, along with the string velocities, determine the position of the peak. This points to the possibility of constraining g_s with CMB, which would perhaps be the first opportunity to constrain this fundamental parameter of string theory with observations.

Most observables, at least those that rely on averaged properties of string networks,

constrain a combination of the string tension μ and their number density, determined by ξ^{-2}. Thus, in principle, it is quite hard to distinguish between the effect of many light strings vs a few heavy ones. Measuring a particular peak position in the B-mode spectrum would be one way to partially break this degeneracy, as we have discussed in this work. In addition, one can explore the fact that different observables constrain different combinations of μ and ξ. For instance, while the amplitude of the CMB spectra is determined by $(\mu/\xi)^2$, the energy density of strings is proportional to μ/ξ^2. We have shown how this difference can be explored in the case of FD networks to partially break the degeneracy between the fundamental string tension μ_F and the coupling g_s by combining the CMB constraints with those from bounds on gravity waves (GW).

The main trends we have identified in this work are largely independent of many of the details of the underlying string theory model, as well as the assumptions that went into the CMB calculation and the predictions for GW. However, we need to improve our understanding of the string interaction rates for different choices of g_s and w, especially in the non-perturbative regime. At very small string couplings, the density of the dominant species becomes so high that the one-scale approximation is almost guaranteed to break down. In such cases, a more sophisticated model is needed to properly describe the scaling of the network and its prediction for the CMB spectra. Whether it will be possible to measure a peak at high ℓ in the B-mode spectrum is another interesting question which will depend strongly on the resolution and sensitivity of the experiments, as well as our ability to clean the contribution from weak lensing. The GW bounds on FD strings depend on the loop size distribution, which is not fully understood at present.

Also, while in all string models considered so far the B-mode from the ordinary

strings is sourced predominately by vector modes, the tensor modes (i.e. large scale GW) were never properly worked out (since it requires accounting for the backreaction). It is our hope that the potentially very exciting opportunity for testing fundamental theory based on the general trends identified in this work will serve as additional motivation for pursuing the remaining open questions.

Chapter 6

Conclusions and Future Directions

In this thesis, we took a journey through the physics of cosmic strings and superstrings with junctions. Cosmic strings are very generic, appearing in many field-theoretic models which exhibit spontaneous symmetry breaking. They also appear at the end of hybrid inflation in SUSY GUTs. Depending on the energy scale in which they have been formed they can have important astrophysical effects, which are mainly characterized by the value of the dimensionless parameter $G\mu$, where G is Newton's constant and μ is the string's tension.

As we saw in Chapter 2, a cosmic string network formed in the early Universe would consist of a collection of infinite strings and closed loops, moving with relativistic velocities. These strings meet each other and exchange partners with a probability that approaches unity, or self-intesect forming closed loops which decay removing energy from the network. The network then evolves towards a scaling regime, where the correlation length and the distance between string segments scale with cosmic time. Numerical simulations agree that the scaling regime is reached, but there is still a

debate regarding important issues like the distribution of loops, the damping of wiggles through gravitational radiation, the class of non self-intersecting loops, the average number of cusps and kinks, and the energy loss via particle production (for a nice overview of this debate, see [94] and references therein). We hope that these issues will be soon resolved using a combination of analytical techniques and high resolution numerical simulations.

Cosmic superstrings are even more exciting and complicated objects. The basic constituents are the F and D strings, which are products of brane inflation models with $G\mu$ in the range $10^{-11} - 10^{-6}$. When these strings meet, they do not necessarily exchange partners. On the contrary, they have a reduced intercommuting probability. In the case of F-strings for example, the reconnection probability is of order g_s^2, where g_s is the string coupling. This means that it can be much smaller than unity.

In this thesis (Chapters 2 and 4), we reviewed the dynamics and observational effects of cosmic strings using the Nambu-Goto approximation, highliting recent progress on the corresponding properties of cosmic strings and superstrings with junctions. In Chapter 3, we extensively studied the evolution and stability of a cosmic string loop with junctions, comparing the Nambu-Goto method with a field theory model that allows composite vortices with corresponding Y-junctions. We showed that the two evolution methods agree until the collision time. In the field theory simulations, a new phenomenon occured, namely the unzipping of the composite vortices to produce new junctions. The string segments between the newly formed junctions can grow, destabilizing the configuration. We modelled this situation modifying the initial conditions in our Nambu-Goto algorithm, and the agreement with field theory was again very good. Our method and numerical code can evolve any loop with junctions — the

reason why we considered the specific configuration, which is highly symmetric, is the difficulty of constructing arbitrary loops with junctions. A possible way to tackle this problem is to try to numerically follow collisions of loops approaching each other with random velocities and decide on the outcome (junction formed or not) based on analytical estimates (see, for example, [228]). Another way to attack the problem of loop junction formation and evolution is by considering the leading order corrections to the Nambu-Goto effective action. The relevant formalism for a single string has been examined by several authors (see [229] and references therein). One starts from the four-dimensional field theoretic action and reduces it to a two-dimensional worldsheet integral, using an expansion in terms of $r_s\kappa$, where r_s is the string thickness and κ a typical scale of the extrinsic curvature of the worldsheet. If we extend this formalism to the modified Nambu-Goto action for strings with junctions, the corrections to the action might be able to model the junction decomposition phenomena.

In Chapter 5, we investigated the scaling patterns and CMB imprints of multi-tension cosmic superstring networks, building on previous work and incorporating the calculated probabilities for an F/D network using string theory methods. More specifically, we investigated networks with different charges (p, q) on the strings and different string couplings g_s, allowing for the formation of junctions between strings of different tensions. We obtained solutions for the characteristic length scales and velocities associated with these networks, finding two distinct patterns depending on the value of g_s. The number density of the network is always dominated by the light F strings, but for small g_s the heavy and rare D strings can dominate the power spectrum density. This leads to a potentially observable signal in the B-mode polarization spectrum: the BB peak position is decreasing with decreasing g_s. We also derived upper bounds on

the value of the fundamental tension μ_F using CMB and pulsar timing constraints.

We believe that our results presented in Chapter 5 can motivate further work towards several directions. First of all, numerical simulations for strings with junctions are needed to give us a better understanding for the dependence of the d_{ij} coefficients on the microscopic probabilities $\mathcal{P}_{ij}$. Studies need to be performed for the quantitative understanding of the string interaction probabilities in the non-perturbative regime as a function of g_s and w. We also need to construct a more sophisticated model in order to model the network's behaviour at small string couplings, since the smallness of the dominant correlation length means that the one-scale approximation breaks down. We can then make firmer predictions for the CMB spectra and especially the B-mode string induced signatures. Finally, it would be very profitable to include loops in our analysis and, in connection with our work in Chapter 3, we would ideally like to have loops with junctions as well.

To conclude, we believe that our results are positively pointing to the direction of probing fundamental theories using cosmological observations. Of course, the open issues we have already stressed need to be addressed. We have recently entered an era of precision cosmology, and we hope that the upcoming observations will provide additional motivation for further research.

Appendices

Appendix A

Field-Theory Initial Conditions

We obtain the initial conditions required for the butterfly configuration by first setting up the appropriate windings in the scalar field and then applying a period of dissipative evolution in order to relax the configuration to the minimum energy configuration. That is, during this period there is an extra term in each of the equations of motion that is proportional to the first time derivative of the corresponding field and so removes energy from the system. Additionally we fix the modulus of the scalar field in the region close to the desired centre lines since otherwise the configuration would simply contract to a point during the dissipative evolution. We apply reflective boundary conditions throughout the simulation.

The initial choice for the phases of the ϕ field for a planar loop of (1,0) string is made as shown in Fig. A.1. If a site is above the plane of the loop then it is given the phase $\pi/2$, if it is below the plane then it is given $3\pi/2$, while if it is in the plane of the loop then it is given either π if it is outside the loop or zero if it is within it. This ensures the correct winding structure of the field but it obviously yields artificially high

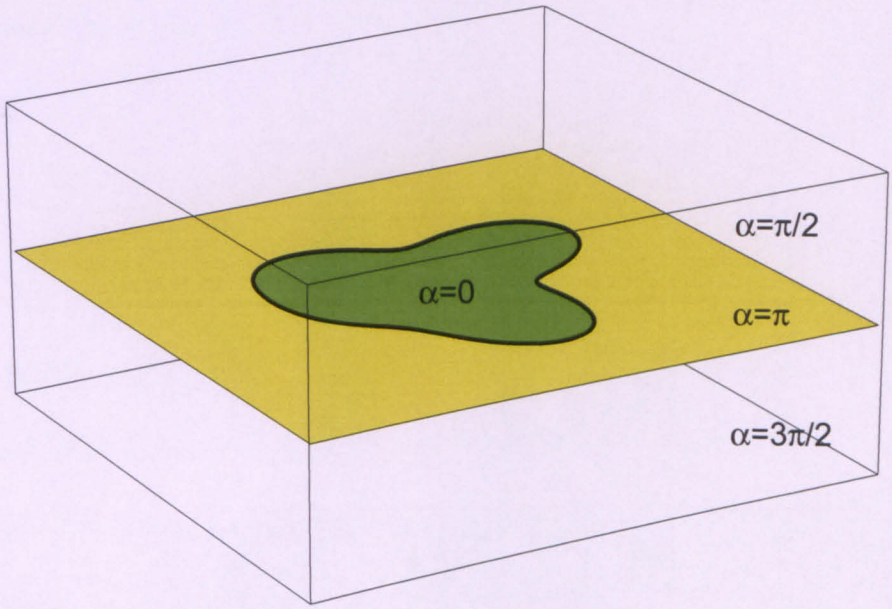

Figure A.1: The initial ϕ phase choice for a planar (1,0) loop, ensuring a winding of 2π in the desired locations.

gradients on the plane of the loop. The modulus of the scalar field is initially chosen so that the field lies on the vacuum manifold, except close to the string centre lines, as will be explained momentarily. During the dissipative evolution the gauge field, which is set to zero initially, quickly grows to counter these phases gradients, while the phase and modulus of ϕ rapidly adjust themselves in order to minimize the energy. Obtaining a (0,1) loop can be achieved by simply swapping ψ for ϕ in the above argument, while a (1,1) loop is obtained by setting up the phases appropriately in both fields. Higher winding numbers cannot be achieved by the direct application of the above approach and will be discussed below.

The modulus of the scalar fields is set inside a tube around the string centre-line according to the solution for an infinite straight string. For a winding $2\pi m$ in the phase of ϕ and $2\pi n$ in the phase of ψ, this has the following form for small displacements r

from the string centre:

$$\phi(r) \approx Cr^m, \tag{A.1}$$

$$\psi(r) \approx Dr^n. \tag{A.2}$$

The constants C and D, which depend on the choice of m and n cannot be found analytically, but are solved for using essentially the approach of Ref. [117]. Note that if m is finite but n is zero, then even though there is no winding in ψ, its modulus is still less than ν near the string as this lowers the total potential term energy. However, $|\psi|$ does remain finite as $r \to 0$. In principle we could fix $|\psi|$ close to the string in this case also, but we choose not to since it would not greatly aid the fixing of the string position and we wish to minimize the artificial restrictions enforced.

The butterfly configuration illustrated in Fig. 3.3 can be constructed by the superposition of a (1,1) loop and a (1,-1) loop after a period of dissipation. Since the equations of motion are non-linear there is no precise means to do this, however a good approximation is simply to sum the gauge fields from each loop A_μ^+ and A_μ^- to give the total:

$$A_\mu = A_\mu^+ + A_\mu^-, \tag{A.3}$$

where the $+$ and $-$ refer to each loop. Then for the scalar fields:

$$\frac{\phi}{\eta} = \frac{\phi_+}{\eta}\,\frac{\phi_-}{\eta}, \tag{A.4}$$

results in a superposition of complex phases [68, 132, 134, 230]. Furthermore, at distances far from any string set up in ϕ_+ (such that the field is approximately constant and close to its vacuum) the form of ϕ is essentially that found in ϕ_-. Using these equations, the time derivatives must then superpose as:

$$\partial_t A_\mu = \partial_t A_\mu^+ + \partial_t A_\mu^-, \tag{A.5}$$

$$\eta\,\partial_t \phi = \phi_+ \partial_t \phi_- + \phi_- \partial_t \phi_+. \tag{A.6}$$

While the wings are largely unaffected by this process and remain close to the minimum energy solution, a further period of dissipation is required to relax the central region, because of the significant interference between the two loops. For the case illustrated in Fig. 3.3 this includes the cancellation of the fluxes in ψ along the central string, which greatly reduces the energy per unit length of that segment.

Bibliography

[1] E. W. Kolb and M. Turner, *The Early Universe*, Addison-Wesley (1990)

[2] J. A. Peacock, *Cosmological Physics*, Cambridge University Press (1999)

[3] P. J. E. Peebles, *Principles of Physical Cosmology*, Princeton University Press (1993)

[4] A. R. Liddle and D. H. Lyth, *Cosmological Inflation and Large Scale Structure*, Cambridge University Press (2000)

[5] A. Vilenkin and E. P. S Shellard, *Cosmic Strings and Other Topological Defects*, Cambridge University Press (1994)

[6] M. B. Hindmarsh and T. W. B. Kibble, Rept. Prog. Phys. **58**, 477 (1995) [arXiv:hep-ph/9411342].

[7] J. Polchinski, Int. J. Mod. Phys. A **20** (2005) 3413 [AIP Conf. Proc. **743** (2005) 331] [arXiv:hep-th/0410082].

[8] E. J. Copeland and T. W. B. Kibble, Proc. Roy. Soc. Lond. A **466** (2010) 623 [arXiv:0911.1345 [hep-th]].

[9] M. Sakellariadou, Phil. Trans. Roy. Soc. Lond. A **366** (2008) 2881 [arXiv:0802.3379 [hep-th]].

[10] A. Achucarro and C. J. A. Martins, arXiv:0811.1277 [astro-ph].

[11] N. Jarosik *et al.*, arXiv:1001.4744 [astro-ph.CO].

[12] D. Larson *et al.*, arXiv:1001.4635 [astro-ph.CO].

[13] C. L. Bennett *et al.*, arXiv:1001.4758 [astro-ph.CO].

[14] E. Komatsu *et al.*, arXiv:1001.4538 [astro-ph.CO].

[15] S. Weinberg, *Gravitation and Cosmology*, John Wiley and Sans, Inc. (1972)

[16] G. Hinshaw *et al.* [WMAP Collaboration], Astrophys. J. Suppl. **180** (2009) 225 [arXiv:0803.0732 [astro-ph]].

[17] A. G. Riess *et al.*, Astrophys. J. **699** (2009) 539 [arXiv:0905.0695 [astro-ph.CO]].

[18] E. P. Hubble, Proc. Natl. Acad. Sci. USA 15, 168173 (1929)

[19] S. Perlmutter *et al.*, Astrophys. J. **517**, 565 (1999)

[20] A. G. Riess *et al.*, Astron. J. **116**, 1009 (1998); Astron. J. **117**, 707 (1999)

[21] M. Kowalski *et al.* [Supernova Cosmology Project Collaboration], Astrophys. J. **686** (2008) 749 [arXiv:0804.4142 [astro-ph]].

[22] R. A. Alpher, H. Bethe and G. Gamow, Phys. Rev. **73** (1948) 803

[23] J. C. Mather *et al.*, Astrophys. J. **512** (1999) 511

[24] T. W. B. Kibble, J. Phys. A **9**, 1387 (1976).

[25] T. W. B. Kibble, Phys. Rept. **67** (1980) 183.

[26] A. A. Starobinsky, JETP Lett. **30** (1979) 682 [Pisma Zh. Eksp. Teor. Fiz. **30** (1979) 719].

[27] A. A. Starobinsky, Phys. Lett. B **91** (1980) 99.

[28] A. H. Guth, Phys. Rev. D **23** (1981) 347.

[29] A. D. Linde, Phys. Lett. B **108** (1982) 389.

[30] A. D. Linde, Phys. Lett. B **129** (1983) 177.

[31] A. D. Dolgov and A. D. Linde, Phys. Lett. B **116** (1982) 329.

[32] J. H. Traschen and R. H. Brandenberger, Phys. Rev. D **42** (1990) 2491.

[33] L. Kofman, A. D. Linde and A. A. Starobinsky, Phys. Rev. D **56** (1997) 3258 [arXiv:hep-ph/9704452].

[34] I. Tkachev, S. Khlebnikov, L. Kofman and A. D. Linde, Phys. Lett. B **440** (1998) 262 [arXiv:hep-ph/9805209].

[35] H. B. Nielsen and P. Olesen, Nucl. Phys. B **61** (1973) 45.

[36] A. Vilenkin, Phys. Rev. D **23** (1981) 852.

[37] Q. Shafi and A. Vilenkin, Phys. Rev. D **29** (1984) 1870.

[38] G. Lazarides and Q. Shafi, Phys. Lett. B **148** (1984) 35.

[39] E. T. Vishniac, K. A. Olive and D. Seckel, Nucl. Phys. B **289** (1987) 717.

[40] R. Jeannerot, Phys. Rev. D **56** (1997) 6205 [arXiv:hep-ph/9706391].

[41] R. Jeannerot, J. Rocher and M. Sakellariadou, Phys. Rev. D **68**, 103514 (2003) [arXiv:hep-ph/0308134].

[42] G. R. Dvali and S. H. H. Tye, Phys. Lett. B **450** (1999) 72 [arXiv:hep-ph/9812483].

[43] S. Kachru, R. Kallosh, A. D. Linde, J. M. Maldacena, L. P. McAllister and S. P. Trivedi, JCAP **0310** (2003) 013 [arXiv:hep-th/0308055].

[44] C. P. Burgess, J. M. Cline, H. Stoica and F. Quevedo, JHEP **0409** (2004) 033 [arXiv:hep-th/0403119].

[45] S. Sarangi and S. H. H. Tye, Phys. Lett. B **536** (2002) 185 [arXiv:hep-th/0204074].

[46] N. T. Jones, H. Stoica and S. H. H. Tye, Phys. Lett. B **563** (2003) 6 [arXiv:hep-th/0303269].

[47] K. Dasgupta, J. P. Hsu, R. Kallosh, A. D. Linde and M. Zagermann, JHEP **0408** (2004) 030 [arXiv:hep-th/0405247].

[48] J. Urrestilla, A. Achucarro and A. C. Davis, Phys. Rev. Lett. **92** (2004) 251302 [arXiv:hep-th/0402032].

[49] M. R. Anderson, *The Mathematical Theory of Cosmic Strings*, Institute Of Physics (2003)

[50] M. Sakellariadou, Nucl. Phys. Proc. Suppl. **192-193** (2009) 68 [arXiv:0902.0569 [hep-th]].

[51] E. J. Copeland, T. W. B. Kibble and D. A. Steer, Phys. Rev. Lett. **97** (2006) 021602 [arXiv:hep-th/0601153].

[52] E. J. Copeland, T. W. B. Kibble and D. A. Steer, Phys. Rev. D **75** (2007) 065024 [arXiv:hep-th/0611243].

[53] G. S. Sharov, arXiv:hep-ph/9809465.

[54] G. 't Hooft, arXiv:hep-th/0408148.

[55] N. Nambu, Phys. Rev. D **4** (1971) 1193

[56] T. Goto, Prog. Theoret. Phys. **46** (1971) 1560

[57] T. W. B. Kibble and N. Turok, Phys. Lett. B **116** (1982) 141.

[58] N. Turok, Nucl. Phys. B **242** (1984) 520.

[59] D. Garfinkle and T. Vachaspati, Phys. Rev. D **36** (1987) 2229.

[60] S. W. Hawking, Phys. Lett. B **246** (1990) 36.

[61] C. J. Burden, Phys. Lett. B **164** (1985) 277.

[62] N. Turok and P. Bhattacharjee, Phys. Rev. D **29** (1984) 1557.

[63] A. Vilenkin, Phys. Rev. D **24** (1981) 2082.

[64] A. Vilenkin, Phys. Rev. Lett. **46** (1981) 1169 [Erratum-ibid. **46** (1981) 1496].

[65] T. Vachaspati and A. Vilenkin, Phys. Rev. D **30** (1984) 2036.

[66] R. J. Scherrer and J. A. Frieman, Phys. Rev. D **33** (1986) 3556.

[67] T. W. B. Kibble, Phys. Lett. B **166** (1986) 311.

[68] E. P. S. Shellard, Nucl. Phys. B **283** (1987) 624.

[69] R. A. Matzner, *Comput. Phys.* **2**, 51.

[70] A. Achucarro and R. de Putter, Phys. Rev. D **74** (2006) 121701 [arXiv:hep-th/0605084].

[71] D. Austin, E. J. Copeland and T. W. B. Kibble, Phys. Rev. D **48** (1993) 5594 [arXiv:hep-ph/9307325].

[72] T. W. B. Kibble, Nucl. Phys. **B252**, 227 (1985) [E **B261 461**]

[73] A. Albrecht and N. Turok, Phys. Rev. D **40** (1989) 973.

[74] B. Allen and E. P. S. Shellard, Phys. Rev. Lett. **64** (1990) 119.

[75] D. P. Bennett and F. R. Bouchet, Phys. Rev. D **41** (1990) 2408.

[76] M. Sakellariadou and A. Vilenkin, Phys. Rev. D **42** (1990) 349.

[77] B. Allen and R. R. Caldwell, Phys. Rev. Lett. **65** (1990) 1705.

[78] D. Austin, Phys. Rev. D **48** (1993) 3422.

[79] C. J. A. Martins and E. P. S. Shellard, Phys. Rev. D **54** (1996) 2535 [arXiv:hep-ph/9602271].

[80] C. J. A. Martins and E. P. S. Shellard, Phys. Rev. D **65** (2002) 043514 [arXiv:hep-ph/0003298].

[81] J. N. Moore, E. P. S. Shellard and C. J. A. Martins, Phys. Rev. D **65** (2002) 023503 [arXiv:hep-ph/0107171].

[82] L. Lorenz, C. Ringeval and M. Sakellariadou, JCAP **1010** (2010) 003 [arXiv:1006.0931 [astro-ph.CO]].

[83] T. Vachaspati and A. Vilenkin, Phys. Rev. D **31** (1985) 3052.

[84] G. R. Vincent, M. Hindmarsh and M. Sakellariadou, Phys. Rev. D **56** (1997) 637 [arXiv:astro-ph/9612135].

[85] V. Vanchurin, K. Olum and A. Vilenkin, Phys. Rev. D **72** (2005) 063514 [arXiv:gr-qc/0501040].

[86] C. Ringeval, M. Sakellariadou and F. Bouchet, JCAP **0702** (2007) 023 [arXiv:astro-ph/0511646].

[87] V. Vanchurin, K. D. Olum and A. Vilenkin, Phys. Rev. D **74** (2006) 063527 [arXiv:gr-qc/0511159].

[88] C. J. A. Martins and E. P. S. Shellard, Phys. Rev. D **73** (2006) 043515 [arXiv:astro-ph/0511792].

[89] K. D. Olum and V. Vanchurin, Phys. Rev. D **75** (2007) 063521 [arXiv:astro-ph/0610419].

[90] J. Polchinski and J. V. Rocha, Phys. Rev. D **74** (2006) 083504 [arXiv:hep-ph/0606205].

[91] J. Polchinski and J. V. Rocha, Phys. Rev. D **75** (2007) 123503 [arXiv:gr-qc/0702055].

[92] F. Dubath, J. Polchinski and J. V. Rocha, Phys. Rev. D **77** (2008) 123528 [arXiv:0711.0994 [astro-ph]].

[93] G. Vincent, N. D. Antunes and M. Hindmarsh, Phys. Rev. Lett. **80** (1998) 2277 [arXiv:hep-ph/9708427].

[94] M. Hindmarsh, S. Stuckey and N. Bevis, Phys. Rev. D **79** (2009) 123504 [arXiv:0812.1929 [hep-th]].

[95] X. Siemens and K. D. Olum, Nucl. Phys. B **611** (2001) 125 [Erratum-ibid. B **645** (2002) 367] [arXiv:gr-qc/0104085].

[96] E. Witten, Phys. Lett. B **153** (1985) 243.

[97] N. Arkani-Hamed, S. Dimopoulos and G. R. Dvali, Phys. Lett. B **429** (1998) 263 [arXiv:hep-ph/9803315].

[98] I. Antoniadis, N. Arkani-Hamed, S. Dimopoulos and G. R. Dvali, Phys. Lett. B **436** (1998) 257 [arXiv:hep-ph/9804398].

[99] L. Randall and R. Sundrum, Phys. Rev. Lett. **83** (1999) 3370 [arXiv:hep-ph/9905221].

[100] L. Randall and R. Sundrum, Phys. Rev. Lett. **83** (1999) 4690 [arXiv:hep-th/9906064].

[101] R. Durrer, M. Kunz and M. Sakellariadou, Phys. Lett. B **614** (2005) 125 [arXiv:hep-th/0501163].

[102] C. P. Burgess, M. Majumdar, D. Nolte, F. Quevedo, G. Rajesh and R. J. Zhang, JHEP **0107** (2001) 047 [arXiv:hep-th/0105204].

[103] J. Garcia-Bellido, R. Rabadan and F. Zamora, JHEP **0201** (2002) 036 [arXiv:hep-th/0112147].

[104] G. Dvali and A. Vilenkin, JCAP **0403** (2004) 010 [arXiv:hep-th/0312007].

[105] M. G. Jackson, N. T. Jones and J. Polchinski, JHEP **0510** (2005) 013 [arXiv:hep-th/0405229].

[106] E. J. Copeland, R. C. Myers and J. Polchinski, JHEP **0406** (2004) 013 [arXiv:hep-th/0312067].

[107] J. Polchinski, arXiv:hep-th/0412244.

[108] A. Sen, JHEP **9803** (1998) 005 [arXiv:hep-th/9711130].

[109] J. H. Schwarz, Phys. Lett. B **360** (1995) 13 [Erratum-ibid. B **364** (1995) 252] [arXiv:hep-th/9508143].

[110] J. Polchinski, Phys. Rev. Lett. **75** (1995) 4724 [arXiv:hep-th/9510017].

[111] E. J. Copeland, H. Firouzjahi, T. W. B. Kibble and D. A. Steer, Phys. Rev. D **77** (2008) 063521 [arXiv:0712.0808 [hep-th]].

[112] P. Salmi, A. Achucarro, E. J. Copeland, T. W. B. Kibble, R. de Putter and D. A. Steer, Phys. Rev. D **77** (2008) 041701 [arXiv:0712.1204 [hep-th]].

[113] N. Bevis and P. M. Saffin, Phys. Rev. D **78** (2008) 023503 [arXiv:0804.0200 [hep-th]].

[114] P. S. Letelier, P. R. Holvorcem and G. Grebot, Class. Quant. Grav. **7**, 597 (1990).

[115] H. Firouzjahi, S. Khoeini-Moghaddam and S. Khosravi, Phys. Rev. D **81**, 123506 (2010) [arXiv:1004.0068 [hep-th]].

[116] P. P. Avelino, C. J. A. Martins and E. P. S. Shellard, Phys. Rev. D **76** (2007) 083510 [arXiv:0710.2210 [hep-ph]].

[117] P. M. Saffin, JHEP **0509**, 011 (2005) [arXiv:hep-th/0506138].

[118] A. Albrecht, R. A. Battye and J. Robinson, Phys. Rev. Lett. **79**, 4736 (1997) [arXiv:astro-ph/9707129].

[119] C. Contaldi, M. Hindmarsh and J. Magueijo, Phys. Rev. Lett. **82**, 679 (1999) [arXiv:astro-ph/9808201].

[120] N. Bevis, M. Hindmarsh, M. Kunz and J. Urrestilla, Phys. Rev. D **75**, 065015 (2007) [arXiv:astro-ph/0605018].

[121] N. Bevis, M. Hindmarsh, M. Kunz and J. Urrestilla, Phys. Rev. Lett. **100**, 021301 (2008) [arXiv:astro-ph/0702223].

[122] A. A. Fraisse, C. Ringeval, D. N. Spergel and F. R. Bouchet, Phys. Rev. D **78**, 043535 (2008) [arXiv:0708.1162 [astro-ph]].

[123] L. Pogosian, S. H. Tye, I. Wasserman and M. Wyman, arXiv:0804.0810 [astro-ph].

[124] M. V. Sazhin, M. Capaccioli, G. Longo, M. Paolillo and O. S. Khovanskaya, arXiv:astro-ph/0601494.

[125] B. Shlaer and S. H. Tye, Phys. Rev. D **72** (2005) 043532 [arXiv:hep-th/0502242].

[126] B. Shlaer and M. Wyman, Phys. Rev. D **72**, 123504 (2005) [arXiv:hep-th/0509177].

[127] K. Kuijken, X. Siemens and T. Vachaspati, arXiv:0707.2971 [astro-ph].

[128] T. Damour and A. Vilenkin, Phys. Rev. Lett. **85**, 3761 (2000) [arXiv:gr-qc/0004075].

[129] X. Siemens, V. Mandic and J. Creighton, Phys. Rev. Lett. **98**, 111101 (2007) [arXiv:astro-ph/0610920].

[130] C. J. Hogan, Phys. Rev. D **74**, 043526 (2006) [arXiv:astro-ph/0605567].
M. R. DePies and C. J. Hogan, Phys. Rev. D **75**, 125006 (2007) [arXiv:astro-ph/0702335].

[131] J. Polchinski, Phys. Lett. B **209**, 252 (1988).

[132] E. J. Copeland and N. Turok, FERMILAB-PUB-86-127-A (1986).

[133] E. P. S. Shellard and P. J. Ruback, Phys. Lett. B **209**, 262 (1988).

[134] R. A. Matzner, Computers in Physics, Sep/Oct, 51 (1988).

[135] M. G. Jackson, JHEP **0709**, 035 (2007) [arXiv:0706.1264 [hep-th]].

[136] A. Hanany and K. Hashimoto, JHEP **0506**, 021 (2005) [arXiv:hep-th/0501031].

[137] A. Avgoustidis and E. P. S. Shellard, Phys. Rev. D **73**, 041301 (2006) [arXiv:astro-ph/0512582].

[138] D. Spergel and U. L. Pen, Astrophys. J. **491**, L67 (1997) [arXiv:astro-ph/9611198].

[139] P. McGraw, Phys. Rev. D **57**, 3317 (1998) [arXiv:astro-ph/9706182].

[140] E. J. Copeland and P. M. Saffin, JHEP **0511**, 023 (2005) [arXiv:hep-th/0505110].

[141] M. Hindmarsh and P. M. Saffin, JHEP **0608**, 066 (2006) [arXiv:hep-th/0605014].

[142] A. Rajantie, M. Sakellariadou and H. Stoica, JCAP **0711**, 021 (2007) [arXiv:0706.3662 [hep-th]].

[143] L. M. A. Bettencourt and T. W. B. Kibble, Phys. Lett. B **332**, 297 (1994) [arXiv:hep-ph/9405221].

[144] J. Urrestilla and A. Vilenkin, JHEP **0802** (2008) 037 [arXiv:0712.1146 [hep-th]].

[145] M. Sakellariadou and H. Stoica, JCAP **0808**, 038 (2008) [arXiv:0806.3219 [hep-th]].

[146] A. Vilenkin, Astrophys. J. **282** (1984) L51.

[147] J. R. Gott, Ap. J. **288** (1985) 422.

[148] D. Huterer and T. Vachaspati, Phys. Rev. D **68** (2003) 041301 [arXiv:astro-ph/0305006].

[149] B. Carter, Phys. Rev. D **41** (1990) 3869.

[150] A. Vilenkin, Phys. Rev. D **41** (1990) 3038.

[151] A. Vilenkin, Nature **322** (1986) 613.

[152] M. Sazhin *et al.*, Mon. Not. Roy. Astron. Soc. **343** (2003) 353 [arXiv:astro-ph/0302547].

[153] E. Morganson, P. Marshall, T. Treu, T. Schrabback and R. D. Blandford, arXiv:0908.0602 [astro-ph.CO].

[154] S. Dyda and R. H. Brandenberger, arXiv:0710.1903 [astro-ph].

[155] R. Brandenberger, H. Firouzjahi and J. Karouby, Phys. Rev. D **77** (2008) 083502 [arXiv:0710.1636 [hep-th]].

[156] R. J. Scherrer, J. M. Quashnock, D. N. Spergel and W. H. Press, Phys. Rev. D **42** (1990) 1908.

[157] D. Garfinkle and G. Comer Duncan, Phys. Rev. D **49** (1994) 2752 [arXiv:gr-qc/9307020].

[158] B. Allen and P. Casper, Phys. Rev. D **50** (1994) 2496 [arXiv:gr-qc/9405005].

[159] B. Allen, P. Casper and A. Ottewill, Phys. Rev. D **50** (1994) 3703 [arXiv:gr-qc/9405037].

[160] P. Casper and B. Allen, Phys. Rev. D **52** (1995) 4337 [arXiv:gr-qc/9505018].

[161] M. Sakellariadou, Phys. Rev. D **42** (1990) 354 [Erratum-ibid. D **43** (1991) 4150] [Phys. Rev. D **43** (1991) 4150].

[162] M. Hindmarsh, Phys. Lett. B **251** (1990) 28.

[163] R. A. Battye and E. P. S. Shellard, Nucl. Phys. B **423** (1994) 260 [arXiv:astro-ph/9311017].

[164] R. Brandenberger, H. Firouzjahi, J. Karouby and S. Khosravi, JCAP **0901** (2009) 008 [arXiv:0810.4521 [hep-th]].

[165] T. Damour and A. Vilenkin, Phys. Rev. D **64**, 064008 (2001) [arXiv:gr-qc/0104026].

[166] T. Damour and A. Vilenkin, Phys. Rev. D **71**, 063510 (2005) [arXiv:hep-th/0410222].

[167] X. Siemens, J. Creighton, I. Maor, S. Ray Majumder, K. Cannon and J. Read, Phys. Rev. D **73** (2006) 105001 [arXiv:gr-qc/0603115].

[168] A. C. Davis, W. Nelson, S. Rajamanoharan and M. Sakellariadou, JCAP **0811** (2008) 022 [arXiv:0809.2263 [hep-th]].

[169] P. Binetruy, A. Bohe, T. Hertog and D. A. Steer, Phys. Rev. D **80** (2009) 123510 [arXiv:0907.4522 [hep-th]].

[170] P. Binetruy, A. Bohe, T. Hertog and D. A. Steer, Phys. Rev. D **82** (2010) 083524 [arXiv:1005.2426 [hep-th]].

[171] P. Binetruy, A. Bohe, T. Hertog and D. A. Steer, arXiv:1009.2484 [hep-th].

[172] E. O'Callaghan, S. Chadburn, G. Geshnizjani, R. Gregory and I. Zavala, Phys. Rev. Lett. **105** (2010) 081602 [arXiv:1003.4395 [hep-th]].

[173] E. O'Callaghan, S. Chadburn, G. Geshnizjani, R. Gregory and I. Zavala, JCAP **1009** (2010) 013 [arXiv:1005.3220 [hep-th]].

[174] E. O'Callaghan and R. Gregory, arXiv:1010.3942 [hep-th].

[175] S. Dodelson, *Modern Cosmology*, Academic Press (2003)

[176] W. Hu and S. Dodelson, Ann. Rev. Astron. Astrophys. **40** (2002) 171 [arXiv:astro-ph/0110414].

[177] W. Hu, Ann. Phys. **303** (2002) 203

[178] A. Challinor, arXiv:astro-ph/0606548.

[179] D. Scott and G. F. Smoot, arXiv:1005.0555 [astro-ph.CO].

[180] D. Baumann and H. V. Peiris, Adv. Sci. Lett. **2** (2009) 105 [arXiv:0810.3022 [astro-ph]].

[181] G. F. Smoot *et al.*, Astrophys. J. **396** (1992) L1.

[182] J. E. Lidsey, A. R. Liddle, E. W. Kolb, E. J. Copeland, T. Barreiro and M. Abney, Rev. Mod. Phys. **69** (1997) 373 [arXiv:astro-ph/9508078].

[183] E. Komatsu *et al.*, Astrophys. J. Supp. **180** (2009) 330

[184] W. Hu and N. Sugiyama, Astrophys. J. **444** (1995) 489 [arXiv:astro-ph/9407093].

[185] R. K. Sachs and A. M. Wolfe, Astrophys. J. **147** (1967) 73

[186] J. Silk, Astrophys. J. **151** (1968) 459

[187] U. Seljak and M. Zaldarriaga, Astrophys. J. **469** (1996) 437 [arXiv:astro-ph/9603033].

[188] A. Lewis, A. Challinor and A. Lasenby, Astrophys. J. **538** (2000) 473 [arXiv:astro-ph/9911177].

[189] C. Contaldi, M. Hindmarsh and J. Magueijo, Phys. Rev. Lett. **82**, 2034 (1999).

[190] R. A. Battye and J. Weller, Phys. Rev. **D61**, 043501 (2000).

[191] F. R. Bouchet, P. Peter, A. Riazuelo, and M. Sakellariadou, Phys. Rev. **D65**, 21301 (2002).

[192] N. Bevis, M. Hindmarsh, and M. Kunz, Phys. Rev.**D70**, 043508 (2004), astro-ph/0403029.

[193] M. Wyman, L. Pogosian and I. Wasserman, Phys. Rev. D **72**, 023513 (2005) [Erratum-ibid. D **73**, 089905 (2006)] [arXiv:astro-ph/0503364].

[194] U. Seljak, A. Slosar and P. McDonald, JCAP **0610**, 014 (2006) [arXiv:astro-ph/0604335].

[195] R. Battye and A. Moss, "Updated constraints on the cosmic string tension," arXiv:1005.0479 [astro-ph.CO].

[196] U. Seljak, U. L. Pen and N. Turok, Phys. Rev. Lett. **79**, 1615 (1997) [arXiv:astro-ph/9704231].

[197] R. A. Battye, arXiv:astro-ph/9806115.

[198] L. Pogosian, S. H. H. Tye, I. Wasserman and M. Wyman, Phys. Rev. D **68** (2003) 023506 [Erratum-ibid. D **73** (2006) 089904] [arXiv:hep-th/0304188].

[199] U. Seljak and A. Slosar, Phys. Rev. D **74** 063523 (2006) [arXiv:astro-ph/0604143].

[200] L. Pogosian and M. Wyman, Phys. Rev. D **77** (2008) 083509 [arXiv:0711.0747 [astro-ph]].

[201] N. Bevis, M. Hindmarsh, M. Kunz and J. Urrestilla, Phys. Rev. D **76**, 043005 (2007) [arXiv:0704.3800 [astro-ph]].

[202] J. Urrestilla, P. Mukherjee, A. R. Liddle, N. Bevis, M. Hindmarsh and M. Kunz, Phys. Rev. D **77**, 123005 (2008) [arXiv:0803.2059 [astro-ph]].

[203] P. Mukherjee, J. Urrestilla, M. Kunz, A. R. Liddle, N. Bevis and M. Hindmarsh, arXiv:1010.5662 [astro-ph.CO].

[204] N. Kaiser and A. Stebbins, Nature **310** (1984) 391.

[205] A. Stewart and R. Brandenberger, JCAP **0902** (2009) 009 [arXiv:0809.0865 [astro-ph]].

[206] L. Pogosian and T. Vachaspati, Phys. Rev. D **60**, 083504 (1999) [arXiv:astro-ph/9903361].

[207] http://www.sfu.ca/~levon/cmbact.html

[208] G. R. Vincent, M. Hindmarsh and M. Sakellariadou, Phys. Rev. D **55**, 573 (1997) [arXiv:astro-ph/9606137].

[209] A. Albrecht, R. A. Battye and J. Robinson, Phys. Rev. D **59**, 023508 (1999) [arXiv:astro-ph/9711121].

[210] R. R. Caldwell, R. A. Battye and E. P. S. Shellard, Phys. Rev. D **54** (1996) 7146 [astro-ph/9607130].

[211] F. A. Jenet *et al.*, Astrophys. J. **653** (2006) 1571 [arXiv:astro-ph/0609013].

[212] K. Dasgupta, C. Herdeiro, S. Hirano and R. Kallosh, Phys. Rev. D **65** (2002) 126002 [arXiv:hep-th/0203019].

[213] A. Avgoustidis, D. Cremades and F. Quevedo, Gen. Rel. Grav. **39** (2007) 1203 [arXiv:hep-th/0606031].

[214] L. Leblond and S.-H. H. Tye, JHEP **0403**, 055 (2004), hep-th/0402072;

[215] S. H. Tye, I. Wasserman and M. Wyman, Phys. Rev. D **71** (2005) 103508 [Erratum-ibid. D **71** (2005) 129906] [arXiv:astro-ph/0503506].

[216] A. Avgoustidis and E. P. S. Shellard, Phys. Rev. D **78** (2008) 103510 [arXiv:0705.3395 [astro-ph]].

[217] N. Bevis, E. J. Copeland, P. Y. Martin, G. Niz, A. Pourtsidou, P. M. Saffin and D. A. Steer, arXiv:0904.2127 [hep-th].

[218] A. Avgoustidis and E. J. Copeland, Phys. Rev. D **81** (2010) 063517 [arXiv:0912.4004 [hep-ph]].

[219] E. Witten, Nucl. Phys. B **460** (1996) 335 [arXiv:hep-th/9510135].

[220] M. Sakellariadou, JCAP **0504** (2005) 003 [arXiv:hep-th/0410234].

[221] A. Avgoustidis, Phys. Rev. D **78** (2008) 023501 [arXiv:0712.3224 [hep-th]].

[222] E. P. S. Shellard and B. Allen, in Cambridge 1989, Proceedings, *The formation and evolution of cosmic strings*, 421-448. (see HIGH ENERGY PHYSICS INDEX 29 (1991) No. 7720)

[223] N. Bevis, M. Hindmarsh, M. Kunz and J. Urrestilla, arXiv:1005.2663 [astro-ph.CO].

[224] http://quiet.uchicago.edu/

[225] http://bolo.berkeley.edu/polarbear/

[226] T. Okamoto and W. Hu, Phys. Rev. D **67**, 083002 (2003) [arXiv:astro-ph/0301031].

[227] K. M. Smith *et al.*, arXiv:0811.3916 [astro-ph].

[228] H. Firouzjahi, J. Karouby, S. Khosravi and R. Brandenberger, Phys. Rev. D **80** (2009) 083508 [arXiv:0907.4986 [hep-th]].

[229] M. R. Anderson, F. Bonjour, R. Gregory and J. Stewart, Phys. Rev. D **56** (1997) 8014 [arXiv:hep-ph/9707324].

[230] K. J. M. Moriarty, E. Myers and C. Rebbi, Phys. Lett. B **207** (1988) 411.